2018

IGDB-2, an IG/FNIII Protein, Binds the ION Channel LGC-34 and Controls Sensory Compartment Morphogenesis in C. Elegans

Wendy Wang

IGDB-2, AN IG/FNIII PROTEIN, BINDS THE ION CHANNEL LGC-34 AND CONTROLS SENSORY COMPARTMENT MORPHOGENESIS IN *C. ELEGANS*

A Thesis Presented to the Faculty of

The Rockefeller University

in Partial Fulfillment of the Requirements for

the degree of Doctor of Philosophy

by

Wendy Wang

June 2018

IGDB-2, AN IG/FNIII PROTEIN, BINDS THE ION CHANNEL LGC-34 AND CONTROLS SENSORY COMPARTMENT MORPHOGENESIS IN *C. ELEGANS*

Wendy Wang, Ph.D.
The Rockefeller University 2018

Sensory organ glia surround neuronal receptive endings (NREs), forming a specialized extracellular space, or compartment, important for neuronal activity, and reminiscent of glia-ensheathed synapses in the central nervous system. Sensory organ glia are conserved across organisms, but our current understanding of how they form sensory compartments is generally lacking. To date, the *Caenorhabditis elegans* amphid sensory organ has provided critical insight into some of these developmental processes. DAF-6, a Patched-related protein, was previously shown to be required in amphid glia to restrict sensory compartment size. LIT-1, a Nemo-like kinase, and SNX-1, a retromer component, antagonize DAF-6 and promote compartment expansion.

My work here further explores the machinery underlying compartment size control. In seeking genes whose inactivation restores normal compartment size to *daf-6* mutants, I identify two novel regulators: IGDB-2, an Ig/FNIII protein, and LGC-34, a ligand-gated ion channel. First, *igdb-2* mutations suppress *daf-6* mutant defects. IGDB-2 acts in glia, where it localizes to glial membranes surrounding NREs, and, together with LIT-1 and SNX-1, regulates compartment morphogenesis. Second, immunoprecipitation followed by mass spectrometry demonstrates that IGDB-2 binds to LGC-34, and *lgc-34* mutations inhibit *igdb-2* suppression of *daf-6*. My

findings thus reveal the novel IGDB-2/LGC-34 membrane protein complex and suggest new molecular mechanisms for how sensory compartment size is controlled.

Acknowledgments

First, I want to thank my advisor, Shai Shaham. Over the last few years, Shai has always been there, gently guiding me through the challenges inherent to science and prodding me to think more critically. Every day, he demonstrates a powerful curiosity that inspires all around him, and provides a rare even keel to help us all navigate to the next interesting idea.

I want to thank the current and past members of my committee: Drs. Hiro Funabiki, Sandy Simon, Monn Myat, Geri Kreitzer, and Jen Zallen for their scientific input and advice that has guided this story to completion. Their perspectives have helped me think more slowly and thoroughly.

I want to thank all the members of the Shaham lab, past and present, for creating a community that gracefully blends perseverance and collegiality. I especially thank Anu and Lena, for their unfailing moral support and loving friendships; my benchmate Wolfgang, for his empathy and his polymathic abilities; Max, Menachem, and Sean for being the first to guide me in lab; Andrea and Jennifer, for their humorous perspectives on life; Elliot and Grigoris for getting this project started; and Yun Lu for her tireless microscopy work; and Maya and Sharon, for keeping the wheels of the lab running smoothly.

I also want to thank the amazing core facilities at Rockefeller, including Alison North at the Bio-Imaging Resource Center, and Milica Tesic-Mark, Joe Fernandez, and Henrik Molina at the Proteomics Resource Center, for making the second half of my thesis work even possible.

I want to thank the MD-PhD program, specifically Elaine and Renee for bringing out the office cheer, and Olaf, for his apt and kind advice and support. I also want to thank Cris and Stephanie at the Dean's Office at Rockefeller, for always being cheerful and helpful with all my questions.

I want to thank Peter, for his love, inimitable humor, and kindness.

Finally, I want to thank my parents, for their fierce optimism, love, and ideas. They have been brave at every juncture and always inspire me to be more so. And I want to thank Stephanie, for being that kindred spirit, who loves and guides her sister.

Table of Contents

Chapter 1: Introduction 1
1.1 Glial compartments surround neuronal receptive endings 1
1.2 Glial compartments in sensory organs 5
1.2.1 In vertebrates 5
1.2.1.1 Sustentacular cells in the olfactory mucosa 7
1.2.1.2 Deiters' cells in the inner ear 7
1.2.1.3 Retinal pigment epithelial cells in the retina 8
1.2.2 In *Drosophila melanogaster* 9
1.2.2.1 Mechanosensory organ 10
1.2.2.2 Olfactory sensory organ 13
1.2.3 In *C. elegans* 14
1.2.3.1 Amphid 14
1.2.3.2 Other sensilla 18
1.2.3.3 Amphid channel morphogenesis 18
1.2.3.3.1 DAF-6 restricts amphid channel expansion 18
1.2.3.3.2 LIT-1 promotes amphid channel expansion 21
1.2.3.3.3 SNX-1 promotes amphid channel expansion 22
1.2.3.3.4 CHE-14, like DAF-6, regulates formation of tubular structures 23
1.2.3.3.5 AMso cell development 25
1.2.3.3.6 Neuronal regulation of amphid channel morphogenesis 26
1.2.3.3.7 Glial regulation of amphid neuron development 27
1.3 Sensory organ glia as models for CNS glia 27
1.4 *C. elegans* as a model for glial compartment morphogenesis 30
1.5 Lumen formation 31
1.5.1 Vertebrate capillaries 34
1.5.2 *C. elegans* excretory cell 35
1.5.3 Madin-Darby canine kidney (MDCK) cells 37
1.5.4 *Drosophila* tracheal system 39

1.5.5 Immunoglobulin (Ig) superfamily (IgSF) members in development of tubular structures 42
1.5.5.1 Neogenin in the zebrafish neural tube lumen 45
1.5.5.2 Cdo and Boc in neural tube patterning 47
1.5.5.3 Neuroglian in the *Drosophila* antennal lobe glial canals 49
1.5.5.4 Robo receptors in astrocytic tunnels 50
1.6 Ion channels in glia 52
1.6.1 K^+ channels in glia 53
1.6.2 Regulation of extracellular K^+ concentrations 53
1.6.3 K^+ concentrations in extracellular space regulation 54
1.6.4 Cdo and Kir2.1 in myoblast differentiation 55
1.6.5 Ligand-gated ion channels 55
1.6.5.1 In astrocytes 56
1.6.5.2 In oligodendrocytes 56
1.6.5.3 In *C. elegans* 57
1.6.5.3.1 LGC-55 58
Chapter 2: IGDB-2, an Ig/FNIII protein, promotes sensory compartment expansion in *C. elegans* 59
2.1 A screen for *daf-6* suppressor mutants 59
2.2 *ns122* suppresses sensory compartment defects of *daf-6* mutants 62
2.3 *ns122* is an allele of *igdb-2*, which encodes an Ig/FNIII protein 65
2.4 *igdb-2* acts in glia and localizes to glial membranes of the sensory compartment 71
2.4.1 *igdb-2* acts in glia, including the AMso glia 71
2.4.2 *igdb-2* is expressed in glia, including the AMso glia 73
2.4.3 IGDB-2 localizes to glial membranes of the sensory compartment 75
2.5 IGDB-2 is *N*-glycosylated 77
2.6 The IGDB-2 membrane-distal extracellular domain is required for compartment morphogenesis 79
2.7 *igdb-2* genetically interacts with other genes controlling compartment size 81

Chapter 3: IGDB-2 binds to and inhibits LGC-34, a predicted ligand-gated ion channel....85
3.1 A screen for IGDB-2 interactors by co-immunoaffinity purification and mass spectrometry analysis....85
3.2 LGC-34, a predicted ligand-gated ion channel, binds to IGDB-2....89
3.3 LGC-34 and IGDB-2 are co-expressed in some cells, including glia....91
3.4 LGC-34 restricts sensory compartment expansion and is inhibited by IGDB-2....93
3.5 F42A8.1, an uncharacterized protein and IGDB-2 interactor candidate, is unlikely to be involved in sensory compartment morphogenesis....95
Chapter 4: Discussion....97
4.1 A model for amphid compartment morphogenesis....97
4.2 IGDB-2 protein domains are found in other lumen-forming proteins....99
4.3 A comparison of IGDB-2-LGC-34 with protein complexes in Hedgehog signaling....102
4.4 A role for IGDB-2 and LGC-34 in glial osmolarity regulation....103
4.5 A ligand for LGC-34 function....103
Chapter 5: Future directions....105
5.1 Structure-function analysis of the IGDB-2-LGC-34 interaction....105
5.2 IGDB-2 regulates LGC-34 localization....106
5.3 Interaction between DAF-6 and IGDB-2....106
5.4 Characterizing other IGDB-2 interactor candidates....107
5.5 LGC-34 and glial (and sensory compartment) osmolarity....108
5.6 Characterizing *ns125*, another *daf-6* suppressor mutant....111
Chapter 6: Materials and methods....113
6.1 *C. elegans* strains....113
6.2 Identification of *igdb-2*(*ns122*)....113
6.3 Extrachromosomal arrays....113
6.4 Integrated arrays....114
6.5 Plasmid construction....114
6.6 Dye-filling assay....115

6.7 Fluorescence and transmission electron microscopy 116
6.8 Co-immunoaffinity purification from worms and mass spectrometry 116
6.9 Cell culture and co-immunoaffinity purification 117
6.10 Immunofluorescence 117
6.11 PNGase F assay 118
6.12 CRISPR/Cas9 generation of *ns793* 119
Appendix. 120
References 126

List of Figures

Figure 1.1. Neuron-glia interactions in the nervous system 4
Figure 1.2. Sensory compartments in vertebrates 6
Figure 1.3. *Drosophila* mechanosensory organ 12
Figure 1.4. *C. elegans* amphid 17
Figure 1.5. *daf-6* mutants show bloated amphid channels, which are suppressed by either *lit-1* or *snx-1* mutations 20
Figure 1.6. A model for sensory compartment morphogenesis in *C. elegans* 24
Figure 1.7. Schematic of Ig/FNIII proteins involved in tissue morphogenesis 44
Figure 2.1. The dye-filling assay 61
Figure 2.2. *ns122* is a *daf-6* suppressor 64
Figure 2.3. Mapping strategy for the *ns122* mutant 66
Figure 2.4. Schematic showing the interval containing the *ns122* locus 68
Figure 2.5. *ns122* is an allele of *igdb-2*, which encodes an Ig/FNIII transmembrane protein 70
Figure 2.6. *igdb-2* acts in glia to regulate amphid channel morphogenesis 72
Figure 2.7. *igdb-2* is expressed in glia, including the AMso glia 74
Figure 2.8. IGDB-2 localizes to the glial membranes of the sensory compartment 76
Figure 2.9. IGDB-2 is *N*-glycosylated 78
Figure 2.10. The N-terminal membrane-distal domain of IGDB-2 is required for IGDB-2 function in amphid channel morphogenesis 80
Figure 2.11. *igdb-2* genetically interacts with other genes controlling compartment size 84
Figure 3.1. IGDB-2 interactors are co-purified from worms 87
Figure 3.2. LGC-34 binds IGDB-2 in HEK293 cells 90
Figure 3.3. LGC-34 and IGDB-2 are co-expressed in a subset of cells in C. elegans. 92

Figure 3.4. *lgc-34* restricts sensory compartment expansion and is inhibited by *igdb-2* 94
Figure 3.5. F42A8.1 does not appear to be involved in sensory compartment morphogenesis 96
Figure 4.1. A model for sensory compartment morphogenesis. 98
Figure 4.2. Possible mechanisms underlying sensory compartment morphogenesis in *C. elegans* 101
Figure 5.1. Environmental osmolarity affects dye-filling in *igdb-2*; *daf-6* mutants. 110
Figure S1. *ns122* suppression of the *daf-6* dye-filling defect correlates with normal amphid channel morphology 121
Figure S2. Mutants of *igdb-2* interactor candidates show various dye-filling phenotypes. 122
Figure S3. *lgc-34* mutants show no significant dye-filling defects as single or double mutants with *daf-6*. 123

List of Tables

Table 1. Mass spectrometry analysis of IGDB2-interacting proteins 84
Table S1. List of abbreviations 120

Chapter 1: Introduction

Animals require sensation to mount appropriate responses to environmental stimuli. Sensory organs detecting external cues are often comprised of sensory neurons and glia, or glia-like cells, wherein the glia form specialized compartments around receptive endings of sensory neurons. This compartment suggests a role for glia in regulating sensory function, much as glia regulate neuronal function in the central nervous system. In my thesis, I sought to understand how glial sensory compartments form and how their size and shape are determined. In this chapter, I will summarize the foundations that led to my thesis work and provide context that will be useful in analyzing my later findings.

1.1 Glial compartments surround neuronal receptive endings

Sensation starts with an environmental stimulus, which is then processed by the nervous system into a response. The nervous system mainly consists of neurons and glia (Figure 1.1). Neurons process stimuli into information through electrical signaling to other cells (e.g. other neurons, muscle cells, and glands) (Shaham, 2005). They connect to these other cells through processes (dendrites and axons, carrying signals to and away from the cell body) that terminate in synapses and gap junctions. The basic sensory circuit involves three neuron types: the sensory neuron, interneuron, and motor neuron (or another type of efferent neuron). This pathway is further modulated by inputs from the central nervous system (CNS) neurons.

Glia, though distinct from neurons, are physically associated with neurons and often share a common lineage. They carry out several critical functions,

including promoting synaptogenesis and regulating neuronal development and signaling (Shaham, 2005). Like neurons, there are several types of glia. In vertebrates, there are four traditional types: Schwann cells in the peripheral nervous system (PNS) and oligodendrocytes, astrocytes, and microglia in the CNS. Schwann cells ensheath axons, either with or without myelin, and provide critical trophic support for PNS neurons (Monk et al., 2015). Oligodendrocytes similarly myelinate and ensheathe axons in the CNS. Astrocytes are the most abundant cell type in the brain (Freeman, 2010) and extend processes that envelop neuronal synapses and also interact with endothelial cells. Finally, microglia are the resident macrophages in the CNS and in contrast to the other glial types, which derive from the ectoderm, are of mesodermal origin.

Together, these neurons and glia are required for proper sensory function, but ultimately, sensation starts with a stimulus and the sensory organ that detects it. Within the sensory organ, glia, or glia-like cells, enclose receptive endings of sensory neurons in specialized extracellular compartments. However, sensory organ glia remain the lesser studied component in this system, though they can be critical for proper sensory function. In support of this, these glia, or glia-like counterparts, are conserved in multiple organisms. I will thus provide an overview of these sensory compartments in vertebrates, *Drosophila melanogaster*, and *Caenorhabditis elegans*. Each highlights not only how the glial compartment regulates sensory neuronal function, but also how much remains to be understood as to how they form.

Unsurprisingly, the most complex sensory compartments are also the least characterized in morphogenesis.

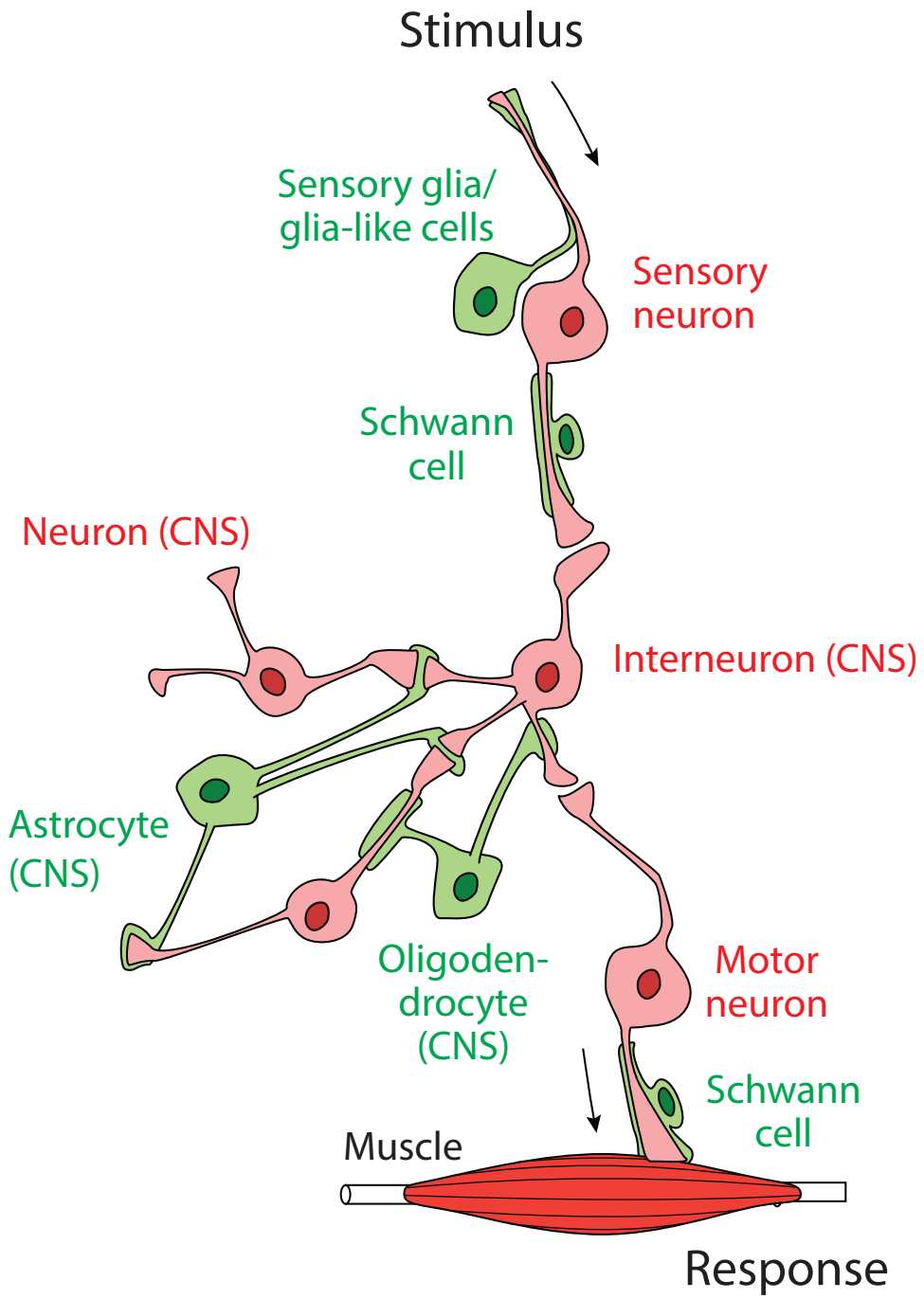

Figure 1.1. Neuron-glia interactions in the vertebrate nervous system. The nervous system consists of neurons (red) and glia (green). Sensory neurons process external stimuli into an electrical signal to interneurons, which process multiple inputs (e.g. from the central nervous system) to ultimately activate a motor neuron. The motor neuron transmits the signal to an effector cell (the muscle fiber shown here). Glia are intimately associated with neurons throughout this signaling network. CNS, central nervous system.

1.2 Glial compartments in sensory organs

1.2.1 In vertebrates

Vertebrate sensory systems range widely in complexity, but in every case, glial or glia-like cells form a specialized compartment for sensory neuronal endings (Figure 1.2). Below, I describe the anatomy and function of the following glia-like cells that form compartments: sustentacular cells in the olfactory mucosa, Deiters' cells in the inner ear, and retinal pigment epithelial cells in the retina. In each case, these glial-like cells serve critical glial functions, including ensheathment and/or isolation of the NREs, trophic support for neurons, phagocytosis of neuronal debris, and maintenance of extracellular ion concentrations. Morphogenesis of these glial compartments remains poorly characterized.

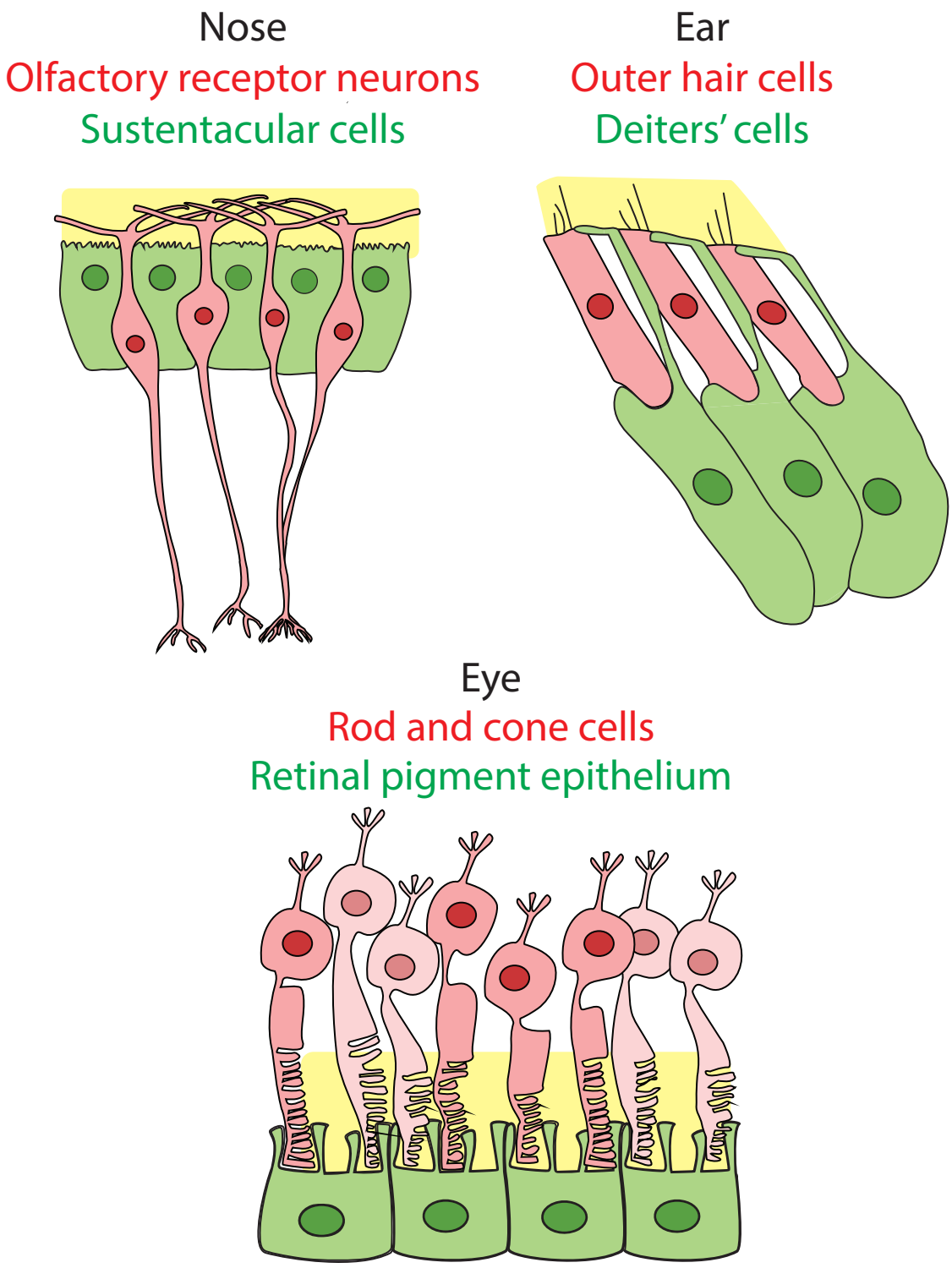

Figure 1.2. Sensory compartments in vertebrates. Glia or glia-like cells (green) form compartments (yellow) around sensory neuronal receptive endings (red).

1.2.1.1 Sustentacular cells in the olfactory mucosa

In the olfactory epithelium, olfactory receptor neurons reside in a compartment between supporting sustentacular cells, which serve several glial functions (Barnett and Chang, 2004). First, the sustentacular cells partially ensheath and isolate the neuronal cilia that project into the nasal cavity. Second, they can phagocytose dead neurons (Suzuki et al., 1996). Third, they help maintain the extracellular ion concentrations for neurons (Getchell, 1986). Finally, they exhibit intracellular calcium signaling similar to that seen in astrocytes (Hegg et al., 2009). These functions demonstrate how sustentacular cells are essential in regulating olfactory receptor neuron functions, but surprisingly few studies address how the sustentacular cells, and its sensory compartment, form. Notch signaling is required to maintain sustentacular cell function (Rodriguez et al., 2008). This regulation of glial survival is a disparate process from sustentacular cell morphogenesis. Considerably less is known about the latter.

1.2.1.2 Deiters' cells in the inner ear

Another glial compartment is seen in the organ of the Corti in the inner ear. Here, Deiters' hair cells structurally support mechanosensory outer hair cells (OHCs) and ensheathe OHC afferent processes (Yu and Zhao, 2009). Deiters' cells express the classic glial marker, glial fibrillary acidic protein (GFAP) (Rio et al., 2002) and help transmit mechanical force to the OHCs via phalangeal processes (Ashmore, 2008). Furthermore, the mechanical coupling to the OHCs allows Deiters' cells to modulate OHC electromotility.

Cell polarity is critical for Deiter's cells to form properly, both during development and after maturation. Mutations in the core planar cell polarity gene, *Van Gogh-like 2* (*Vangl2*) lead to disorganized apical surfaces and misplaced phalangeal processes in Deiters' cells and another support cell, outer pillar cells (OPCs) (Copley et al., 2013). Additionally, postnatal *Cdc42* depletion in mice leads to defective F-actin belt formation in Deiters' cells and OPCs, ectopic lumen formation between cells, and loss of polarity (Anttonen et al., 2012). However, polarity is affected in both types of support cells, which makes it harder to distinguish the contributions from each individual cell type. Moreover, beyond actin regulation, we know little about other pathways that shape the auditory sensory compartment.

1.2.1.3 Retinal pigment epithelial cells in the retina

A third sensory compartment is in the vertebrate retina, where retinal pigment epithelial (RPE) cells maintain the extracellular environment for rod and cone photoreceptors. RPE cells lie in close association with the photoreceptors, separated by a thin compartment of interphotoreceptor matrix (IPM) (Strauss, 2005) (Figure 1.2, picture on right, yellow region). RPE cells importantly provide nutrients and ions, process retinol, and phagocytose outer segments shed by the photoreceptor cells via microvilli that ensheath these outer segments (Bok, 1993).

These apical microvilli are established via apical-basal polarity processes and are critical for RPE function, but how do they develop? Morphologically, this process starts with a ciliated pseudostratified RPE, which converts to a simple cuboidal layer (Marmorstein et al., 1998). When the photoreceptor cells extend their outer

segments, RPE cells extend the microvilli in response, and simultaneously develop basal membrane foldings. Just as in Deiters' cells, apical-basal polarity appears tightly regulated. In RPE cells, increases in apical membranes concurrently occur to an equal extent on the basolateral side.

Ezrin is known to be essential for apical microvilli development, and membrane proteins like Na^+/K^+-ATPase and NCAM-140 (involved in neurite outgrowth and cell-cell adhesion) are trafficked to the apical membrane (Strauss, 2005). However, little else is known about factors regulating RPE morphogenesis. Moreover, the RPE microvilli are intimately associated with the photoreceptor outer segments and only separated by the IPM, but the processes that shape the IPM remain unknown. This presents a significant challenge in studying glial morphogenesis in this system.

1.2.2 In *Drosophila melanogaster*

The neuron-glia sensory structure is conserved in invertebrates, such as *Drosophila melanogaster*, as are the supportive functions of the glia. Invertebrate mechanosensory and olfactory sensory organs are structurally simpler. For example, the vertebrate organ of Corti alone counts inner and outer pillar cells and Deiters' cells as support cells. The simplicity in *Drosophila* has allowed for more glial cell lineage studies and insight into cell fate specification pathways, but again, these questions are distinct from how the glial cells acquire their shapes. Our knowledge about the latter is considerably lacking.

1.2.2.1 Mechanosensory organ

Drosophila mechanosensory organs are bristles found on the dorsal thorax and classified by size and location as macrochaetes or microchaetes (Furman and Bukharina, 2008). Each organ consists of four cells: a single-dendrite sensory neuron and concentrically ensheathing support cells (shaft, socket, and sheath) (Figure 1.3) (Hartenstein and Posakony, 1989). The shaft and socket cells contribute to the external portion of the bristle, and the socket cell wraps around the base of the shaft. Importantly, the sheath cell wraps around the neuron, recalling glial cells of vertebrate sensory organs. Because the sheath cell physically contacts the neuron, the sheath cell transduces mechanical stimuli to the neuron, like how Deiters' cells help convey mechanical force to OHCs in the inner ear (Chung et al., 2001). This is at least partially due to the dendritic cap, a matrix-filled compartment secreted by the sheath cell (highlighted in yellow, Figure 1.3). The dendritic cap also requires expression of NompA, a zona pellucida-domain protein, for proper stimulus transduction.

The sequence of events leading to development of the mechanosensory organ has been well described by Hartenstein and Posakony (Hartenstein and Posakony, 1989). This process initiates when a sensory organ precursor (SOP) cell is chosen from a cluster of ectodermal cells, called the "proneural cluster," through lateral inhibition of Notch signaling: only the cell expressing the highest levels of four basic helix-loop-helix transcription factors, known as the *achaete-scute* (AS-C) gene complex, escapes inhibition and becomes the SOP (García-Bellido and de Celis,

2009). Using bromodeoxyuridine (BrdU) labeling, they found that the SOP divides twice to produce four precursor cells: the eventual neuron, sheath, socket, and shaft cells (Hartenstein and Posakony, 1989). The neuronal precursor moves interiorly and extends an axon, which eventually fasciculates with neighboring bristle axons, and a dendrite, which pierces through the sheath cell. The socket and shaft cells then extend processes around the sheath cell. These processes remain in place, while the cell bodies migrate interiorly. Eventually, these processes grow apically into a shaft and socket, and the sheath secretes the dendritic cap (Hartenstein and Posakony, 1989).

These studies demonstrate an inherent strength of simpler sensory structures: it is easier to track the development of individual neurons and glia and to thus perform lineage analysis of each cell type. However, in other respects, the mechanosensory organ is as poorly characterized as its vertebrate counterparts. For instance, the AS-C gene complex is known to regulate cell fate (García-Bellido and de Celis, 2009), but we still face a considerable void as to how the support cells, like the sheath cell, actually form.

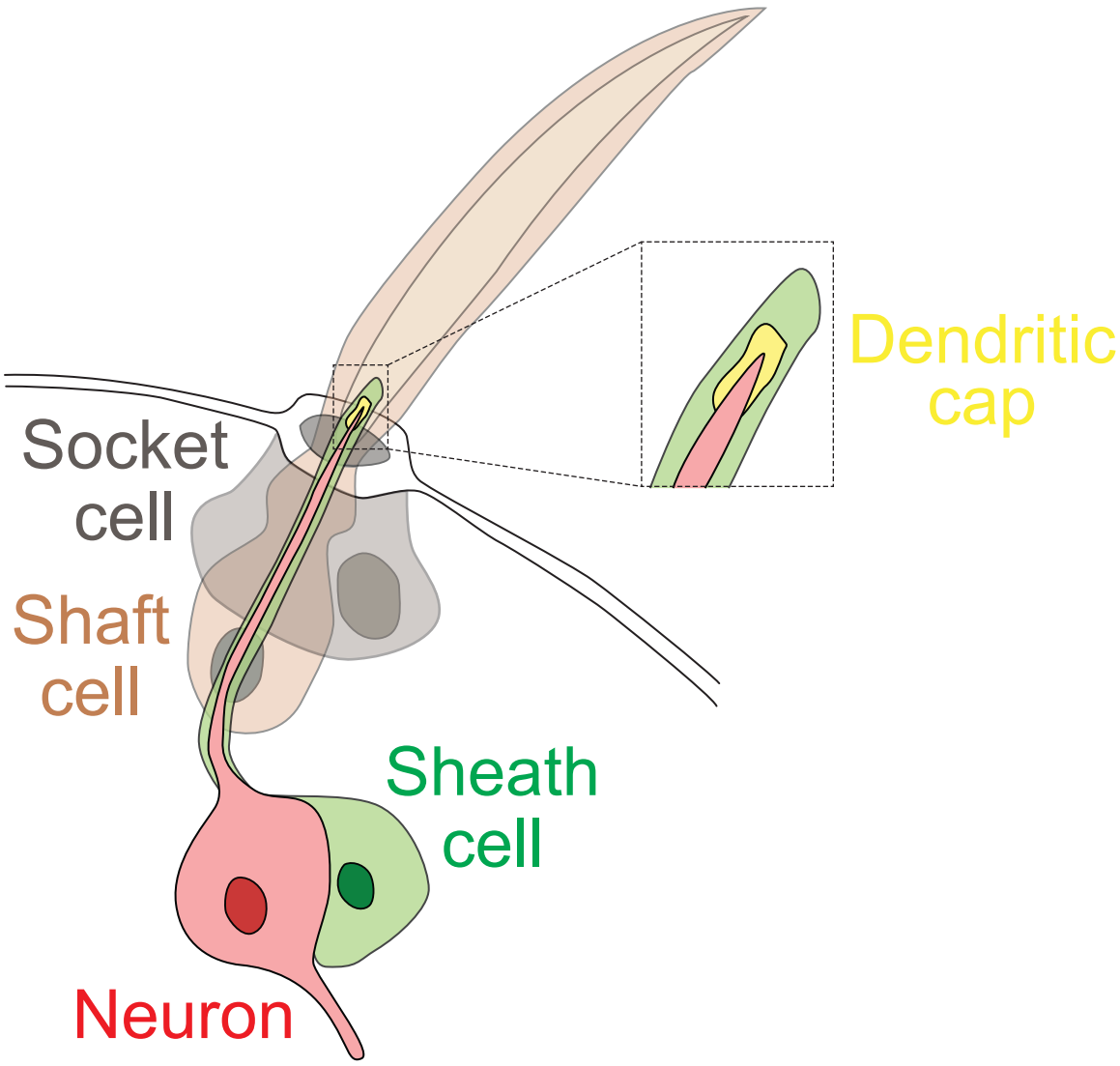

Figure 1.3. *Drosophila* mechanosensory organ. The single-dendrite sensory neuron (red) is ensheathed by three supporting cells: a glia-like sheath (green), socket (gray), and socket (gray). The sheath cell secretes the dendritic cap, a matrix-filled compartment (yellow) at the tip of the sensory neuron. Adapted from Fabre et al., 2008.

1.2.2.2 Olfactory sensory organ

The basic anatomy of the *Drosophila* mechanosensory organ is also found in the animal's other peripheral sensory organs. For example, the olfactory sensory organ also consists of the same four cell types: the sensory neuron and accessory (sheath, shaft, and socket) cells, though there can be multiple neurons in each organ (Shanbhag et al., 2000). Similarly, the sheath cell ensheaths the neuronal dendrite, and is in turn enveloped by the socket and shaft cells. However, the dendrite does not extend beyond the cuticle into the dendritic cap, but instead into a lymph-filled cavity within the socket and shaft cells.

Just as Notch signaling and the AS-C genes specify neural fate for the mechanosensory SOP cell (García-Bellido and de Celis, 2009), Notch signaling and *amos*, another bHLH transcription factor, regulate SOP selection of the olfactory sensory organ (Goulding et al., 2000). However, the olfactory SOP recruits other ectodermal cells to differentiate into the accessory cells, rather than dividing to give rise to them itself. Interestingly, the AS-C genes, *amos*, and *atonal*, another bHLH gene, can account for SOP specification of most of the *Drosophila* PNS, suggesting conservation of the mechanisms governing sensory organ development. Furthermore, these mechanisms are likely evolutionarily conserved, as *Drosophila atonal* is able to fully rescue the phenotype of mice null for *Math1*, the mouse homolog (Wang et al., 2002).

Despite the conservation of neural fate pathways among these different sensory structures and the extensive lineage studies, the regulation of subsequent

steps, specifically glial (e.g. sheath cell) morphogenesis, are still unclear. For example, in some vertebrate sensory structures, apical-basal polarity features prominently in glial morphogenesis (Copley et al., 2013), but its function in the mechanosensory and olfactory sensory organs in *Drosophila* is currently not apparent.

1.2.3 In *C. elegans*

The neuron-glia sensory structure is also conserved in *C. elegans*. Sensory organs like the amphid in the worm display an anatomic complexity similar to those in *Drosophila* (Ward et al., 1975). Amphid glia are also required for sensory function (Bacaj et al., 2008), a feature conserved from sensory organ glia in vertebrates and *Drosophila*. A significant advantage of the amphid is our greater understanding of the factors regulating glial morphogenesis in this sensory structure (see Section 1.2.3.3), which allows greater focus on the mechanisms and subcellular processes governing morphogenesis.

1.2.3.1 Amphid

The amphid is the primary chemosensory organ of the worm. Each *C. elegans* possesses bilaterally symmetric amphid sensory organs in the head. Each amphid is composed of 12 sensory neurons and two glial cells: a socket glial cell (AMso) and a sheath glial cell (AMsh) (Ward et al., 1975) (Figure 1.4A, B). The neuron cell bodies are located between the anterior and posterior bulbs of the pharynx. They extend ciliated dendrites anteriorly, with some passing through a matrix-filled tubular

channel (amphid channel) that opens to the environment, and axons posteriorly into the nerve ring (Perkins et al., 1986).

The AMso and AMsh cells also extend processes anteriorly to form the anterior and posterior sections, respectively, of a sensory compartment called the amphid channel. These discrete sections are joined by tight junctions to form a continuous tube. Similar junctions attach glia to sensory neuron dendrites, sealing the posterior portion of the channel to form an isolated compartment surrounding ciliary NREs (Figure 1.4C). The AMsh cell actively secretes matrix into this compartment (Fig 1.4C, yellow region). Interestingly, some matrix proteins are required for proper sensory function (Bacaj et al., 2008).

Eight of the twelve sensory neurons extend ciliated dendrites through the amphid channel (six neurons extend single cilia, and two extend double cilia) (Ward et al., 1975). Collectively, these neurons are required to sense osmolarity, dauer pheromone (which signals animals to arrest in dauer, an alternate developmental phase to tolerate environmental stress (see below)), and chemical and mechanical stimuli (Inglis et al., 2007). The remaining four neurons differ in cilia shape: three have winged cilia, and one has a single cilium surrounded by many microvilli. The winged cilia travel through the amphid channel and terminate within the AMsh cell. Likewise, the microvilli of the last neuron are embedded in the AMsh cell, but without any contact with the amphid channel. The wing neurons sense volatile odorants, while the neuron with microvilli senses temperature.

The amphid structure demonstrates the close association between the sensory neurons and AMsh and AMso cells, a relationship conserved in sensory structures in vertebrates and *Drosophila*. Moreover, the simplicity of this structure (only two glial cells) is a considerable boon. It allows us to interrogate individual functions of the AMsh and AMso glia, as well as their individual contributions to the amphid channel.

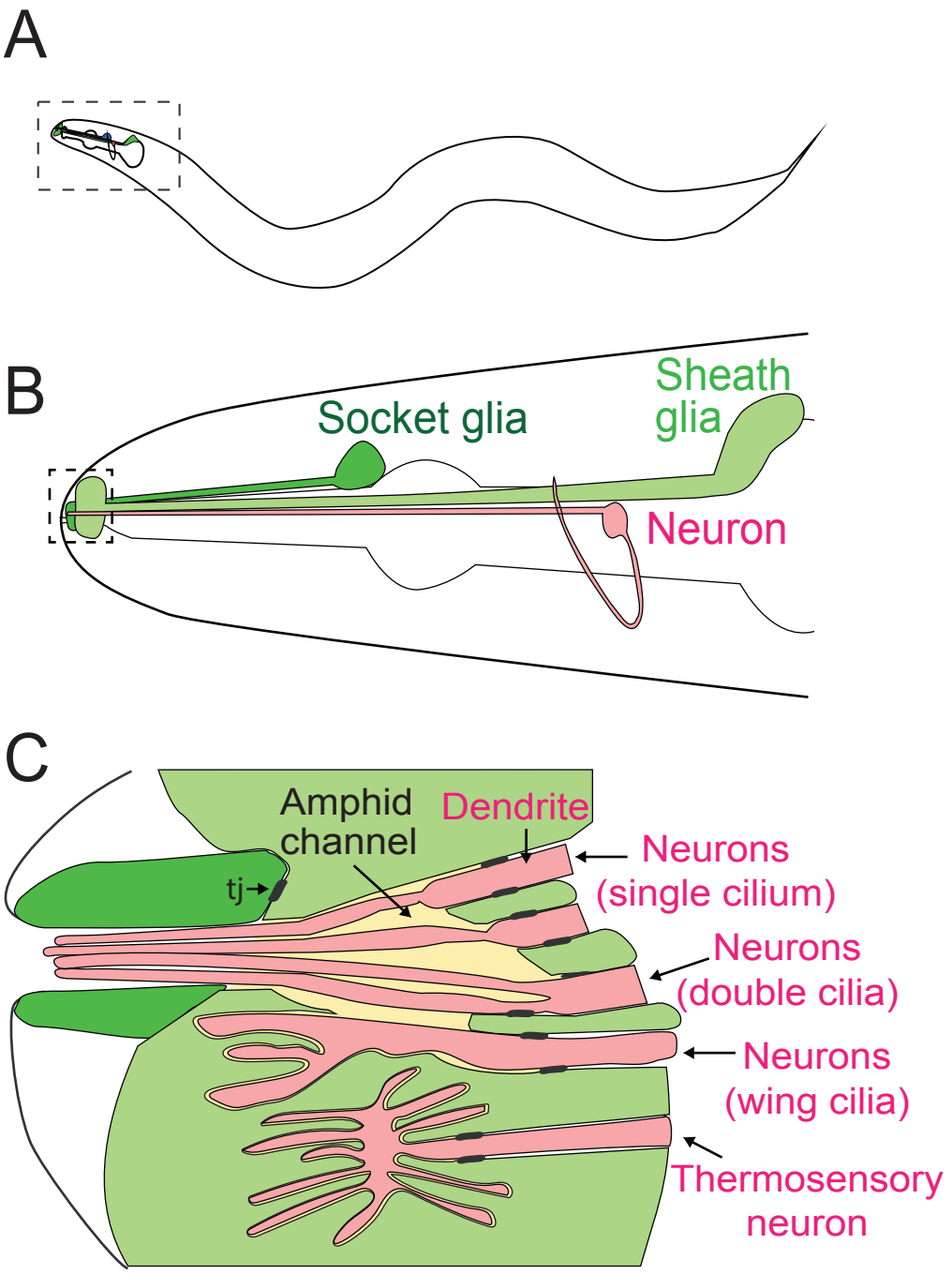

Figure 1.4. *C. elegans* amphid. (A) The amphid is the primary chemosensory organ found in the head. **(B)** Each of two bilaterally symmetric amphids consists of 12 amphid neurons (one shown in red) and the sheath (light green) and socket glia (dark green). **(C)** The amphid channel (yellow) is the sensory compartment formed by the sheath and socket glia. It is filled with matrix proteins secreted by the sheath glia. Tj, tight junctions. Adapted from Perkins et al., 1986.

1.2.3.2 Other sensilla

The neuron-glia anatomy of the amphid, specifically the sheath and socket glial compartment that isolates NREs, is also seen in these other *C. elegans* sensory structures: the cephalic sensilla, inner and outer labial sensilla, anterior and posterior deirids, and the phasmid. Furthermore, male animals have additional sensilla that help with mating: the hook, spicules, post-cloacal sensilla, and sensory rays (Sulston et al., 1980). These male sensilla also contain glial compartments. For example, in each sensory ray, two sensory neurons extend dendrites through a compartment formed by the structural glial cell (Oikonomou and Shaham, 2011). Generally, these structures consist of neuronal dendrites enclosed by a glial compartment, and thus roughly resemble the amphid. It also suggests that what we learn about amphid channel morphogenesis may be applicable to these other structures.

1.2.3.3 Amphid channel morphogenesis

1.2.3.3.1 DAF-6 restricts amphid channel expansion

Of these sensory organs, the *C. elegans* amphid has been one of the most studied in terms of morphogenesis. Amphid channel morphogenesis requires glial DAF-6, a Patched-related protein that restricts amphid channel expansion during development (Oikonomou et al., 2011; Perens and Shaham, 2005). *daf-6* (*daf*, dauer formation-defective) was first identified in a screen for mutants that failed to enter dauer, an alternate developmental state (Albert et al., 1981). Dauer entry is induced

by dauer pheromone released upon environmental stress, like crowding or starvation (Hu, 2007).

These dauer defects are likely due to amphid channel defects in *daf-6* mutants, based on several observations. First, the channel is severely bloated, thus occluding neuronal cilia from the environment, and full of matrix-filled vesicles (Figure 1.5, compare C and D to A and B) (Albert et al., 1981; Oikonomou et al., 2011; Perens and Shaham, 2005). Second, *daf-6* mutants are also defective in other sensory modes that require direct access to the environment, such as osmotic avoidance and chemosensation of water-soluble solutes (Albert et al., 1981; Perkins et al., 1986). Third, *daf-6* mutants fail to uptake lipophilic dyes, like diI, from the environment (Perkins et al., 1986). Wild-type animals can take up these dyes into a subset of amphid neurons. This uptake is blocked when sensory cilia are defective or cannot access the environment, as in the *daf-6* mutant.

These severe sensory defects highlight the importance of the amphid channel in sensory function, recalling the supportive functions of sensory organ glia in vertebrates and *Drosophila*. DAF-6 function in amphid channel expansion also hints at intriguing new mechanisms for glial morphogenesis in these other systems. For instance, as a Patched-related protein, DAF-6 implicates a role for membrane dynamics in amphid channel growth. This is further supported by known functions of other components that regulate amphid channel morphogenesis (see Sections 1.2.3.3.2-1.2.3.3.4).

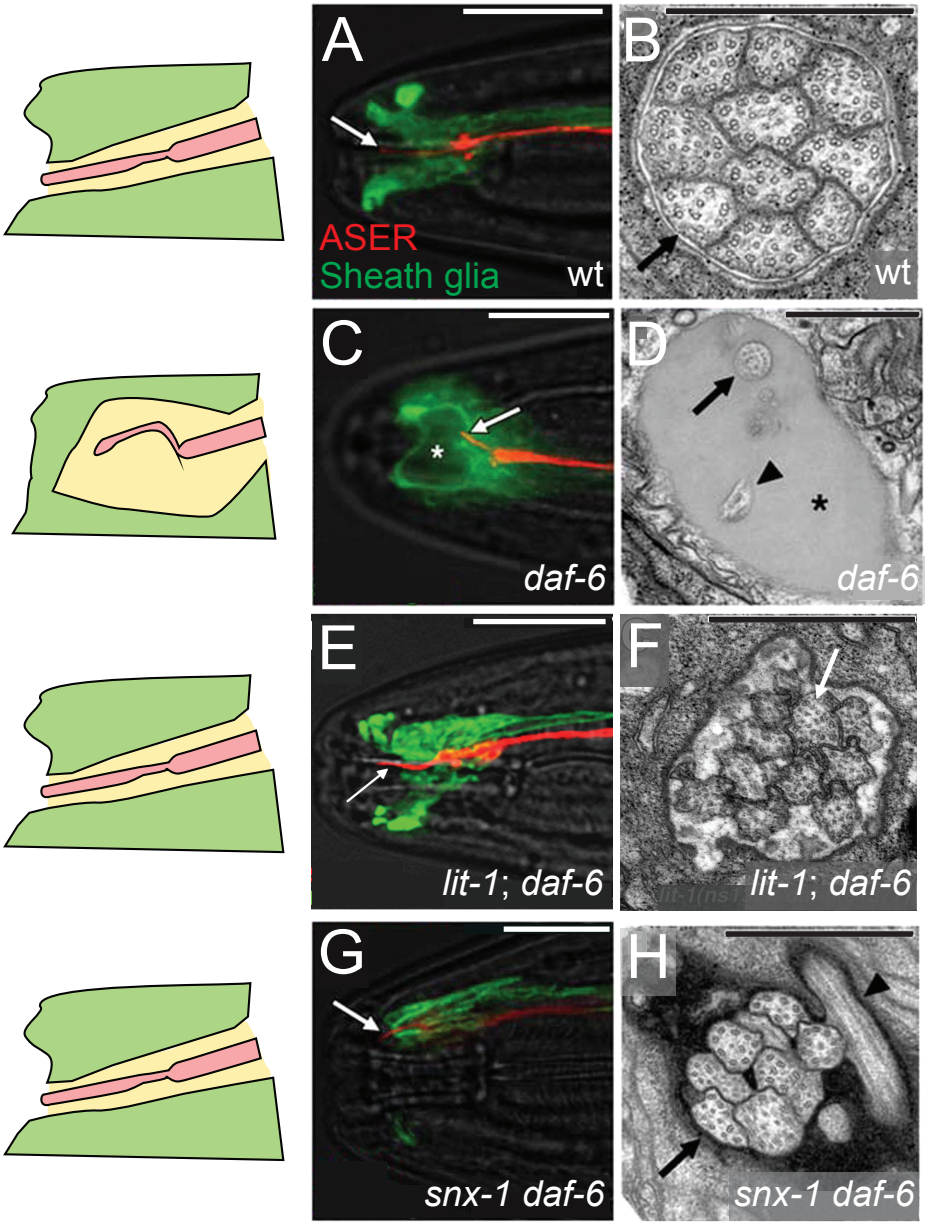

Figure 1.5. *daf-6* mutants show bloated amphid channels, which are suppressed by either *lit-1* or *snx-1* mutations. (A,C,E,G) The amphid channel (arrow) in **(A)** wild-type, **(C)** *daf-6*, **(E)** *lit-1*; *daf-6*, and **(G)** *snx-1 daf-6* adult animals. The ASER neuron is visualized with mCherry (red, driven by the *gcy-5* promoter) and the sheath glia with GFP (green, *T02B11.3* promoter). Left is anterior. The asterisk marks bloated amphid channel. Scale bar, 5 μm. Cartoons of the amphid channel are on the left (neuron in red, glia in green, channel in yellow). **(B, D, F, H)** Transmission electron micrographs of cross-sections through the amphid channel in **(B)** wild-type, **(D)** *daf-6*, **(F)** *lit-1*; *daf-6*, and **(H)** *snx-1 daf-6* adult animals. Arrows point to cilia, arrowheads to bent cilia, and the asterisk to the bloated amphid channel. Scale bar, 0.5 μm. Note the difference in scale between **(B, F, and H)** and **(D)**. Adapted from Oikonomou et al., 2012 and Oikonomou et al., 2011.

1.2.3.3.2 LIT-1 promotes amphid channel expansion

Bloated channels in *daf-6* mutants can be restored to their proper size by mutations in *lit-1* (Oikonomou et al., 2011), which encodes a Nemo-like kinase (Figure 1.5, compare E and F to C and D). This suggests that LIT-1 antagonizes DAF-6 and promotes amphid channel growth. Indeed, *lit-1* mutants alone exhibit abnormally constricted amphid channels.

LIT-1 was previously known to regulate Wnt signaling: the β-catenin WRM-1 activates LIT-1, to transduce anterior/posterior polarity signals in asymmetric cell divisions during embryogenesis (Rocheleau et al., 1999). However, the only other Wnt pathway component involved in amphid compartment morphogenesis is MOM-4, a LIT-1-activator kinase. Mutations in *mom-4* can suppress the dye-filling defects of the *daf-6* mutant (Oikonomou et al., 2011; Shin et al., 1999). This suggests a Wnt-independent role for LIT-1 in sensory compartment size control.

This novel role for LIT-1 is further supported by the following LIT-1 protein interactors. LIT-1 binds WSP-1, the *C. elegans* homolog of the Wiskott-Aldrich Syndrome Protein (WASP), which transduces signals from cell surface receptors to the actin network (Oikonomou et al., 2011). Like *lit-1* and *mom-4*, *wsp-1* mutations suppress the *daf-6* dye-filling phenotype. LIT-1 can also bind actin, which was also enriched along the amphid channel. These findings suggest a function for LIT-1 in regulating actin dynamics in amphid glial morphogenesis, possibly downstream of a cell surface receptor. DAF-6 could act as such a receptor, like Patched in Hedgehog

signaling. However, this remains to be determined, and how such a signal could be transduced to LIT-1 is unresolved.

1.2.3.3.3 SNX-1 promotes amphid channel expansion

Like *lit-1* mutations, mutations in *snx-1*, which encodes a retromer component, also suppress the *daf-6* amphid channel defects (Oikonomou et al., 2012) (Figure 1.5, compare G and H to C and D). The retromer complex is involved in recycling proteins from the endosome to the Golgi apparatus (Seaman, 2005). It consists of a cargo-selection module that recognizes cytoplasmic tails of endocytosed proteins, made of VPS26, VPS29, and VPS35, and a membrane-coating/bending subunit that promotes cargo vesicle budding from endosomes, made of sorting nexins SNX1/2 and SNX5/6 (Seaman, 2005). Besides SNX-1, two other retromer components, VPS-29 and SNX-3, were found to promote amphid compartment growth; *vps-29* and *snx-3* mutants each suppressed *daf-6* dye-filling defects (Oikonomou et al., 2012).

To test whether *snx-1* genetically interacts with *lit-1*, Oikonomou et al. generated *lit-1*; *snx-1 daf-6* triple mutants, and found a synergistic suppression of *daf-6* dye-filling defects, suggesting that *snx-1* and *lit-1* act in parallel pathways to promote amphid channel expansion.

Since these retromer components traditionally regulate vesicle trafficking, this pathway could conceivably regulate how membrane is delivered to the amphid channel. An alternative explanation is that they regulate internalization of a specific

cell surface protein to regulate its function at the cell surface, such as DAF-6 or other unidentified membrane proteins.

1.2.3.3.4 CHE-14, like DAF-6, regulates formation of tubular structures

Another regulator of amphid compartment morphogenesis is CHE-14, a Dispatched homolog, required for apical secretion from the AMsh glia. *che-14* mutants share *daf*-6 amphid channel defects, such as in dye-filling, osmotic avoidance, and dauer formation (Michaux et al., 2000). *che-14* mutants also accumulate matrix-containing vacuoles in AMsh cells (Perkins et al., 1986). Given these similarities, Perens et al. tested for genetic interactions between *che-14* and *daf-6* by generating *che-14*; *daf-6* double mutants. Interestingly, these mutants showed severe defects in tubular structures, such as the amphid channel and excretory canal (Perens and Shaham, 2005), suggesting a common morphogenetic mechanism for these tubular structures.

However, in contrast to their suppression of *daf-6* defects, *lit-1* and *snx-1* actually enhance *che-14* dye-filling defects. These results suggest *lit-1*, *snx-1*, and *che-14* each promote expansion of the amphid compartment (Figure 1.6). CHE-14's role in apical secretion adds a cell polarity aspect to our speculations about vesicle and protein trafficking pathways that may underlie amphid channel morphogenesis. For instance, if LIT-1 and SNX-1 do regulate trafficking of a membrane protein, CHE-14 may promote the final steps of secretion, and this protein may associate with the matrix.

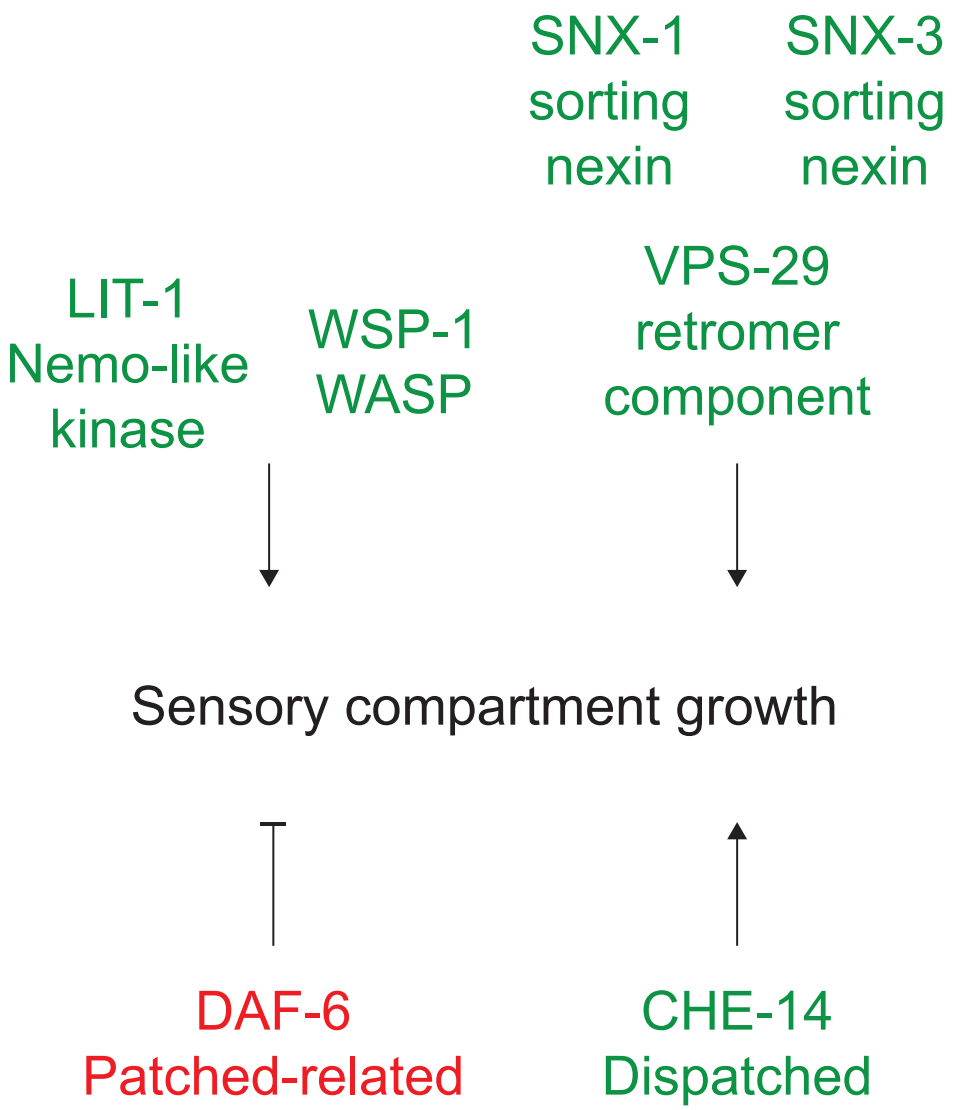

Figure 1.6. A model for sensory compartment morphogenesis in *C. elegans*. DAF-6 (red) restricts sensory compartment expansion, while all the other proteins listed promote expansion (green). Adapted from Oikonomou et al., 2012.

1.2.3.3.5 AMso cell development

Much of the work on amphid channel morphogenesis has focused on the AMsh glia. *daf-6* mutants showed vesicle accumulation primarily in the AMsh glia (Albert et al., 1981). Mosaic analysis also demonstrated *daf-6* functions in the AMsh glia for normal channel morphogenesis (i.e. dye-filling) (Herman, 1987).

However, the AMso glia may deserve more attention, since the *daf-6* suppressors, *lit-1* and *snx-1*, may function in both the AMsh and AMso glia ((Oikonomou et al., 2012; Oikonomou et al., 2011). Cell-specific rescue experiments for both *lit-1* and *snx-1* used a *lin-26* promoter fragment, expressed in both AMsh and AMso glia (Landmann et al., 2004), to drive expression of *lit-1* and *snx-1*.

AMso cell shape can affect the integrity of the amphid channel, as seen in the *alr-1* mutant (Tucker et al., 2005). *alr-1* encodes the ortholog of Aristaless, a paired class homeobox transcription factor in *Drosophila* (Galliot et al., 1999). *alr-1* mutants show progressive defects in dye-filling and chemotactic responses through larval development (Tucker et al., 2005). These defects are partially rescued with AMso cell-specific *alr-1* expression. Moreover, they correspond with morphological changes in the AMso cell during the larval-to-adult transition: the cell protrudes abnormal membrane extensions, and becomes detached from the cuticle and AMso cell. These finding thus highlight the importance of the AMso glia and proper cell attachments in regulating sensory function.

Interestingly, mutations in the human *aristaless*-related homeobox gene, ARX, have been linked to several X-linked neurodevelopmental disorders (Kato et al.,

2004; Stromme et al., 2002). ARX knockout mice resemble the disorder, X-linked lissencephaly with abnormal genitalia (XLAG), with defects in forebrain neuronal proliferation and migration (Kitamura et al., 2002). Given the *alr-1* AMso cell defects, the vertebrate phenotype may also arise from cell morphological and adhesion abnormalities.

These studies highlight the structural importance of the AMso cell, but there are some notable caveats. For example, AMso cell-specific expression for *alr-1* only partially rescued the *alr-1* defect, suggesting it may function from other cells as well, such as the neighboring AMsh cell. In fact, this situation resembles the multiple sensory organ glia present in vertebrate sensory structures. However, since the amphid only has the AMsh and AMso glia, it is likely easier to discriminate between the functions of the two cells, further underscoring the strengths of the amphid as a model sensory structure.

1.2.3.3.6 Neuronal regulation of amphid channel morphogenesis

Since the amphid channel tightly ensheaths neuronal cilia, it is possible neuronal signals play a role in regulating amphid channel morphogenesis. DAF-6, LIT-1, and SNX-1 proteins all function in amphid glia, and localize to the amphid channel surface (Oikonomou et al., 2012; Oikonomou et al., 2011; Perens and Shaham, 2005). However, in the *daf-19* cilia mutant (*daf-19* encodes a transcription factor required for sensory neuronal cilia formation (Swoboda et al., 2000)), DAF-6, LIT-1, and SNX-1 become mislocalized, concentrating instead at the AMsh-AMso cell junction (Oikonomou et al., 2012; Oikonomou et al., 2011; Perens and Shaham,

2005). This intriguing finding suggests that neuronal signals regulate localization of these amphid channel morphogenetic factors. The potential trafficking roles of LIT-1, WSP-1, and SNX-1, if verified, may occur downstream of any neuronal signals, if they exist.

1.2.3.3.7 Glial regulation of amphid neuron development

Conversely, AMsh glial studies have demonstrated a glial role in regulating neuronal cell shape and development. Notably, Singhvi et al. reported that AMsh glial protein KCC-3, a K/Cl transporter, regulates microvilli shape of the AFD thermosensory neuron (Singhvi et al., 2016). KCC-3 thus also controls the animal's thermosensory behavior. Specifically, KCC-3 regulates extracellular Cl^- concentrations (in the compartment between the AFD neuron and AMsh glia). Cl^- ions in turn inhibit the AFD-specific guanylyl cyclase, GCY-8, which synthesizes cyclic GMP (cGMP), and high cGMP levels antagonize WSP-1, thus limiting AFD NRE growth. Therefore, these findings provide a precedent for glia-to-neuron morphogenetic signaling. It is thus plausible that neuron-to-glia signaling also occurs, as in a neuronal ligand that regulates AMsh cell shape (see Section 1.2.3.3.7). Finally, this study further testifies to how *C. elegans* is a powerful system for studying individual glia-neuron interactions.

1.3 Sensory organ glia as models for CNS glia

Sensory organ glia share several features with glial cells that surround excitatory synapses in vertebrate nervous systems. Anatomically, the sensory organ glia surrounding sensory NREs (some of which are dendritic tips, like in the amphid)

resembles astrocytes and microglia that ensheath dendritic spines. Developmentally, glia in both systems can influence NRE shape. As mentioned above, in the *C. elegans* amphid, the AMsh glia regulates NRE shape of the AFD neuron, by way of KCC-3-enriched glial microdomains that surround the NREs (Singhvi et al., 2016). Similarly, in the mouse hippocampus, astrocytes regulate postsynaptic dendritic spine shape and retraction in pyramidal neurons (Murai et al., 2003). This is mediated through repulsion between the ephrin-A3 ligand, localized on the astrocytic processes that envelop dendritic spines, and the EphA4 receptor tyrosine kinase, enriched on the spines.

Both types of glia also provide trophic support for neurons, such as by maintaining extracellular ion and signaling molecule concentrations. In the amphid, as previously described, the AMsh glia regulates extracellular Cl^- concentration to control proper NRE morphogenesis (Singhvi et al., 2016). Astrocytes are similarly critical in maintaining extracellular K^+ concentrations in the extracellular space surrounding neurons (for more on this, see Sections 1.6.1.1 and 1.6.1.2 below). Changes in K^+ concentrations and volumes of extracellular spaces affect neuronal excitability, and have been implicated in the pathophysiology of seizures and epilepsy (Devinsky et al., 2013).

Another maintenance function for sensory organ and CNS glia is to engulf shed neuronal membranes. For instance, as mentioned above, retinal pigment epithelial cells ensheath and phagocytose outer segments shed by the photoreceptor cells (Bok, 1993). Likewise, in the *Drosophila* mushroom body, glia are required for

programmed axonal pruning during metamorphosis, specifically by engulfing axonal varicosities (Awasaki and Ito, 2004).

Furthermore, both types of glia exhibit complex intracellular calcium signaling in response to upstream stimuli. In the mouse olfactory epithelium, sustentacular cells can generate two types of calcium signals: intercellular calcium waves that propagate to neighboring cells (possibly through gap junctions) and intracellular calcium oscillations, downstream of G-protein-coupled muscarinic and purinergic receptor stimulation (Hegg et al., 2009). Similarly, vertebrate astrocytes show both calcium signals (Perea and Araque, 2005). The intracellular calcium signaling occurs downstream of metabotropic receptors, and provides a means of neuron-to-glia communication.

Finally, both sensory organ and CNS glia express common glial cell markers. For instance, Deiters' cells in the inner ear and astrocytes both express glial fibrillary acid protein (GFAP), an intermediate filament protein (Rio et al., 2002). This is also true of olfactory ensheathing cells associated with olfactory neurons in the olfactory bulb (Ramón-Cueto and Valverde, 1995), non-myelinating Schwann cells in the PNS, and glia in the enteric nervous system (Yang and Wang, 2015).

Therefore, understanding how sensory organ glia compartments arise and affect neuron receptive endings (NREs) may shed light on activities of their central nervous system (CNS) counterparts (Shaham, 2010). They also provide unique insights into how glial cells form. For instance, LIT-1 and SNX-1 have been identified

as regulators of amphid channel morphogenesis, but were not previously implicated in CNS glial development.

1.4 *C. elegans* as a model for glial compartment morphogenesis

Sensory organ glia are important in both how they form compartments that regulate sensory function and in their parallels to CNS glia. However, as summarized above, development of sensory organ glia is not well characterized in vertebrate systems, and glial cell complexity presents a significant obstacle to individual cell studies. An added challenge arises from the trophic role of glia in vertebrates and even *Drosophila*. In these organisms, glial ablation or removal leads to neuronal death, thus obscuring how glia regulate neuronal function (Ghosh et al., 2011; Ullian et al., 2001).

Fortunately, the nematode *C. elegans* provides a unique arena to study glial development and glia-neuron interactions, as developmental constraints allow neurons to survive even in the absence of glia (Bacaj et al., 2008). Glial loss or manipulation in this animal leads to profound sensory and synaptic deficits, as they do in other organisms (Bacaj et al., 2008; Colón-Ramos et al., 2007; Felton and Johnson, 2011; Singhvi et al., 2016; Wallace et al., 2016). Importantly, interactions between single glia and neurons can be interrogated at the level of neuronal activity and animal behavior (Oikonomou and Shaham, 2011). Thus, glial regulation of sensory function is well-conserved in *C. elegans*, and the simplicity of its sensory organ structures makes it a pliable system to uncover general mechanisms for glial morphogenesis.

1.5 Lumen formation

Sensory organ glia form specialized compartments to house NREs. Often, these compartments consist of a lumen in which the NREs reside. How does this lumen form? Some insight may come from studying the development of other luminal structures. For example, *daf-6* and *che-14* regulate the size and shape of not only the amphid channel, but also several other luminal structures, such as the excretory canal and vulval lumen (Michaux et al., 2000; Perens and Shaham, 2005). This implies a common developmental mechanism for these luminal structures.

Tubular structures consist of epithelial or endothelial cells that are either: 1) connected by seams (intercellular or autocellular junctions; this first category is the most common), 2) seamless and single (no junctions), or 3) a mixture of both (Iruela-Arispe and Beitel, 2013). These structures generally arise from one of the following five cellular mechanisms. First, "wrapping" entails a sheet of epithelial cells invaginating, with the edges meeting and sealing off a lumen. This occurs in neural tube formation (Lubarsky and Krasnow, 2003). Second, "budding" involves cells invaginating and extending orthogonally from an existing sheet or tube, creating a secondary tube with a lumen continuous from the original. This mechanism gives rise to structures like the mammalian lung and *Drosophila* tracheal system.

Third, "cavitation" starts with a cylinder of cells, from which the central cells are removed (e.g. by apoptosis), as in mouse salivary glands. Fourth, "cord hollowing" resembles cavitation, but without removing any cells (i.e. cell number

remains the same), as in the *C. elegans* gut (Leung et al., 1999) and Madin-Darby canine kidney (MDCK) cultured cells (Pollack et al., 1998). Fifth, "cell hollowing" involves the lumen forming within and spanning a single cell. This occurs in the *C. elegans* excretory canal cell (Buechner, 2002) and endothelial cells in vertebrate capillaries (Wolff and Bär, 1972). These latter three mechanisms can also apply to tubular structures of nonepithelial origin (e.g. endothelial cells).

Nevertheless, despite the anatomical and cellular diversity of these tubular structures, they share certain basic elements: establishment of apical-basal polarity, interplay between cell adhesion molecules (e.g. between cells, and cells and the ECM), and ultimately formation of a single lumen. These processes are also crucial for normal glial compartment formation. For example, apical-basal polarity is a known requirement for Deiters' cell organization and function.

Key apical polarity complexes are the Par complex (Par3, Par6, and atypical protein kinase C (aPKC)) and Crumbs complex (Crumbs, Stardust, and PATJ (PALS1 (protein-associated with Lin7, Stardust, MPP5)-associated tight junction protein)) (Suzuki et al., 1996). Briefly, the Par complex directs apical distribution of the Crumbs complex, while restricting a third complex, the Scribble polarity module (Scribble, Discs large, and Lethal giant larvae), to basolateral membranes (Bilder et al., 2003). The Scribble module conversely helps maintain apical localization of the Par complex (Hutterer et al., 2004). The Par complex also interacts with small GTPases like Rac1/Cdc42 to regulate cytoskeletal changes (Joberty et al., 2000), and Cdc42 is thought to transmit polarity cues to the Par complex (Etienne-Manneville

and Hall, 2001). It is unsurprising then that Cdc42 (see Section 1.2.1.2.) function is also critical for sensory organ glia like Deiters' cells, with a similar role in cell polarity.

The cell adhesion molecules, such as integrins, interact with these polarity complexes to establish cell polarity. For instance, loss of β1 integrin in the endothelium leads to loss of polarity and lumen occlusion (Zovein et al., 2010). The endothelial cells appear cuboidal (normally flattened), and cell-cell adhesion molecules (e.g. VE-cadherin) become mislocalized; these are normally distributed according to the apical-basal axis (Zovein et al., 2010). Moreover, the β1 integrin functions upstream of Par3, of the Par complex (Suzuki and Ohno, 2006). Cell adhesion also plays a prominent role in maintaining sensory compartments. For example, the amphid channel is continuous through adherens junctions between the AMso-AMsh glia, and this boundary is lost in *daf-6* mutants. Thus, several aspects of lumen formation overlap with sensory compartment development, and tubular structure studies may inform our current understanding of glial morphogenesis.

Below, I describe a few classic luminal structures and their development in more detail: vertebrate capillaries, MDCK cultured cells, the *C. elegans* excretory canal, and the *Drosophila* tracheal system. Each system highlights roles of vesicle trafficking and fusion and cell polarity, which may also figure into sensory compartment development.

1.5.1 Vertebrate capillaries

Capillaries are the smallest and most basic blood vessels and thus provide perspective into tubulogenesis at its simplest. They consist of tubes of endothelial cells, joined end to end by intercellular junctions. Capillary walls are only a single cell thick, hence allowing easy diffusion of oxygen, nutrients, etc. As mentioned previously, cell hollowing is a well-established mechanism for lumen formation in capillaries. Each cell generates vesicles that fuse into a large vacuole that is ultimately continuous with those of adjacent endothelial cells (Wolff and Bär, 1972). This intracellular vacuole may arise from pinocytic events (Davis and Camarillo, 1996) However, depending on the context, other mechanisms also underlie capillary growth, such as budding in angiogenic sprouting (Iruela-Arispe and Davis).

As described above, integrin signaling is a fundamental early step in lumen formation, with several purposes. First, integrin interacts with the ECM (such as with collagen and fibronectin), which can determine whether vessel formation occurs (Davis and Senger, 2005). Second, integrin signaling activates the Rho GTPases, Cdc42 and Rac1, to target vesicles to the intracellular vacuole compartment; dominant-negative mutants of Cdc42 and Rac1 inhibited formation of the vacuole, and thus the lumen (Bayless and Davis, 2002). Cdc42 is known to bind Par6 of the Par complex, and both are required for lumen formation. However, it is still unclear if the other polarity complexes (Crumbs and Scribble) are involved in angiogenesis. Third, integrin signaling activates the Src and FAK kinases to stabilize the tube structure (Eliceiri et al., 2002).

Much of the work on capillary formation has been done in 3D matrices of collagen or fibrin. In this environment, matrix metalloproteinases (MMPs) were also identified as key players of capillary development (Davis et al., 2007). One is the membrane-anchored MT1-MMP, which is necessary to create vascular guidance tunnels into which the nascent vessels can grow (Chun et al., 2004). Thus, capillaries highlight basic aspects of tubulogenesis: vesicle fusion, integrin signaling in cell polarity, and matrix involvement. These may also feature in lumen formation in sensory glia.

1.5.2 *C. elegans* excretory cell

Another simple tubular organ is the *C. elegans* excretory system, which includes three connected unicellular tubes: the canal, duct, and pore cells (Nelson et al., 1983). Similar to vertebrate capillaries, these tubes are only one cell thick. In fact, the excretory canal is made of a single excretory cell, an H-shaped cell that extends bilateral canals the entire length of the animal. This excretory cell connects to the duct cell, which in turn connects to the pore, which opens to the environment, thus allowing the animal to eliminate excess water and waste, and maintain its osmolarity. Interestingly, these three cells do not all form their respective lumens via the same mechanism; the excretory cell uses hollowing and the duct and pore cells use wrapping (Sundaram and Buechner, 2016).

As the largest cell that forms the excretory canal, the excretory cell has been well-studied in its development. The cell is born one-third of the way through embryogenesis and subsequently extends processes dorsolaterally (Sundaram and

Buechner, 2016). This canal extension requires some signaling mechanisms that also regulate neuronal process outgrowth. For example, the netrin, UNC-6, and its receptor, UNC-5, directionally guide both the excretory canal and axonal commissures (Hedgecock et al., 1990). Additionally, *pat-3* (paralysed arrest at two-fold) encodes β_1-integrin (Gettner et al., 1995), and the *pat-3* mutant exhibits both shortened neural tracts and excretory canals (Buechner, 2002).

As the excretory cell extends processes, vacuoles appear within the cell body that coalesce into a lumen with an apical surface (Buechner, 2002). The lumen is initially full of an electron-dense ECM, which disappears by the time of hatching. Several "Exc" lumen mutants have been identified, in which the lumen swells into fluid-filled cysts, though the range of lumen diameter changes varies by mutant. Some of these Exc mutants affect apical cytoskeletal proteins. One of these is SMA-1, a β_H-spectrin (McKeown et al., 1998). The excretory canal in the *sma-1* mutant swells during larval growth, ultimately into a single cyst in the adult. The apical terminal web is also detached from the luminal membrane, suggesting SMA-1 normally helps bind the two, as SMA-1 localizes to apical surfaces. Another is EXC-5, a GDP-GTP exchange factor that activates Cdc42 (its human homolog is FGD1 (Faciogenital dysplasia, Aarskog-Scott syndrome)) (Suzuki et al., 2001). *exc-5* mutants have large excretory cysts, but only the apical membranes are distended, suggesting EXC-5 and Rho GTPases may regulate the balance of apical-basal membrane growth. These cysts evoke an interesting comparison to the vacuoles in

the amphid channel in *daf-6* mutants, once again suggesting roles for the apical network and cell polarity in sensory compartment shape.

Besides these cytoskeletal components, other regulators of excretory canal lumen size have been identified such as *exc-4*, which encodes a chloride intracellular channel (CLIC) family member (Berry et al., 2003). *exc-4* mutants show large cysts near the excretory cell body. Interestingly, *exc-4* is also expressed in the phasmid and labial sheath glia, specifically at the distal tips of their processes that envelop neuronal dendrites. These findings suggest that *exc-4* may regulate luminal osmolarity across several structures, including the amphid compartment.

1.5.3 Madin-Darby canine kidney (MDCK) cells

MDCK cells were derived from a cocker spaniel's kidney tissue and have subsequently served as a good *in vitro* model for tubulogenesis. They can form different 3D structures depending on their cell culture substrate. On a thin layer of collagen, they form a monolayer that has allowed for apical-basal polarity studies (Montesano et al., 1991). When suspended in a 3D collagen matrix, they instead form spherical cysts. Furthermore, if hepatocyte growth factor (HGF) is added to the collagen matrix, MDCK cells extend branching tubules.

To form these tubules, the MDCK cells undergo a series of structural changes that highlight the importance of apical polarity in tubulogenesis (Pollack et al., 1998). First, single cells form extensions from the cyst. Second, a chain several cells long but a single cell thick extends off the main sphere. In leaving behind their contacts with the cyst (or lumen), they lose apical-basal polarity. Polarity markers

become redistributed; E-cadherin, a basolateral marker, now becomes uniformly distributed, and gp135, an apical marker, disappears from the cells in the chain. Third, the chain thickens to a diameter of 2-3 cells. At this point, gp135 is expressed again, but only at sites of cell-cell contact, where the future lumen will form. E-cadherin still remains uniformly expressed. Fourth, the cords mature into tubules, with the appearance of discontinuous lumens. Eventually these lumens fuse with each other and with the lumen of the cyst. gp135 localizes to luminal surfaces and E-cadherin redistributes to basolateral surfaces in the tubules.

Work in MDCK cells has also shed light on the vacuole machinery that drives lumen formation. When dissociated to single cells, MDCK cells form an intracellular vacuolar apical compartment (VAC) with microvilli (Vega-Salas et al., 1987). The VAC selectively accumulates apically targeted membrane proteins. This targeting may involve the exocyst machinery, which also redistributes during tubulogenesis (Lipschutz et al., 2000). Moreover, overexpression of Sec10, the exocyst subunit that binds to vesicles for docking, stimulated cyst and tubule formation (Lipschutz et al., 2000), and synthesis of basolateral and secretory proteins (Lipschutz et al., 2003).

VAC formation also depends on Cdc42 activity, as depletion of Cdc42 inhibits fusion of VACs into a lumen (Martin-Belmonte et al., 2007). Cdc42 helps establish polarity by binding and localizing the Par complex to the apical membrane. Cdc42 also interacts with the exocyst complex and may thus coordinate vesicle docking (Zhang et al., 2001). This finding suggests that vesicle docking is a tightly regulated

step in establishing polarity in the lumen, and thus worth exploring in the context of sensory compartment morphogenesis.

1.5.4 *Drosophila* tracheal system

The *Drosophila* tracheal system consists of a network of branched tubules, starting with the trachea, which takes in air from the environment through openings called spiracles (Krasnow and Manning, 1993). This air passes through progressively branched tubules to reach tracheal termini for gas exchange. These tubules originate as tracheal placodes, made of epithelial cells, invaginate into the body cavity and undergo stereotyped budding to form branches.

Detailed studies of how the multicellular branches formed have underlined the role for cell intercalation. By following single cells during tubulogenesis, Ribeiro et al. found that a majority of branches form through a cell intercalation process that starts with two cells level at the bud axis and ends with two cells joined end to end along the bud axis. This entails converting intercellular adherens junctions (AJs) into autocellular AJs (made of E-cadherin complexes), as each cell forms its own lumen (Ribeiro et al., 2004). One regulator of cell intercalation is Spalt (Sal), a zinc-finger protein and Wnt-activated gene. Sal expression inhibits formation of autocellular AJs, which is in turn suppressed by Decapentaplegic (Dpp) signaling (Ribeiro et al., 2004).

The apical ECM is also an important feature of tracheal system development. As the tracheal branches expand and lengthen, their lumen is transiently filled with a matrix of chitin and zona pellucida (ZP) domain proteins (i.e. Piopio and Dumpy)

(Tonning et al., 2005). Notably, this recalls the development the *C. elegans* excretory cell, which also features a temporarily ECM-filled lumen. In the tracheal system, these matrix proteins are secreted into the luminal space to inflate the lumen and regulate its diameter (Tsarouhas et al., 2007). This secretion requires Sar1 (secretion-associated Ras-related protein), a small Ras-like GTPase that regulates COPII vesicle formation and trafficking from the endoplasmic reticulum (ER) to the Golgi apparatus (Sato and Nakano, 2007). Loss of the matrix, such as of chitin, leads to formation of cysts and lumen constrictions, suggesting the apical ECM is important for proper cytoskeletal rearrangements.

When the branches have terminated growth, the luminal ECM is cleared and replaced with gas (Tsarouhas et al., 2007). This clearing process is mediated by endocytic pathways involving Rab5.

The ECM further plays a role in determining tracheal tube length, specifically through interactions with the apical membrane of the lumen. These three types of proteins restrict tube elongation. First, there are ECM proteins: Serpentine and Vermiform encode matrix proteins with chitin-binding and deacetylase domains, which are secreted into the lumen and required for normal chitin structure (Luschnig et al., 2006). This secretion is regulated in part by septate junction proteins (Wang et al., 2006). Second, apical membrane proteins regulate tubule length, including the Crumbs transmembrane protein. Third, there are proteins connecting the ECM to the apical membrane, such as the ER protein O-linked N-acetylglucosamine transferase (Dong et al., 2014). It would be interesting to probe

whether similar connections between the apical membranes of sensory compartments and the ECM also regulate lumen dimensions.

Tracheal tube diameter is regulated by actin rings, so proteins that regulate formation of these actin rings in turn affect tube diameter (Hayashi and Dong, 2017). For instance, the formin DAAM (Dishevelled-associated activator of morphogenesis) is required to organize these actin rings, and *daam* mutants lack organized actin rings (shorter, improperly cross-linked actin bundles) (Matusek et al., 2006). These mutants thus show collapsed trachea and lack the cuticle normally secreted onto the lumen's apical surface.

The tracheal system, due to the extent of its branching, requires a mechanism to connect the various lumens, or form anastomoses, which was previously uncharacterized. Recently, Caviglia et al. found that secretory lysosome-related organelles are involved in lumen fusion in the fusion tip cells that guide branch migration. These vesicles carry the calcium-binding protein Unc-13-4/Staccato (Stac), which is specific to these tip cells, and the Rab39 GTPase (a late endosomal marker) (Caviglia et al., 2016). Another GTPase, Arl13, is also exclusively expressed in these cells, and is necessary and sufficient for Stac localization to these vesicles. Importantly, Arl13 promotes fusion of the Stac vesicles to apical membranes, thus forming a transcellular lumen, and fusion events correlate with increases in local calcium concentrations. These findings thus identify new roles for calcium signaling and apical vesicle trafficking in lumen formation between neighboring cells. The integrity of intercellular boundaries is also important in sensory compartment

formation, such as between the AMsh and AMso cells of the amphid channel, and principles governing lumen continuity may also hold for glial compartments.

1.5.5 Immunoglobulin (Ig) superfamily (IgSF) members in development of tubular structures

A subset of nervous system tubular structures, such as the neural tube, involves the functions of certain Ig SF member proteins. This superfamily comprises large secreted or cell-surface glycoproteins with at least one Ig domain (Zinn and Özkan, 2017). Members of the the Ig cell adhesion molecules (IgCAM) subfamily typically have extracellular several Ig and fibronectin type III (FNIII) domains. Both domains feature a β-sandwich, made of two opposing antiparallel β-sheets, that allow binding to several other protein domains. IgCAM proteins are hence found in homophilic or heterophilic interactions amongst ECM components and cell surface proteins. Accordingly, IgCAMs mediate neuron-neuron and neuron-glia interactions, and thus play an important role in neurodevelopment (Sytnyk et al., 2017).

The IgSF consists of a wide range of proteins. In humans, there are approximately 500 protein members (excluding antibodies and T cell receptors) (Zinn and Özkan, 2017). In *Drosophila*, there are about 130 proteins (Zinn and Özkan, 2017), and in *C. elegans*, more than 60 proteins (Teichmann and Chothia, 2000). Below, I provide a brief overview of a selection of IgSF and IgCAM proteins that regulate the development of nervous system tube structures (Figure 1.7). In each case, the IgSF proteins interact with other proteins (e.g. ligands, other receptors, matrix proteins) to carry out their functions, in some cases to establish

cell polarity. It is thus worth considering how surface protein interactions may similarly shape the sensory compartment.

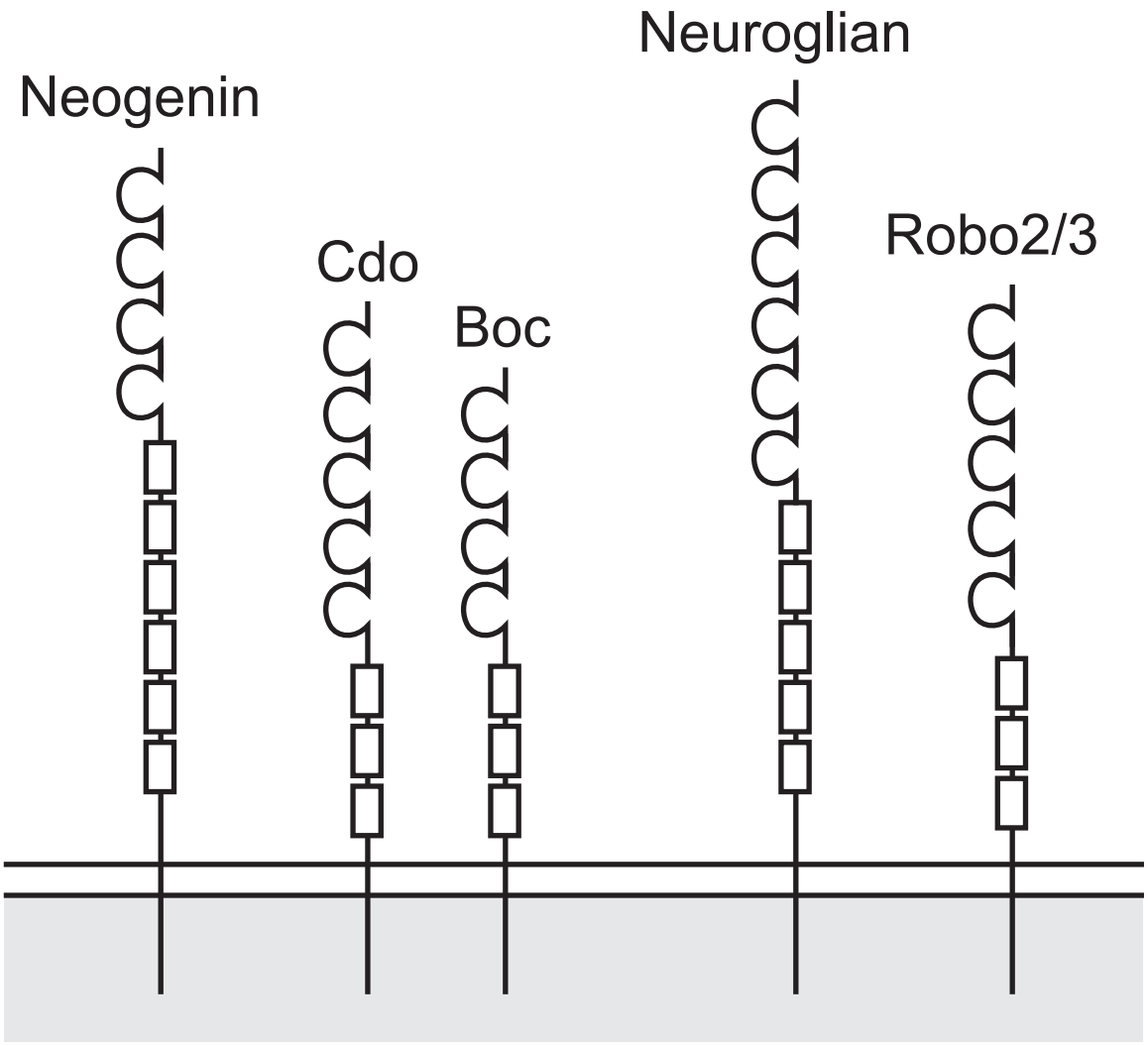

Figure 1.7. Schematic of Ig/FNIII proteins involved in tissue morphogenesis. Ig domains are represented by the C-shaped loops, and FNIII domains by rectangles. Neogenin is a netrin receptor (Wilson and Key, 2007), Cdo and Boc are Hedgehog co-receptors (Allen et al., 2011), Neuroglian is the *Drosophila* homolog of the L1 IgCAM (Sytnyk et al., 2017), and Robo2/3 are two of four Robo receptors for the Slit ligand (Blockus and Chédotal, 2016).

1.5.5.1 Neogenin in the zebrafish neural tube lumen

Neogenin is a single-pass transmembrane receptor with four extracellular Ig and six FNIII domains (Wilson and Key, 2007). Neogenin has a vertebrate homolog, deleted in colorectal cancer (DCC), which are both homologs of UNC-40 in *C. elegans* and frazzled in *Drosophila*. Both Neogenin and DCC are receptors for the axon guidance molecule, netrin, and the repulsive guidance molecule (RGM), a glycosylphosphatidylinositol (GPI)-linked glycoprotein. Netrin-neogenin interactions are involved in many developmental processes, such as mammary gland development (Srinivasan et al., 2003) and vascular smooth muscle cell migration during angiogenesis (Kang et al., 2004). Both of these processes have required cell adhesive properties of the netrin-neogenin interaction, rather than the traditional attraction/repulsion role required in axon guidance (Wilson and Key, 2006).

More recent work has uncovered a role for neogenin in neural tube formation, specifically in regulating cell adhesion and polarity. This began with the discovery that in zebrafish, neogenin is required for neural rod cavitation; subsequently, neogenin knockdown embryos lacked a neural tube lumen (Mawdsley et al., 2004). This was likely due to widespread neuronal cell death in the developing brain. These embryos also developed thinner and wider somites with less polarized epithelial boundary cells, the first hint that Neogenin helps establish cell polarity.

Subsequently, Neogenin interactions with netrin and RGMa (one of three mouse RGM proteins) have been implicated in neural tube closure in *Xenopus*.

Morpholino knockdowns of Neogenin and RGMa disrupt neural tube closure. This resulted from a loss of apical-basal polarity in the neuroepithelium and subsequent cell detachment, both during neural tube formation and after neural tube closure (Kee et al., 2008). Similarly, morpholino knockdown of *Xenopus* netrin-1 also delays neural tube closure, but through a different mechanism: defective migration of neuroectodermal cells to the midline (Kee et al., 2013).

The mechanism of Neogenin function appears related to actin machinery. Neogenin was most recently identified as a key component of the actin nucleation machinery that stabilizes adherens junctions (Lee et al., 2016). Neogenin interacts directly with the WAVE regulatory complex (WRC) through a WRC-interacting receptor sequence (WIRS) (Lee et al., 2016). This binding then recruits the WRC and Arp2/3 to adherens junctions (Lee et al., 2016). Neogenin also maintains stability of adherens junctions by regulating E-cadherin recycling (Lee et al., 2016). Neogenin-RGMa similarly maintain adherens junctions and cell polarity in a 3D cyst morphogenesis *in vitro* culture system (Srinivasan et al., 2003). However, it remains to be seen how Neogenin interactions with RGMa and/or netrin relate to these WRC interactions. Nevertheless, these findings present a novel interaction between an Ig/FNII protein and an actin regulatory complex (Lee et al., 2016). It is also worth exploring whether Ig/FNIII protein interactions play any role in sensory compartment morphogenesis.

1.5.5.2 Cdo and Boc in neural tube patterning

Note: Unlike Neogenin, Cdo and Boc do not regulate physical aspects of neural tube formation (e.g. neural tube folding or lumen formation), but do regulate cell patterning in the neural tube. Their interactions with Patched (see below) provide some context for the Discussion (Section 5.3), and are thus briefly described in this neural tube section.

CAM-related/downregulated by oncogenes (Cdo) and brother of Cdo (Boc) are single-pass transmembrane proteins in the vertebrate IgSF family (*Drosophila* orthologs: Interference Hedgehog (Ihog) and Brother of Ihog (Boi), respectively). They possess multiple Ig and FNIII repeats (Briscoe and Thérond, 2013). Along with growth arrest-specific 1 (Gas1) (a vertebrate-specific protein), they belong to a group of Sonic Hedgehog (Shh) co-receptors. These co-receptors form separate complexes with the canonical Hedgehog receptor, Patched (Ptc), a twelve-pass transmembrane protein (Briscoe and Thérond, 2013).

Hedgehog (Hh) signaling is essential for patterning of embryonic tissues in invertebrates and vertebrates (McMahon et al., 2003). In mammals, this includes patterning of the ventral neural tube, which ultimately gives rise to V3, V2, and V1 interneurons, as well as motor neurons. Because of its prominent developmental role, dysfunctional Hh signaling leads to congenital syndromes, like holoprosencephaly, or cancers, like medulloblastoma (Briscoe and Thérond, 2013).

The Hh signaling pathway was first identified by genetic analysis in *Drosophila* (Briscoe and Thérond, 2013). Briefly, Hh binds to Ptc, which releases

suppression of the G protein-coupled receptor (GPCR), Smoothened (Smo) (Briscoe and Thérond, 2013). This leads to activation of the Gli zinc-finger transcription factors (or Ci in *Drosophila*), which can activate or inhibit transcription of Hh target genes (Briscoe and Thérond, 2013).

Subsequent work has shown that the Hh co-receptors, Cdo, Boc, and Gas1, also transduce the Hh signal, together with Ptc. Removing individual co-receptors has little effect on Shh-dependent neural patterning, but removing any two leads to a severe patterning defects (e.g. markedly fewer interneuron and motor neuron progenitors) (Allen et al., 2011). Removing all three co-receptors leads to almost complete loss of Hh signaling, such as a complete lack of ventral neural tube patterning (phenocopying *Shh*$^{-/-}$ mutants), and early embryonic lethality. This combinatorial analysis demonstrates the partially overlapping functions of Cdo, Boc, and Gas1.

Similarly, in *Drosophila*, Ihog and Boi are essential for Hh signaling. Cells in the developing eye and wing disc lacking both genes showed an absence of Hh signaling (Camp et al., 2010). Cells lacking both *Ihog* and *Boi* also lack Ptc expression (one of the Hh transcriptional targets) (Zheng et al., 2010). Furthermore, *ihog*; *boi* double mutant larvae die shortly after hatching, but single mutants are viable, further confirming the redundant functions of the Hh co-receptors (Camp et al., 2010).

Structure-function analysis demonstrated that Ihog interacts with Hedgehog *in vitro* (Yao et al., 2006) and with Patched through its first and second FNIII

domains (Zheng et al., 2010), respectively (Ihog has four Ig domains and two FNIII domains). Moreover, both FNIII domains are required for Ihog to form a complex with Ptc and Hh and to properly transduce the Hh signal. These findings thus link specific physical interactions with Hh (co)receptor function. The overlapping functions of these coreceptors also demonstrate how Ig/FNIII proteins and Ptc can be more finely regulated from within a complex. Notably, DAF-6 is a Ptc-related protein, and these interactions hint at the possibility of DAF-6 regulation by other membrane proteins. However, unlike *Drosophila* and vertebrates, *C. elegans* lacks several key components of the Hedgehog pathway, including Hh and Smo, and instead has several Hh-related and Ptc-related genes (Bürglin and Kuwabara, 2006).

1.5.5.3 Neuroglian in the *Drosophila* antennal lobe glial canals

Neuroglian is the *Drosophila* homolog of the L1 IgCAM, which functions in neurodevelopment, ranging from axon guidance to synapse formation (Sytnyk et al., 2017). Neuroglian and L1 both have six Ig domains and five FNIII repeats. Like L1, Neuroglian has several protein isoforms and depending on the isoform is expressed in cells besides neurons, including glia and muscle cells (Hortsch et al., 1990).

Neuroglian's glial function has recently been uncovered in the development of the *Drosophila* antennal lobe, the neuropil structure that shares similarities with the vertebrate olfactory bulb. A distinct population of glia, the Transient-Interhemispheric-Fibrous-Ring (TIFR) glia, are transiently associated with but required for the developing antennal lobe commissural bundle during metamorphosis (Chen and Hing, 2008). Neuroglian functions specifically in the TIFR

glia for olfactory receptor neurons (ORNs) to project axons across the midline of the brain. Without these glia, the antennal lobes become disconnected and displaced.

Neuroglian is required for TIFR glial morphogenesis, as loss of *Nrg* leads to misshapen TIFR glia and, subsequently, agenesis of the antennal lobe commissure (Chen and Hing, 2008). Notably, the TIFR normally have four canal structures (ORN axons are ensheathed by one of these canals). Strikingly, in a *Neuroglian* mutant, these canals are missing. Moreover, Neuroglian requires its intracellular ankyrin-binding motif for its glial functions, suggesting that its cell adhesion properties may regulate morphogenesis of these glial tube structures.

Although the role for Neuroglian in cell adhesion is poorly characterized compared to Neogenin in actin nucleation, this finding is notable in its specific regulation of glial morphogenesis. It thus hints at potential Ig/FNIII protein functions in glial compartment and lumen formation.

1.5.5.4 Robo receptors in astrocytic tunnels

Roundabout (Robo) receptors are single-pass transmembrane IgSF receptors for the large secreted Slit proteins (Blockus and Chédotal, 2016). In vertebrates there are three Slit proteins (Slit1-3) and four Robo receptors (Robo1-4). There is one Robo ortholog in *C. elegans*, SAX-3, and three in *Drosophila*. Except for Robo4, the Robo receptors have five extracellular Ig and three FNIII domains (Kidd et al., 1999; Zallen et al., 1998).

Slit-Robo signaling is traditionally known to mediate axon repulsion to regulate midline crossing (Kidd et al., 1999; Zallen et al., 1998), but more recently,

studies have uncovered roles in other developmental processes, such as neurogenesis and angiogenesis (Blockus and Chédotal, 2016).

Notably, Slit-Robo signaling is required for forming and maintaining astrocytic tunnels, or tubes, that lead from the subventricular zone to the olfactory bulb in adult mammals (Kaneko et al., 2010). Young neurons travel in chains along this path, called the rostral migratory stream (RMS), and via the astrocytic tunnels. Defects in the astrocytic tunnel subsequently disrupt neuronal chain migration. These astrocytes express Robo2 and Robo3, which respond to Slit1 secreted by the migrating neurons (which also express Robo2 and Robo3, but at a lower level). Removal of Slit1 led to disorganized astrocytic tunnels, in which their processes invaded the neuronal chains. This may be due to a failure in Slit1-Robo signaling, so that astrocytes fail to change cell shape to properly appose membranes of nearby neurons. If so, this finding presents a new mechanism of glial cell morphogenesis: cell repulsion. Given the similarities previously noted between astrocytes and sensory organ glia, *trans* membrane protein interactions may also regulate the sensory compartment.

This function in tube formation is not unprecedented for Slit-Robo signaling, as it also regulates branching morphogenesis in the mammary gland (Macias et al., 2011) and cardiac tube lumen formation in *Drosophila* (Medioni et al., 2008; Santiago-Martinez et al., 2008). In the latter case, Slit-Robo signaling specifies subcellular luminal (membrane that forms lumen) and adherent domains (membrane that forms adherens junctions that fuse the cell) in bilateral rows of

cardioblasts, which fuse to form the cardiac tube (Medioni et al., 2008). The cardiac tube lumen differs from traditional epithelial tube formation in that the luminal side expresses basal components, and lacks the typical apical markers and vesicle fusion that usually contribute to the lumen. Therefore, Slit-Robo signaling may function via alternative lumen morphogenesis pathways in cardiac tube formation, and possibly even in astrocytic tunnel development.

1.6 Ion channels in glia

Note: The following section summarizes select functions of ion channels in glia and other cells (muscle cells in Sections 1.6.1.3 and 1.6.2.3.1). Although the relevance of ion channels to Ig/FNIII protein function is not immediately apparent based on the background information detailed above, my thesis work uncovers a relationship between the two protein types. This summary will thus provide a context for my findings described in Chapter 2.

Ion channels are membrane proteins that allow ions to pass through a pore(s) (Alberts et al., 2002). In regulating ion flow, they regulate a wide range of cellular properties, including resting membrane potentials, action potentials, and cell volume (Alberts et al., 2002). One way of classifying ion channels is by ion type; some common ions are K^+, Na^+, Cl^-, Ca^{2+}, and H^+ (Sulston et al., 1980). Another method of classification is by gating mechanism; prominent classes are voltage-gated, ligand-gated, and second messenger-gated (e.g. ATP) (Alberts et al., 2002). Glial cells express a variety of these ion channels and transporters, not only to regulate the extracellular ion environment for neurons, but also for signaling to neurons, and

even for morphogenesis and differentiation (Verkhratsky and Steinhäuser, 2000). Below, I describe some glia-specific functions of K^+ and ligand-gated ion channels (LGICs).

1.6.1 K^+ channels in glia

K^+ channels are the most studied and most abundant ion channels in glia (Verkhratsky and Steinhäuser, 2000). K^+ flow also dominates glial conductance, and thus largely determines their resting membrane potential (Olsen et al., 2015).

1.6.2 Regulation of extracellular K^+ concentrations

Early glial studies established a role in regulating extracellular K^+ levels, which elevate upon neural activity. This occurs in two steps: K^+ uptake and K^+ spatial buffering. K^+ uptake occurs through K^+ channels, as well as the Na^+/K^+-ATPase and NKCC (Na^+-K^+-$2Cl^-$) cotransporters (Leiserson and Keshishian, 2011). The K^+ channels are predominantly inwardly rectifying K^+ channels (K_{ir}s), which are enriched at distal ends of astrocytic processes (Verkhratsky and Steinhäuser, 2000). The K_{ir}s "siphon" K^+ ions from regions of high K^+ and transfer them to regions with low K^+. This K^+ redistribution by glia can occur within a single cell or among several cells in a glial syncytium; this constitutes K^+ spatial buffering.

There is an interesting correlation between glial cell maturity and K^+ buffering capacity, as fluctuations in extracellular K^+ diminish in nenonatal rat spinal cords as they age (Jendelová and Syková, 1991), and young animals express very low levels of K_{ir}s until P7 (Bringmann et al., 1999). Additionally, glial K_{ir} currents diminish after injury and in some CNS diseases, suggesting a change in the

extracellular K^+ environment (Verkhratsky and Steinhäuser, 2000). An important function of glia is thus to maintain extracellular ion concentrations. This role was also seen previously in the AMsh cell, which regulates extracellular Cl^- to signal to the AFD neuron (Singhvi et al., 2016), suggesting several ions may be relevant in glial compartments.

1.6.3 K^+ concentrations in extracellular space regulation

An additional consequence of K^+ flux into glia is an increase in glial cell volume, due to the osmotic force of the K^+ ions; subsequently, the extracellular space decreases (Leiserson and Keshishian, 2011). The NKCC1 cotransporter mediates this swelling in astrocytes, as inhibition of the cotransporter reduces the extent of swelling (MacVicar et al., 2002). As previously mentioned, since extracellular K^+ levels increase from neural activity, it follows that the extracellular volume would increase as a result (Svoboda and Sykova, 1991). Conversely, changes in extracellular space can alter neuronal excitability, by changing the local K^+ concentration (Devinsky et al., 2013). A decrease in extracellular space (and thus increase in neuronal and glial cell volume) increases neuronal excitability. This has pathologic implications, as greater neuronal excitability can lead to seizures. This phenomenon also has therapeutic applictions: the diuretic, furosemide, blocks the NKCC co-transporter and, because of its action in glia, has antiepileptic effects (Hochman, 2012). On the same principle, glial aquaporin-4 (AQP4), a water channel, is also implicated in epilepsy, and mice lacking AQP4 have altered seizure susceptibility (Binder et al., 2012).

1.6.4 Cdo and Kir2.1 in myoblast differentiation

Note: This section addresses K_{ir} function in myoblast differentiation, not glia. However, it provides a precedent and some context for a protein interaction postulated in the Discussion in Section 5.4.

Kir2.1 is a classical K_{ir} channel. Like other K_{ir}s, it consists of two membrane-spanning domains linked by a pore-forming region, with cytoplasmic N- and C-termini (Hibino et al., 2010). Kir2.1 is a well-known myoblast differentiation factor in skeletal muscle. Myoblasts express Kir2.1 to drive hyperpolarization, this allows Ca^{2+} to enter the cells, and cells fuse into multinucleated muscle fibers (Fischer-Lougheed et al., 2001).

Kir2.1 expression and function are regulated by Cdo, the Hh co-receptor and Ig/FNIII protein. Cdo forms a complex with Kir2.1 and increases cell surface expression of Kir2.1 in differentiating myoblasts (Leem et al., 2016). *Cdo*$^{-/-}$ primary myoblasts show defective Kir2.1 activity, and thus defective differentiation. This surface regulation by Cdo occurs through p38MAPK, since treatment with a p38MAPK inhibitor similarly reduces Kir2.1 surface expression. This myoblast model hence adds two additional regulators that interact with Cdo, an ion channel and a protein kinase; other Ig/FNIII proteins may similarly carry out functions through such interactors.

1.6.5 Ligand-gated ion channels

Besides K^+ channels, another class of ion channels with interesting glial functions is the ligand-gated ion channels (LGICs). Their ligand molecules are

neurotransmitters, including glutamate, glycine, GABA (γ-Aminobutyric acid), and ATP (Verkhratsky and Steinhäuser, 2000). LGICs are expressed in several cell types, such as astrocytes and oligodendrocytes in vertebrates and in neurons and glia in *C. elegans*.

1.6.5.1 In astrocytes

LGICs mediate several signaling processes in astrocytes. For example, glutamate can activate AMPA receptors, which increases intracellular Na^+ levels and blocks outward rectifying K^+ currents (Robert and Magistretti, 1997). In rat astrocytes, K^+ channel blockers can reduce cell proliferation, suggesting a role for AMPA receptors in this process as well. Another type of signaling found in astrocytes is calcium signaling. A subtype of AMPA receptors, that lacks one of the four possible subunits, GluR2, is capable of generating calcium currents. This was first demonstrated in astrocytes in the rat cerebellum called Bergmann glia (Burnashev et al., 1992). Furthermore, glutamate receptors can induce morphological changes in astrocytes (i.e. filopodia formation), which hints at a mechanism by which astrocytes respond to synaptic activity (Cornell-Bell et al., 1990). Long-term changes may also result from LGIC activity in astrocytes. This was shown by gene expression changes induced by AMPA receptors (McNaughton and Hunt, 1992).

1.6.5.2 In oligodendrocytes

LGIC function is not limited to astrocytes. They play some of the same roles in oligodendrocytes. For instance, AMPA receptors in oligodendrocyte progenitor cells

(OPCs) are also Ca^{2+}-permeable (Holtzclaw et al., 1995), and Ca^{2+} influx can lead to changes in gene expression (Liu and Almazan, 1995). Glutamate receptors can also regulate proliferation and differentiation of OPCs, through membrane depolarization and increases in intracellular Na^{+} concentrations (Knutson et al., 1997). LGIC function spans a wide gamut, from regulating K^{+} currents to Ca^{2+} signaling to gene expression regulation. It would be interesting to identify whether these functions are conserved among different glial types, beyond astrocytes and oligodendrocytes.

1.6.5.3 In *C. elegans*

A subset of LGICs is the cysteine (Cys)-loop superfamily, which includes nicotinic acetylcholine (nAChR), $GABA_A$, and glycine receptors. Cys-loop receptors are pentameric channels with a characteristic extracellular N-terminal loop of 13 amino acids between two Cys residues that form a disulfide bridge (Connolly and Wafford, 2004). The extracellular N-terminal domain is followed by four transmembrane domains. The largest Cys-loop superfamily exists in *C. elegans*, with 90 LGICs, compared to 45 and 20 in humans and *Drosophila* (Jones and Sattelle, 2008). Some overlap with vertebrates and *Drosophila* (e.g. cation-permeable nAChR, anion-permeable $GABA_AR$), but some appear unique to *C. elegans* (e.g. anion-permeable nAChR). However, many remain uncharacterized and thus exciting future research directions.

1.6.5.3.1 LGC-55

One of the Cys-loop LGICs recently identified and characterized is LGC-55, a tyramine-gated chloride channel (Ringstad et al., 2009). *lgc-55* mutants resemble tyramine-deficient animals; both exhibit defects in suppressing small rapid head movements in response to touch. LGC-55 is expressed in head neurons, glia-like GLR cells, and head muscles. Muscle-specific expression of LGC-55 fails to rescue the movement defect, suggesting it functions from the neurons and/or GLR cells. LGC-55 thus provides a precedent for Cys-loop receptors acting in neurons and/or glia.

Chapter 2: IGDB-2, an Ig/FNIII protein, promotes sensory compartment expansion in *C. elegans*

Summary

In this chapter, I describe my studies of IGDB-2, an Ig/FNIII protein, and its role in sensory compartment expansion. I show that *daf-6* amphid channel defects are suppressed by mutations in *igdb-2*. Moreover, like other regulators of sensory compartment morphogenesis, *igdb-2* acts as a *daf-6* suppressor and is expressed in the glia, including the AMso glia. Moreover, *igdb-2* appears enriched along the amphid channel portion of the AMso glia, suggesting IGDB-2 may function at the cell surface.

IGDB-2 is notably a transmembrane protein, like DAF-6 and CHE-14, two other factors in the amphid compartment machinery. Like other secreted or membrane proteins, IGDB-2 is *N*-glycosylated. Structure-function analysis showed its N-terminal membrane-distal domain, which includes one Ig and two FNIII domains (out of a total of two Ig and five FNIII domains), are required for function, suggesting a role for these domains in extracellular signaling. Genetic analysis suggests that *igdb-2* acts on the same cell processes as *lit-1* and *snx-1*. These factors may thus be similarly involved in a signaling pathway that promotes compartment expansion.

2.1 A screen for *daf-6* suppressor mutants

Since *daf-6* mutants have an abnormally bloated amphid sensory compartment, other factors may counteract *daf-6* activity to promote compartment expansion. To identify such factors, Elliot Perens performed a *daf-6* suppressor

screen (Perens, 2006). He made use of a *daf-6* phenotype that likely results from the amphid channel defects: an inability to form dauer larvae (Albert et al., 1981). The dauer phase is an alternate developmental state, induced by a pheromone released upon environmental stress, like crowding or starvation (Hu, 2007). Dauer entry is easily scored, as dauer animals are resistant to environmental stresses, including 1% sodium dodecyl sulfate (SDS). In *daf-6*(*e1377*) mutants, the inability to form dauer is fully penetrant and recessive, so SDS treatment kills these animals. Elliot reasoned that *daf-6* suppressor mutants would survive SDS exposure. Thus, he mutagenized *daf-6*(*e1377*) animals using ethyl methanesulfonate (EMS), starved F2 animals to induce dauer, and treated them with SDS.

To exclude mutations that affected downstream steps in dauer formation, he subsequently assayed dye-filling in the suppressor mutants. *daf-6* mutants fail to uptake lipophilic dyes, like diI, from the environment, again as a result of their amphid channel defects (Figure 2.1) (Perkins et al., 1986). Thus, *daf-6* suppressor mutants could presumably take up dye.

In total, Elliot screened 60,000 F2s and isolated seven mutants that both survived SDS treatment and dye-filled. Grigorios Oikonomou identified *ns132* and *ns133* as mutations in *lit-1* and *snx-1* genes, respectively (Oikonomou, 2011), and I later found the *ns123* mutant as a second mutation in *snx-1*.

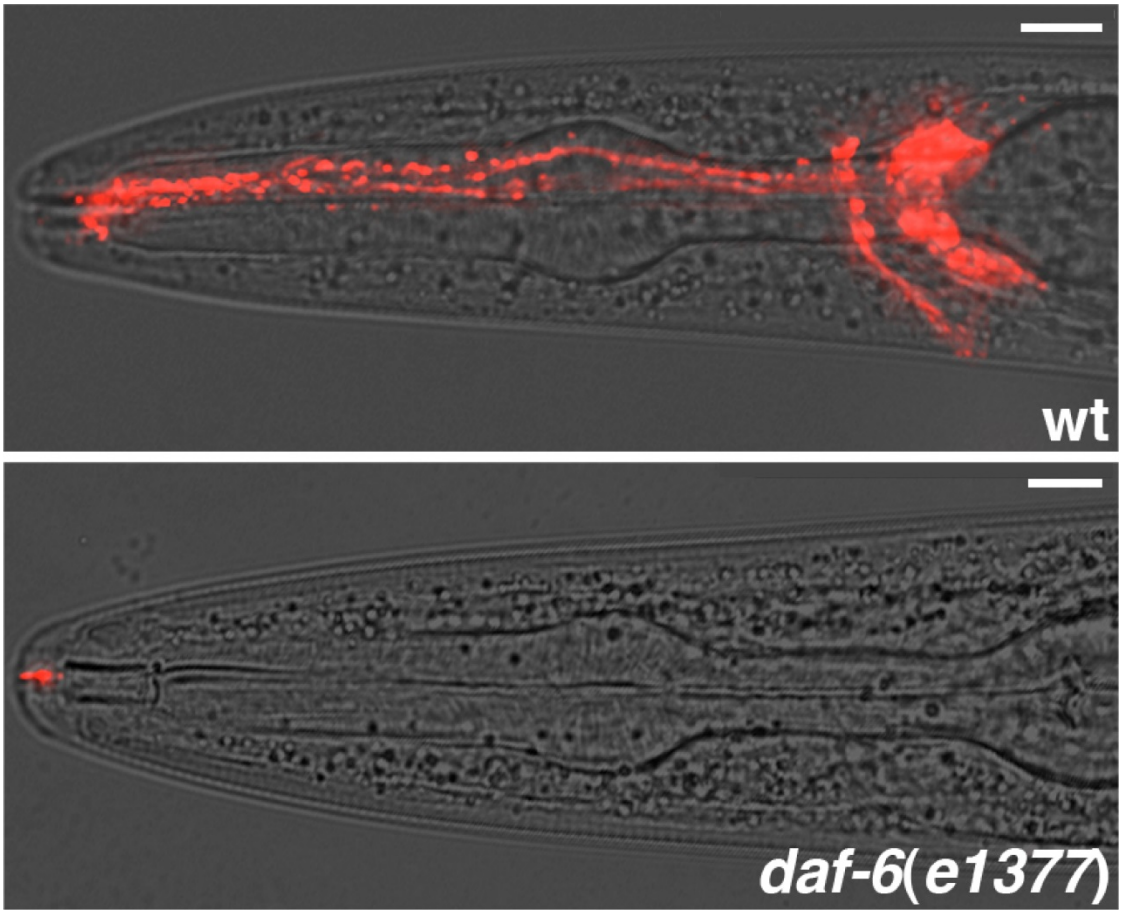

Figure 2.1. The dye-filling assay
Overlay of DIC and fluorescence microscopy images of wild-type and *daf-6* mutant animals after dye-filling with diI (see Materials and methods). Scale bar, 10 μm. Adapted from Oikonomou, 2011.

2.2 *ns122* suppresses sensory compartment defects of *daf-6* mutants

A third suppressor mutant, with allele designation *ns122*, was also isolated by Elliot but not characterized. My thesis work focuses on characterizing the gene corresponding to *ns122*. To determine whether *ns122* indeed restores normal channel morphology to *daf-6* mutants, I examined *ns122*; *daf-6* double mutants carrying transgenes driving GFP expression in AMsh glia and mCherry in the ASER amphid sensory neuron. I found that the ASER cilium in the double mutant extends through a channel as in the wild type in 20% of animals (n=10, compare Figure 2.2E to A, and note difference from C). To confirm these observations, Yun Lu performed serial-section transmission electron microscopy (TEM) on double mutants. As shown in Figure 2.2F, the amphid channel indeed appears largely normal, with cilia tightly bundled and exposed to the environment (n=3, compare Figure 2.2F to B, and note difference from D; Figure S1). However, cilia are not arranged in a 3:4:3 pattern, suggesting partial suppression.

To assess channel defects more quantitatively, I used the diI dye-filling assay. Consistent with our imaging assays, while neurons of *daf-6* mutants all fail to accumulate dye, 37% of *ns122*; *daf-6*(*e1377*) double mutants exhibit neuronal dye-filling in at least one of the two amphid sensory organs (Figure 2.2G), confirming that *ns122* suppresses *daf-6* mutant defects. Crossing the *ns122* allele to another *daf-6* mutant, *m186*, results in a comparable dye-filling increase (Figure 2.2G). Furthermore, three *ns122*; *daf-6*(*e1377*) animals that accumulated dye in only one amphid organ displayed only one amphid channel of more normal morphology by

EM (Figure S1), suggesting that dye-filling can serve to report on channel morphogenesis.

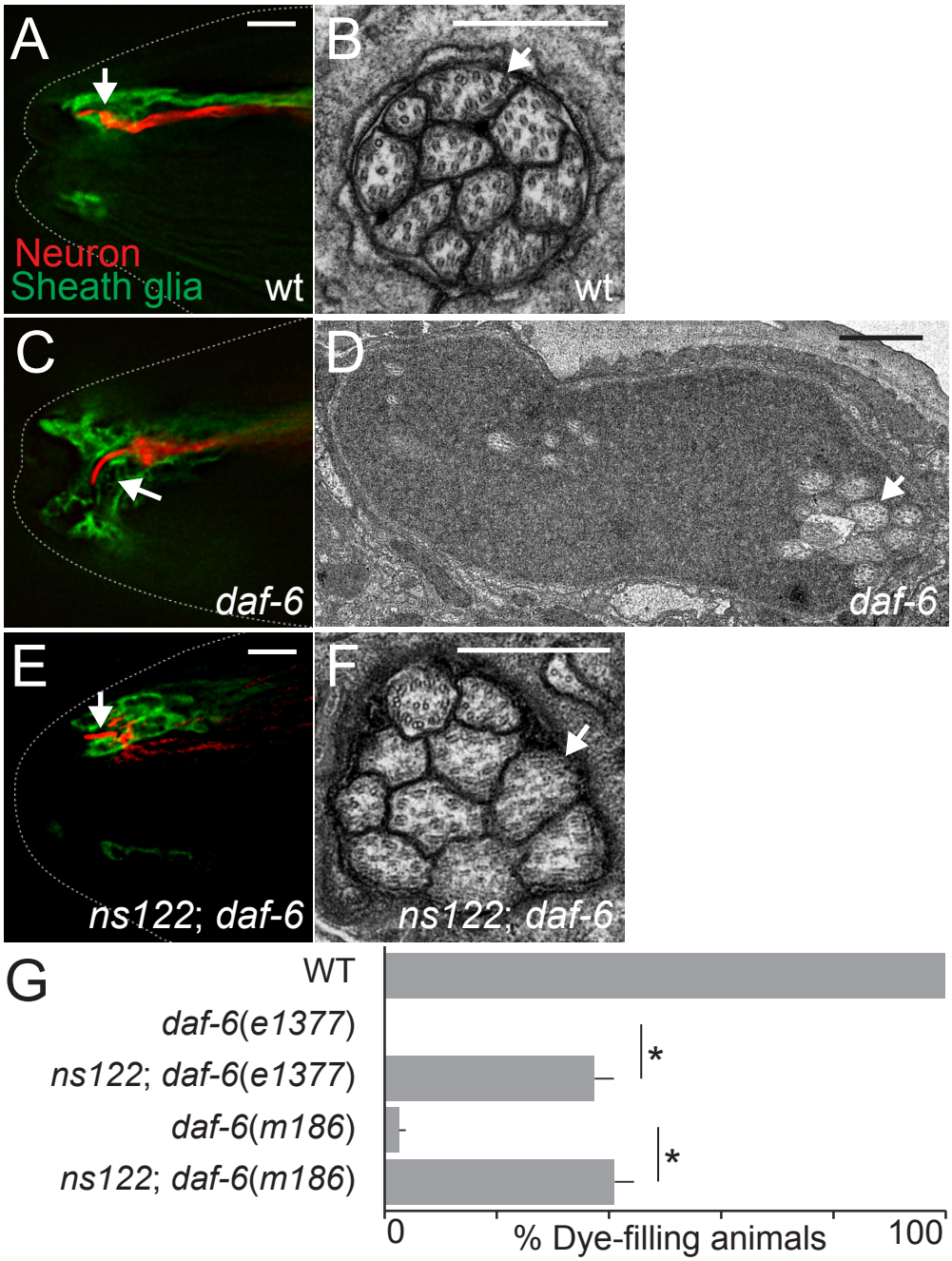

Fig. 2.2. *ns122* is a *daf-6* suppressor. (A, C, E) The amphid channel (white arrow) in wild-type **(A)**, *daf-6*(*e1377*) **(C)**, and *ns122*; *daf-6*(*e1377*) **(E)** adult animals. The ASER neuron is visualized with mCherry (red, driven by the *gcy-5* promoter) and the sheath glia with GFP (green, *T02B11.3* promoter). Left is anterior. Scale bar, 5 µm. **(B, D, F)** Transmission electron micrographs of cross-sections through the amphid channel in wild-type **(B)**, *daf-6*(*e1377*) **(D)**, and *ns122*; *daf-6*(*e1377*) **(F)** adult animals. White arrows point to cilia. Scale bar, 0.5 µm. Note the difference in scale between **(D)** and **(F)**. **(G)** *ns122* suppresses *daf-6* dye-filling defects. $n \geq 100$. Error bars, standard error of the mean (SEM), from ≥ 3 experiments. *$p < 0.0001$, unpaired *t*-test.

2.3 *ns122* is an allele of *igdb-2*, which encodes an Ig/FNIII protein

To identify the gene defective in *ns122* mutants, I used single nucleotide polymorphism (SNP) mapping to narrow down the interval containing *ns122* (Wicks et al., 2001). This mapping entails crossing the mutant strain, of the N2 Bristol background, to a wild-type strain, of the Hawaiian background. N2 and Hawaiian backgrounds differ in more than 6,000 known SNPs. By recovering the mutant phenotype and identifying the N2 SNPs that cosegregate with it, the mutant locus can be identified.

To map *ns122, ns122*; *daf-6* animals (N2) were crossed to CB4856 animals (Hawaiian), F2 animals were singled to individual plates, and F3 animals were assayed for dye-filling (Figure 2.3). *ns122*; *daf-6* mutant animals showed 37% dye-filling. However, the mapping method required a few adjustments. Because *ns122* was semidominant (9% of F1 males from *ns122*; *daf-6* x CB4856 dye-filled), it was hard to distinguish between *ns122* homozygous and heterozygous animals. This significantly hindered identification of *ns122* mutants at the F3 stage.

To circumvent this, I instead recovered F3 animals that were wild type at the *ns122* locus and mutant for *daf-6* , i.e. animals with little to no dye-filling (Figure 2.3). N2 SNPs should presumably co-segregate with the wild type phenotype. I then singled a few F3 animals to individual plates to confirm the wild-type phenotype in the F4 generation, and prepared genomic DNA from the remaining F3 animals for SNP genotyping.

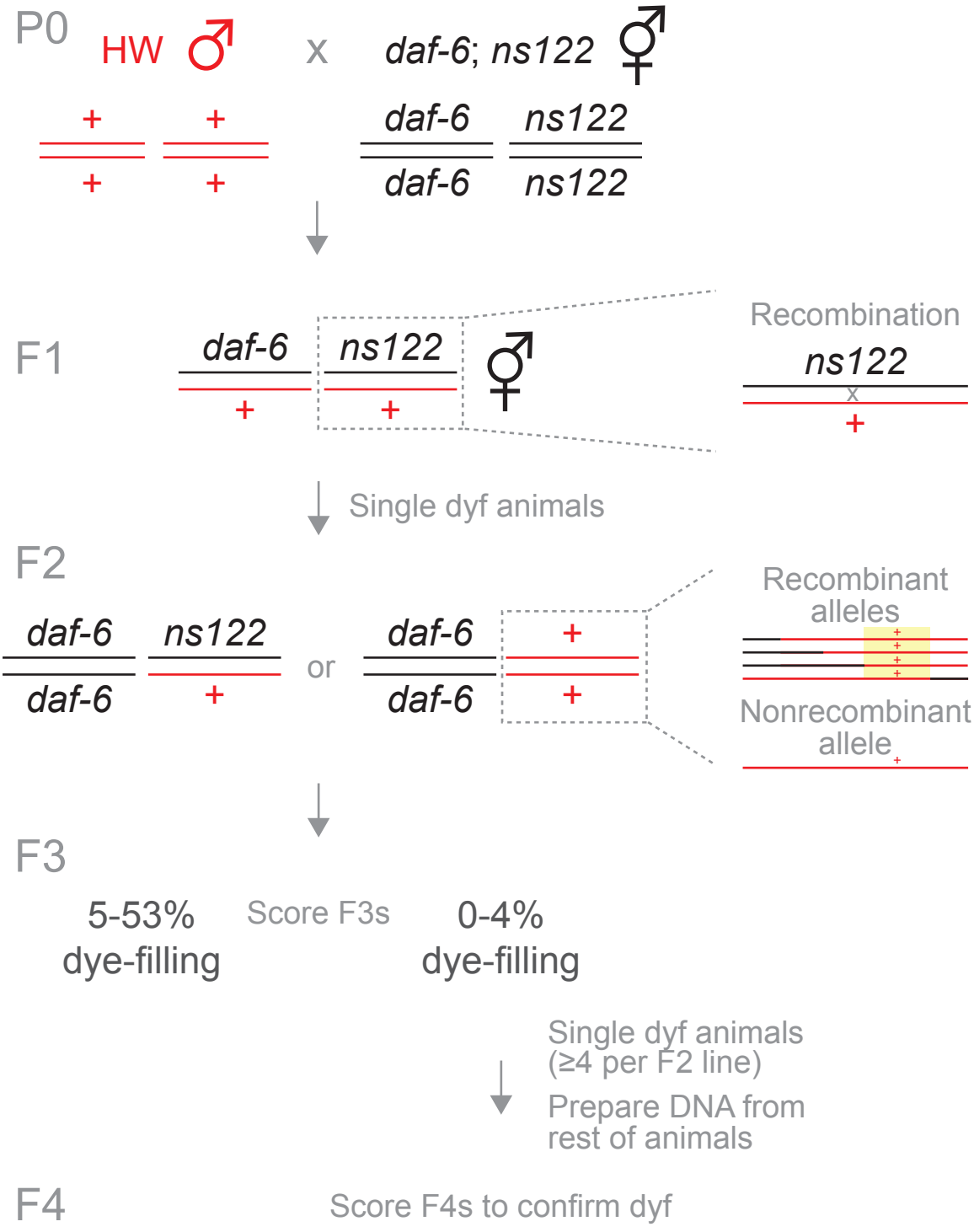

Figure 2.3. Mapping strategy for the *ns122* mutant. Hawaiian DNA is shown in red, and N2 in black. Yellow highlights the *ns122* locus. The generation number is shown in gray to the left. dyf, dye-filling defective (i.e. <5% animals dye-fill).

SNP mapping placed *ns122* in the region between +4.96 and +6.44 on LG IV, which spanned three fosmids (Figure 2.4). Fosmid rescue experiments narrowed the mapping interval to the WRM0629bG01 fosmid, between LG IV +5.97 and +5.98. Next, to identify specific mutations in this interval, Grigoris Oikonomou performed whole-genome sequencing of the *ns122*; *daf-6* strain, and the results were analyzed using galign (Shaham, 2009). Mutations were found in two genes: *igdb-2* (Q579ochre) and *T04A11.1* (D186N). Both genes reside in a duplication of a block of genes, but *igdb-2* is only partially duplicated (*igdb-1* is the C-terminal half of *igdb-2*), whereas *T04A11.1* is fully duplicated (*T04A11.4*).

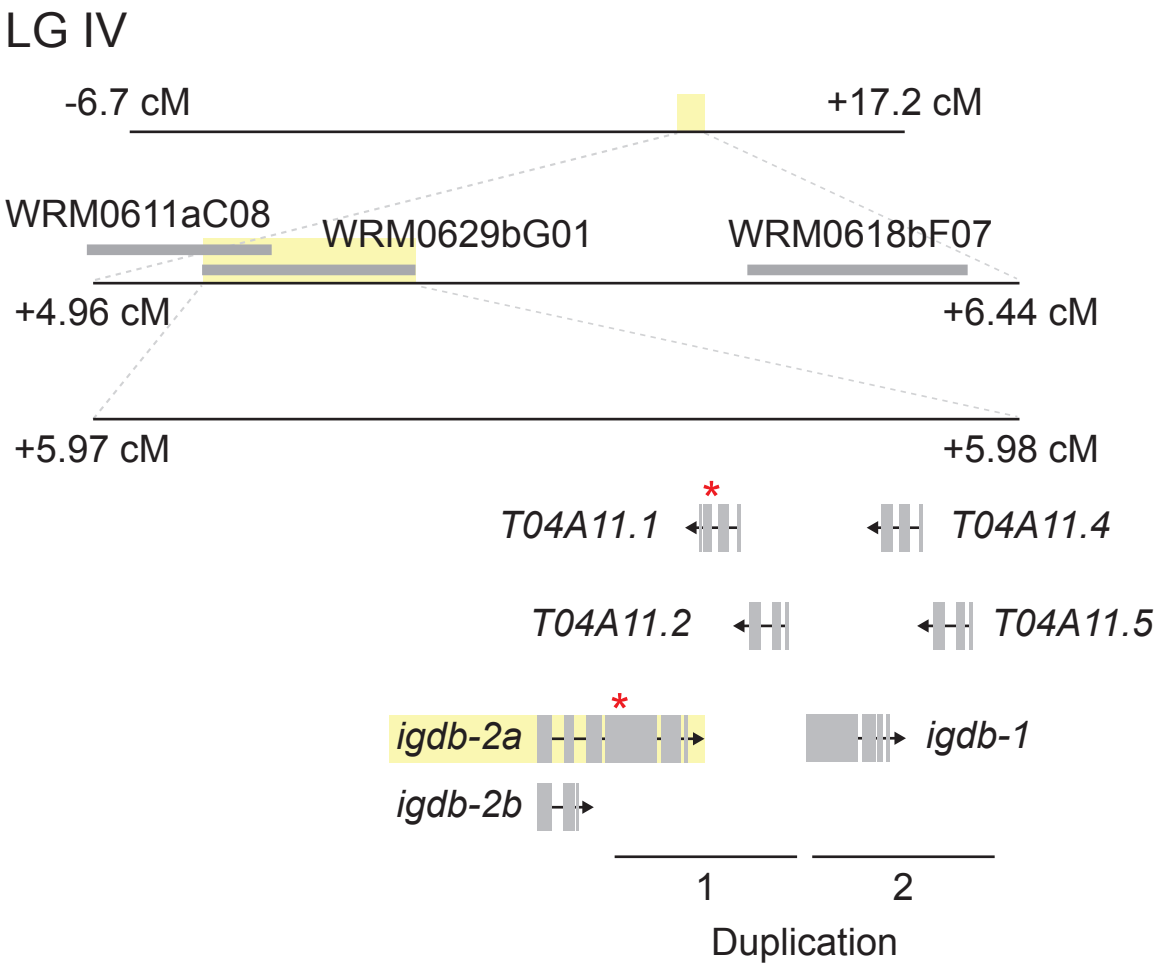

Figure 2.4. Schematic showing the interval containing the *ns122* locus. Yellow highlights the mapped interval at each step. (First row) SNP mapping narrowed the interval to a region of LG IV. (Second row) WRM0629bG01, one of three fosmids in that interval rescued the *ns122* defect. (Third row) *igdb-2* and *T04A11.1* had point mutations, and were both part of a block duplication.

igdb-2 encodes a single-pass transmembrane protein with multiple Ig-like and fibronectin type III (FNIII) domains (Figure 2.5A). The Q579ochre mutation in *igdb-2*(*ns122*) mutants leads to a predicted truncation of the IGDB-2 protein, preserving the first Ig and FNIII domains. To determine whether this *igdb*-2 mutation is responsible for restoring wild-type channel shape to *daf-6* mutants, I crossed another *igdb-2* allele, *gk214668*, to *daf*-6 mutants (Figure 2.5B). This allele harbors a Q78ochre mutation and leaves only the first Ig domain intact (Figure 2.5A). 22% of *igdb-2*(*gk214668*); *daf-6*(*e1377*) double mutants exhibit dye-filling, suggesting that *igdb-2* is indeed the relevant gene (Figure 2.5B). Further supporting this conclusion, dye uptake in *igdb-2*(*ns122*); *daf-6*(*e1377*) mutants carrying an extrachromosomal array containing the *igdb*-2 fosmid is reduced from 37% (no transgene) to 3% (Figure 2.5B). Similarly, *igdb-2*(*ns122*); *daf-6*(*e1377*) mutants carrying a transgene containing the *igdb-2* genomic region (from 5.4 kb upstream of the start codon to 0.4 kb downstream of the stop codon) have reduced dye-filling (Figure 2.5B); the same is true using the *igdb-2* promoter region to drive expression of an *igdb-2* cDNA::GFP fusion. Together, these data demonstrate that lesions in *igdb-2* restore wild-type channel morphology to *daf-6* mutants.

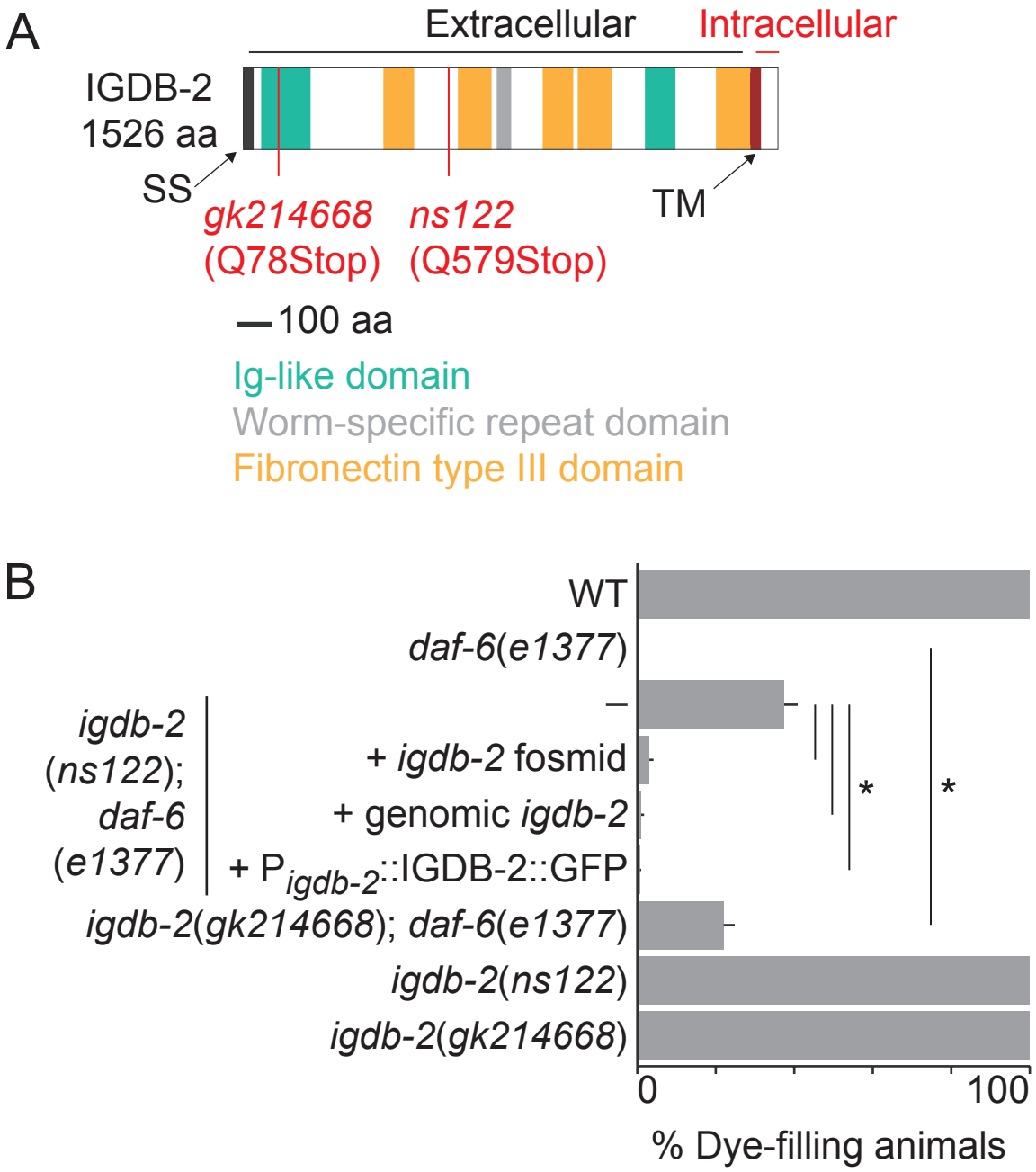

Figure 2.5. *ns122* is an allele of *igdb-2*, which encodes an Ig/FNIII transmembrane protein. (A) Schematic of the IGDB-2 protein, marking truncations predicted in *ns122* and *gk214668*. SS, signal sequence. TM, transmembrane domain. **(B)** Dye-filling assay for indicated genotypes. Alleles used are: daf-6(e1377) and igdb-2(ns122). (—) indicates no transgene. *igdb-2* fosmid is WRM0629bG01. $n \geq 87$. Error bars, SEM, from ≥ 3 experiments. *$p < 0.0082$, unpaired *t*-test.

2.4 *igdb-2* acts in glia and localizes to glial membranes of the sensory compartment

2.4.1 *igdb-2* acts in glia, including the AMso glia

To determine whether *igdb-2* functions in neurons or glia to regulate channel morphogenesis, I performed cell-specific rescue experiments. As shown in Figure 2.6, *igdb-2*(*ns122*); *daf-6*(*e1377*) mutants expressing an *igdb-2* cDNA::GFP fusion transgene under control of the glia-specific *mir-228* promoter, expressed during channel morphogenesis (Miska et al., 2007), have significantly reduced dye accumulation compared to non-transgenic animals. *igdb-2* cDNA::GFP expression in AMso glia alone, using an *itr-1* promoter fragment (Gower et al., 2001), also significantly reduces dye uptake. Importantly, *igdb-2* cDNA::GFP expression using the ciliated sensory neuron-specific *dyf-7* promoter, also active at the time of compartment morphogenesis (Heiman and Shaham, 2009), does not affect dye filling of *igdb-2*(*ns122*); *daf-6*(*e1377*) mutants. Thus, *igdb-2* functions at least in part in AMso glia and not in neurons to regulate compartment shape.

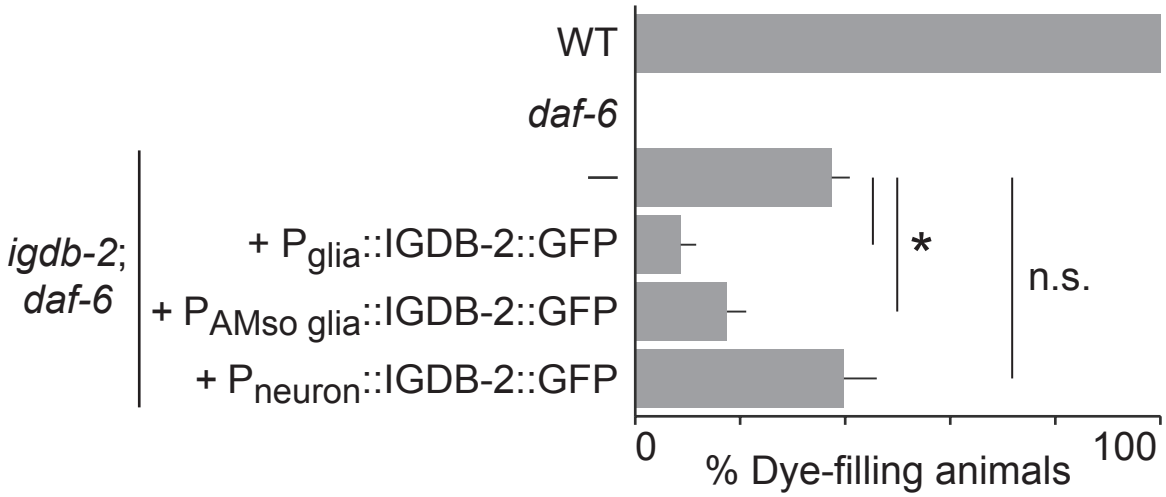

Figure 2.6. *igdb-2* acts in glia to regulate amphid channel morphogenesis. Dye-filling assay for indicated genotypes. Alleles used are: *daf-6*(*e1377*) and *igdb-2*(*ns122*). (—) indicates no transgene. Promoters used for expression in glia, AMso glia, and neurons are $P_{mir\text{-}228}$ (Miska et al., 2007), $P_{itr\text{-}1}$ (Gower et al., 2001), and $P_{dyf\text{-}7}$ (Heiman and Shaham, 2009), respectively. $n \geq 100$. Error bars, SEM, from ≥ 3 experiments. *$p < 0.0048$, n.s. not significant, unpaired *t*-test.

2.4.2 *igdb-2* is expressed in glia, including the AMso glia

The *igdb-2* gene expression pattern also supports this conclusion. Animals co-expressing *igdb-2* promoter::nuclear-RFP and glial *mir-228* promoter::GFP exhibit signal co-localization in glia, among other cells (Figure 2.7A). A similar experiment using *itr-1* promoter::GFP to mark AMso glia, revealed co-localization with *igdb-2* promoter::GFP in these cells (Fig. 2.7B), consistent with our rescue studies.

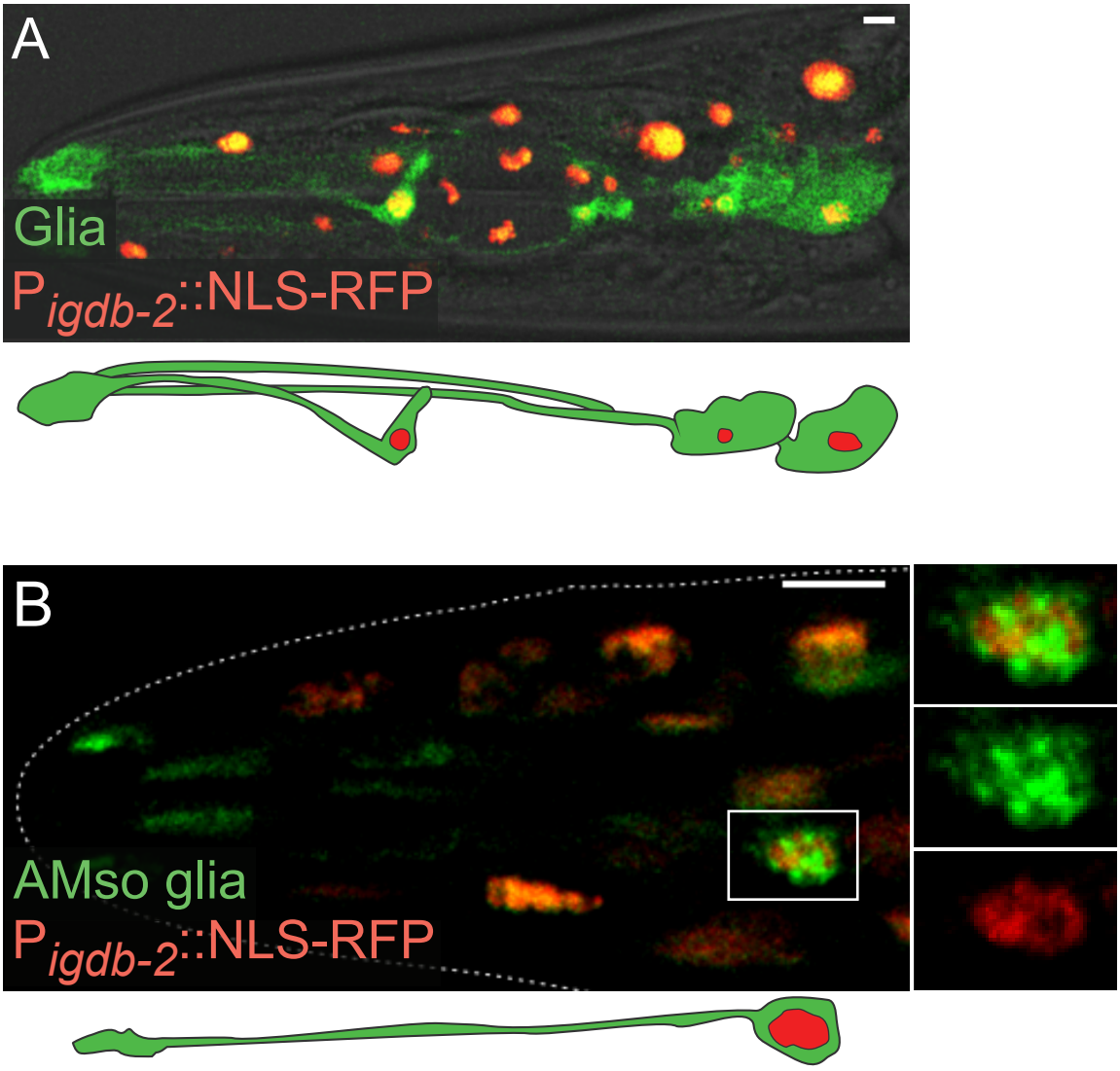

Figure 2.7. *igdb-2* is expressed in glia, including the AMso glia. Image of an adult animal (head) expressing $P_{igdb\text{-}2}$::NLS-RFP (red) and either **(A)** $P_{mir\text{-}228}$::GFP (in all glia, green) or **(B)** $P_{itr\text{-}1}$::GFP (in socket glia, green). Schematic of glia is shown below **(A)** and **(B)**. Outlined area in **(B)** is shown in greater detail in inset. Scale bars, 5 μm. Left is anterior.

2.4.3 IGDB-2 localizes to glial membranes of the sensory compartment

To examine where IGDB-2 protein localizes within AMso glia, I generated animals carrying a transgene driving *igdb-2* cDNA::GFP expression in these cells. I found an enrichment of IGDB-2 near the amphid channel (Figure 2.8) and in vesicular structures in the cell body. This supports the notion that IGDB-2 is trafficked on vesicles to the amphid channel, where it participates in channel morphogenesis. These observations are consistent with previous findings demonstrating that DAF-6, LIT-1, and SNX-1 also localize to the amphid channel (Oikonomou et al., 2012; Oikonomou et al., 2011; Perens and Shaham, 2005).

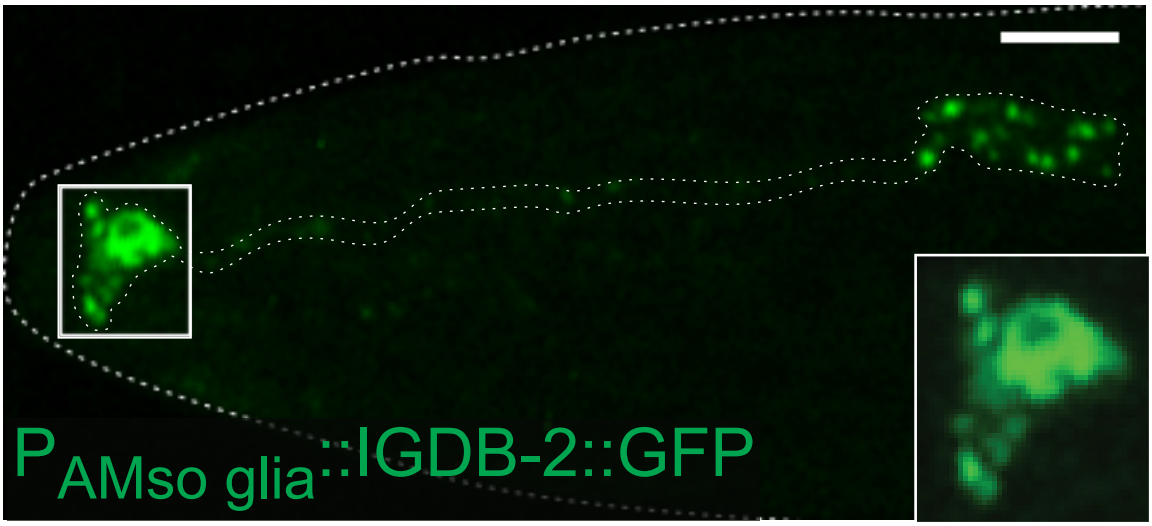

Figure 2.8. IGDB-2 localizes to the glial membranes of the sensory compartment. Adult expressing $P_{itr\text{-}1}$:::IGDB-2::GFP (in AMso glia, green). Outlined area is shown in greater detail in inset. Scale bar, 5 μm. Left is anterior.

2.5 IGDB-2 is *N*-glycosylated

The IGDB-2 protein has a large extracellular domain containing Ig-like and FNIII protein-protein interaction domains. As a predicted transmembrane protein, IGDB-2 may also undergo glycosylation, which is common to secreted proteins. The predominant form of glycosylation is *N*-linked (to asparagine residues), which has a wide range of functions, from regulating protein stability to mediating protein-protein interactions and signaling (Arey, 2012).

To determine whether IGDB-2 is glycosylated, I performed a peptide-*N*-glycosidase F (PNGase F) assay on IGDB-2 purified from worm extract. PNGase F cleaves the innermost sugar from the asparagine residue and removes the major types of *N*-glycans from glycoproteins (Maley et al., 1989). PNGase F treatment under denaturing conditions (which increase enzymatic efficiency) produced a downward shift of the smear of IGDB-2 by SDS-PAGE (Figure 2.9). This indicates that IGDB-2 is indeed *N*-glycosylated. This observation provides a basis to study the potential of glycosylation in IGDB-2 stability, or its interactions with other proteins in the future.

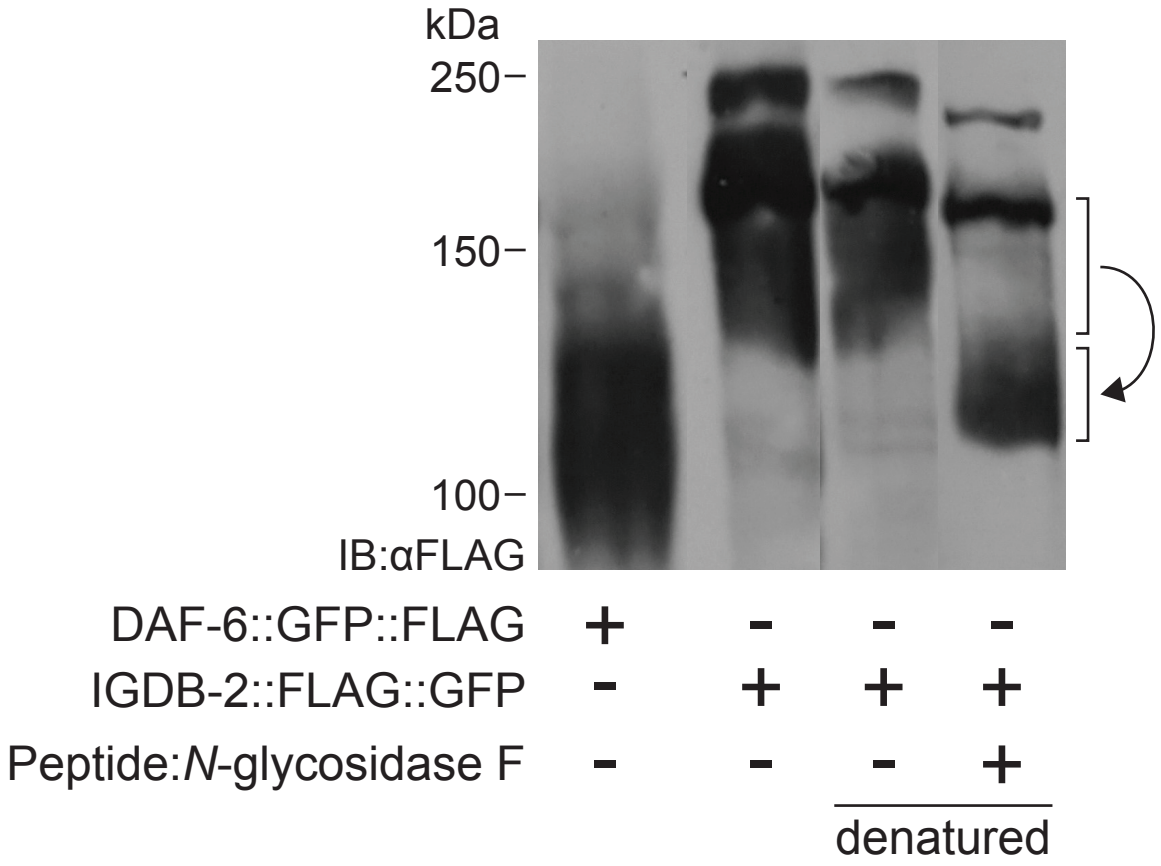

Figure 2.9. IGDB-2 is *N*-glycosylated. IGDB-2 was purified from worms with anti-FLAG beads (3 lanes on right) and treated with PNGase F (2 lanes on right) under denaturing conditions (rightmost lane), which produced a downward shift in IGDB-2 protein species by SDS-PAGE. DAF-6 was purified as a control (leftmost lane). IB, immunoblot. Representative of two experiments.

2.6 The IGDB-2 membrane-distal extracellular domain is required for compartment morphogenesis

The IGDB-2 protein consists of a large extracellular domain containing Ig-like and FNIII protein-protein interaction domains, as well as a short intracellular domain, which could be used for signal transduction. To uncover the functional significance of these domains, I generated *igdb-2*(*ns122*); *daf-6*(*e1377*) animals carrying transgenes in which the *igdb-2* promoter drives expression of truncated *igdb-2* cDNA::GFP proteins. As shown in Figure 2.10, animals expressing IGDB-2ΔN::GFP, lacking membrane-distal extracellular sequences, exhibit dye accumulation comparable to non-transgenic mutants. However, in mutants expressing either IGDB-2Δmiddle::GFP or IGDB-2ΔC::GFP, only 6% and 16% of animals take up dye, respectively, indicating that these transgenes remain functional. Based on GFP signal, these truncated proteins are expressed. These results, therefore, indicate that the N-terminal membrane-distal domain of IGDB-2, containing one Ig domain, two FNIII domains, and a single nematode-specific repeat domain, is required for IGDB-2 channel morphogenesis functions, and that the membrane-proximal and intracellular domains are dispensable for activity. Thus, IGDB-2 is unlikely to function through intracellular signaling, at least on its own, and likely influences compartment shape by interacting with extracellular moieties.

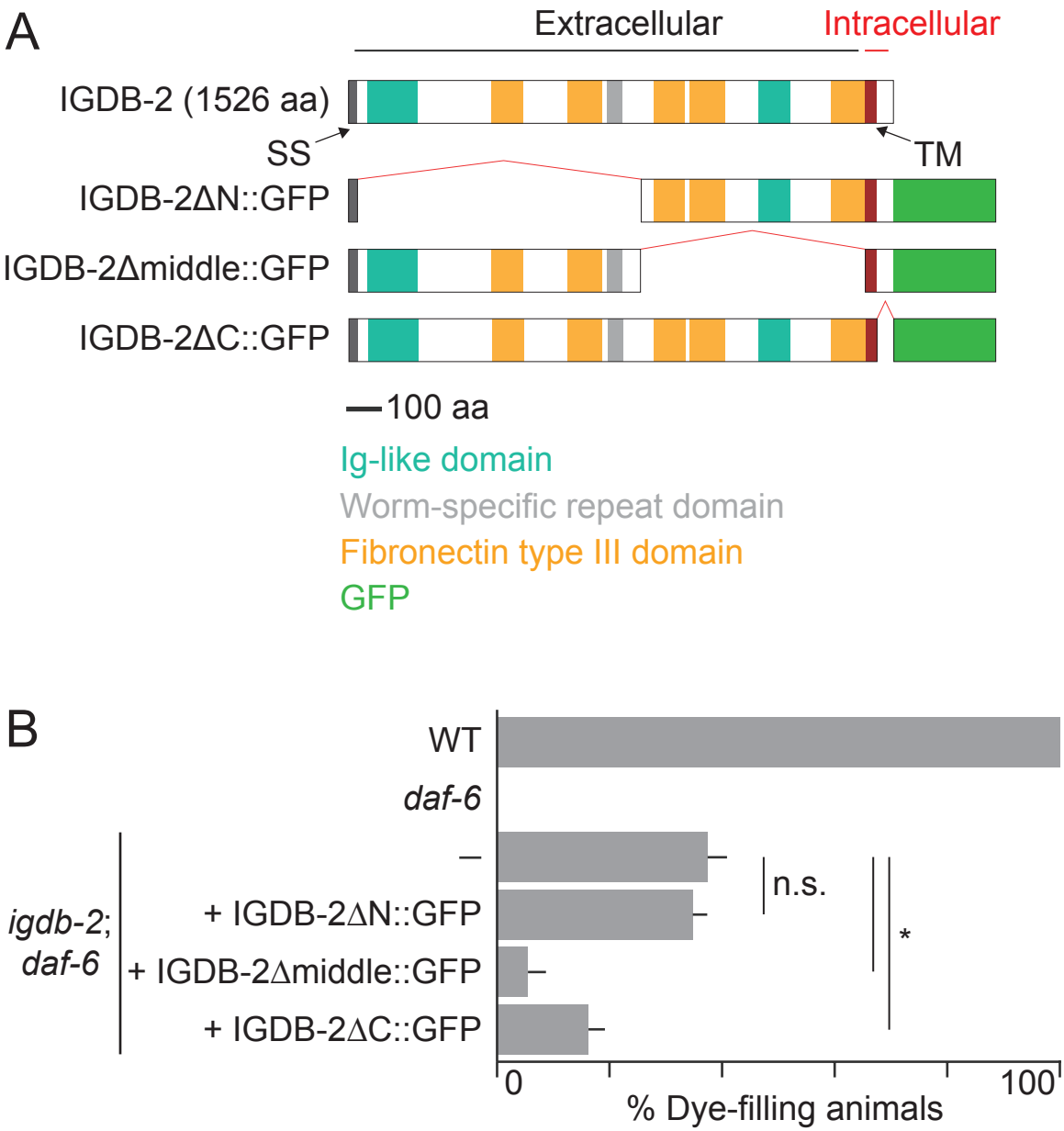

Fig. 2.10. The N-terminal membrane-distal domain of IGDB-2 is required for IGDB-2 function in amphid channel morphogenesis.

(A) Schematic of wild-type and truncated IGDB-2::GFP proteins. **(B)** Dye-filling assay for indicated genotypes. Alleles used are: *daf-6*(*e1377*) and *igdb-2*(n*s122*). (—) indicates no transgene. $n \geq 100$. Error bars, SEM, from ≥ 3 experiments. *$p < 0.0024$, n.s. not significant, unpaired *t*-test.

2.7 *igdb-2* genetically interacts with other genes controlling compartment size

Like *igdb-2* mutations, lesions in *lit-1* and *snx-1* only partially suppress *daf-6* mutant defects. One explanation for this is that more than one pathway drives compartment expansion; thus, disruption of a single pathway may not be sufficient to restore wild-type sensory channel morphology to *daf-6* mutants. I therefore sought to determine whether *igdb-2*, *lit-1*, and *snx-1* function in independent pathways. To this end, I generated the following triple mutants: 1) *lit-1*; *igdb-2*; *daf-6*, 2) *igdb-2*; *snx-1 daf-6*, and 3) *lit-1*; *snx-1 daf-6*. I then assessed their ability to take up dye, and compared with the relevant *daf-6* double mutants. I found that 39%, 26%, and 45% of triple mutants accumulate dye in amphid sensory neurons, respectively (Figure 2.11). Neither *lit-1*; *igdb-2*; *daf-6* nor *igdb-2*; *snx-1 daf-6* mutants were statistically different from the corresponding double mutants, suggesting that *igdb-2* acts with *lit-1* and *snx-1.* On the other hand, *lit-1*; *snx-1 daf-6* mutants showed a significantly higher suppression (45%) than *lit-1*; *daf-6* (25%) mutants, suggesting parallel functions for *lit-1* and *snx-1*, as previously reported (Oikonomou et al., 2012). However, this synergistic effect was much weaker than observed earlier (Oikonomou et al., 2012), and not even seen when comparing *lit-1*; *snx-1 daf-6* mutants to *snx-1 daf-6* mutants (34%). These differences from earlier findings may be due to accumulations of background mutations in the double or triple mutants. Given the weakness of this synergy, and the lack of synergy between either *lit-1* or

snx-1 and *igdb-2*, these values together do not support parallel pathways between *lit-1*, *snx-1*, and *igdb-2*.

To verify this epistasis analysis, we generated *lit-1*; *igdb*-2; *snx-1 daf*-6 quadruple mutants. 44% of animals could take up dye, statistically comparable to the *lit-1*; *igdb-2*; *daf-6* and *igdb-2*; *snx-1 daf-6* triple mutants. This again supports a common pathway model. There was a slight difference between the quadruple mutant and *igdb-2*; *snx-1 daf-6*, which could suggest a parallel function for *lit-1*. However, once again, this is not supported by other results, namely the *lit-1*; *snx-1 daf-6* to *snx-1 daf-6* comparison (statistically insignificant). Thus, none of these values significantly support parallel pathway models. Taken together, these results suggest either that IGDB-2, LIT-1, and SNX-1 function in the same process, or that *daf-6* mutant defects cannot be suppressed much beyond ~45%. However, the latter is unlikely, since there is another *daf-6* suppressor mutant, *ns125*, which greatly suppresses the *daf-6* dye-filling defect, in 70-90% of animals (see Section 5.6).

To further distinguish between these models, I tested whether *igdb-2* interacts genetically with *che-14*/Dispatched, which also regulates amphid channel morphogenesis (Michaux et al., 2000). I previously showed that *lit-1* and *snx-1* mutations enhance dye-filling defects in *che-14* mutants, in contrast to their suppression of *daf-6* defects (Oikonomou et al., 2012; Oikonomou et al., 2011). To determine if *igdb-2* acts similarly, I crossed *igdb-2*(*ns122*) to *che-14* mutants. 6% of double mutants took up dye, significantly less than the 34% in *che-14* single mutants,

demonstrating that *igdb-2* does enhance the *che-14* dye-filling defect. I thus favor a model in which IGDB-2 acts in the same process as LIT-1 and SNX-1.

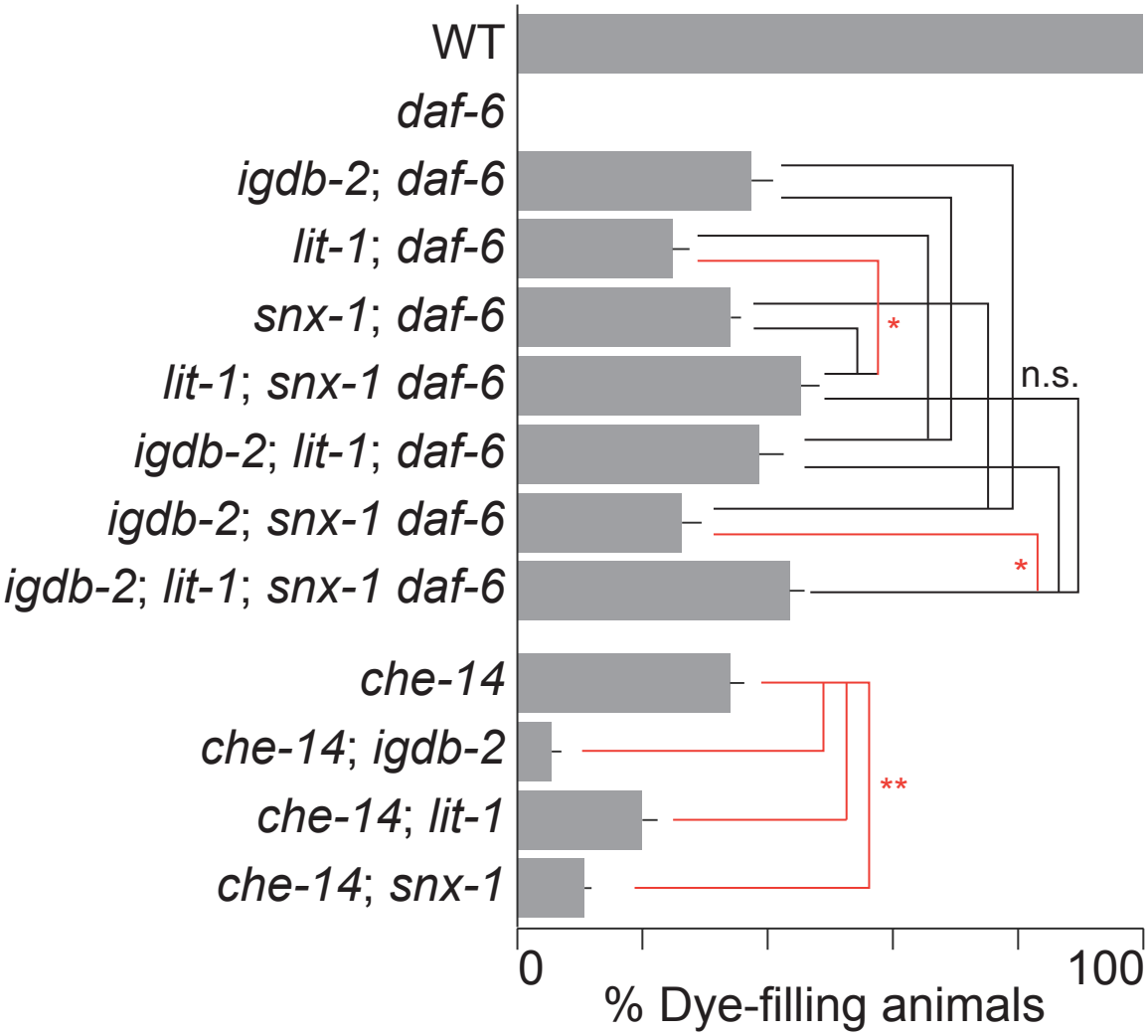

Fig. 2.11. *igdb-2* genetically interacts with other genes controlling compartment size. Dye-filling assay for indicated genotypes. Alleles used are: *daf-6*(*e1377*), *igdb-2*(*ns122*), *lit-1* (*ns132*), *snx-1*(*ns133*), and *che-14*(*ok193*). Note: we previously observed a strong synergistic suppression of the *daf-6* dye-filling defect by *lit-1* and *snx-1* mutations (Oikonomou et al., 2012), but it was now weak, possibly due to changes in the triple mutant genetic background. $n \geq 100$. Error bars, SEM, from ≥ 3 experiments. n.s. not significant (black lines), *$p < 0.019$ (red lines), one-way ANOVA analysis with Bonferroni's multiple comparisons. **$p < 0.0044$ (red lines), unpaired *t*-test.

Chapter 3: IGDB-2 binds to and inhibits LGC-34, a predicted ligand-gated ion channel

Summary

In this chapter, I describe a screen for IGDB-2 interactor proteins and the subsequent characterization of two: LGC-34 and F42A8.1. As hinted in the last chapter, IGDB-2 may function through interactions with other proteins, given its Ig and FNIII domains. To explore this, I use a co-immunoaffinity purification approach, coupled with mass spectrometry analysis, to isolate IGDB-2 interactors from whole worms. One of these interactors, LGC-34, is a predicted ligand-gated ion channel. I verify its interaction and co-localization with IGDB-2 in both worms and cell culture. Importantly, genetic analysis shows that *igdb-2* inhibits *lgc-34* in promoting sensory compartment expansion, thus providing some insight into how IGDB-2 functions. However, a second IGDB-2 interactor candidate, F42A8.1, does not appear to have a role in regulating the sensory compartment, though the list of candidates is by no means exhausted.

3.1 A screen for IGDB-2 interactors by co-immunoaffinity purification and mass spectrometry analysis

To identify IGDB-2 interactors that may also direct sensory compartment morphogenesis, I generated animals expressing a FLAG-tagged IGDB-2 protein, detectable by Western blot (Figure 3.1A), and performed co-immunoaffinity purification of this fusion protein using anti-FLAG beads (Figure 3.1B) (see Materials and methods). As a control, I purified LIT-1 from a strain expressing

FLAG-tagged LIT-1. Precipitates were subjected to MS/MS mass spectrometry to identify interacting proteins (see Materials and methods). Importantly, peptides derived from WRM-1/β-catenin, a known LIT-1-interacting protein, were found in the LIT-1, but not in the IGDB-2 precipitate, demonstrating both the success and specificity of this method. Interactor candidates were ordered by ranked by quantity (or area under the curve plotting intensity of a particular mass/charge over time) in the IGDB-2 sample, relative to that in the LIT-1 sample (Table 1). The two highest scoring candidates were LGC-34, a ligand-gated ion channel, and F42A8.1, a protein of unknown function.

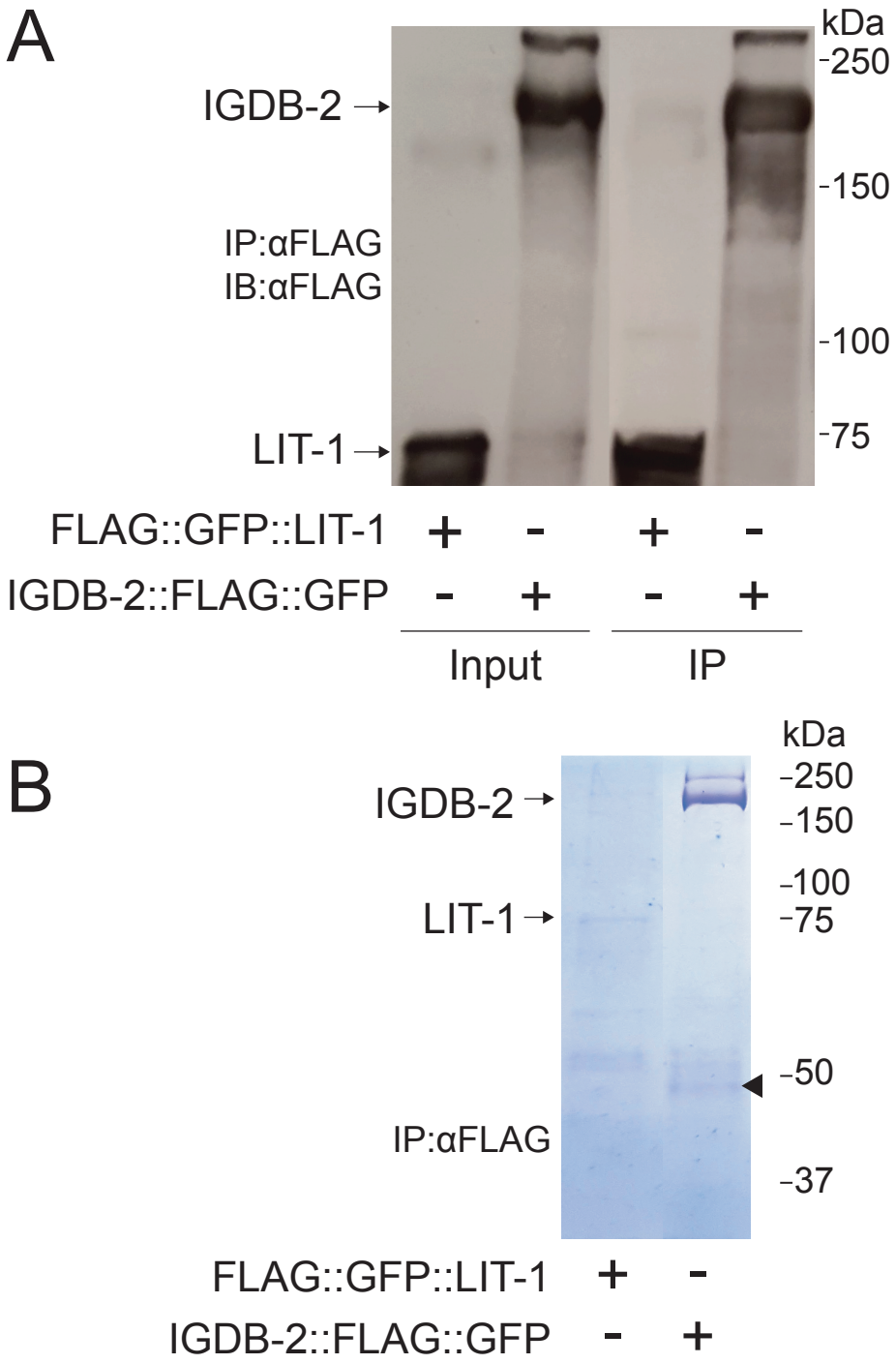

Figure 3.1. IGDB-2 interactors are co-purified from worms. (A) IGDB-2::FLAG was purified from animals with anti-FLAG beads and detected by Western blot. FLAG::LIT-1 was expressed and purified as a control. IP, immunoprecipitated. IB, immunoblot. **(B)** Proteins co-immunoprecipitated with IGDB-2::FLAG were resolved by SDS-PAGE and the gel stained with Coomassie Blue. The arrowhead marks LGC-34. Representative of two experiments.

Table 1. Mass spectrometry analysis of IGDB2-interacting proteins.
Proteins are ordered by ratio of area under the curve (plotting intensity of a particular mass/charge over time) in the IGDB-2 eluate to that in the LIT-1 eluate.

Protein	ΣCoverage	Σ# Proteins	Σ# Unique Peptides	Σ# Peptides	Σ# PSMs	Ratio Area IGDB2:LIT1
LGC-34 Ligand-gated ion channel	29.49	1	10	10	14	338.7
F42A8.1	49.19	1	21	21	24	335.0
IGDB-2 Ig-like and FNIII	70.77	3	110	110	672	321.3
SKPO-3 Peroxidase domain	32.71	2	25	25	31	304.2
DSL-1 Delta-like	23.41	1	5	5	8	262.4
ELO-1 Fatty acid elongase	6.60	2	3	3	5	145.0
TEP-1 Endopeptidase	12.59	3	15	15	15	90.2
T02H6.9 Vitelline membrane outer layer	31.82	1	4	4	5	84.3
PUF-5 Pumilio	9.58	1	5	5	5	78.0
CDR-2 Cadmium-responsive	16.91	1	3	6	6	68.3
DHS-24 Short-chain dehydrogenase	14.84	1	5	5	5	60.1
ACIN-1 Apoptotic chromatin condensation inducer	9.31	1	5	5	6	58.0
H04M03.3	18.32	1	5	5	5	57.8
ARL-1 ADP-ribosylation factor-like	25.00	2	5	5	6	41.8

3.2 LGC-34, a predicted ligand-gated ion channel, binds to IGDB-2

To confirm the IGDB-2-LGC-34 interaction, we co-expressed IGDB-2-FLAG and LGC-34-GFP in HEK293 cells, using expression of either IGDB-2-FLAG or LGC-34-GFP alone as controls (Fig. 6C). Immunoprecipitation using anti-GFP beads specifically pulled down IGDB-2-FLAG only when co-expressed with LGC-34-GFP (Figure 3.2B, compare right to left lane in top IP panel). Conversely, immunoprecipitation using anti-FLAG beads also precipitated LGC-34-GFP (Fig. 6C, compare right to left lane in bottom IP panel). We should note that anti-FLAG beads nonspecifically bind a residual amount of LGC-34-GFP, when expressed alone (Fig. 6C, left lane of bottom IP panel). However, when co-expressed with IGDB-2-FLAG, much more LGC-34-GFP was precipitated (Fig. 6C, right lane of bottom IP panel), despite lower expression levels (Fig. 6C, right lane of bottom input panel), suggesting that LGC-34 indeed co-immunoprecipitates with IGDB-2. Taken together, the co-immunoprecipitation experiments revealed that these two proteins specifically interact in this setting as well.

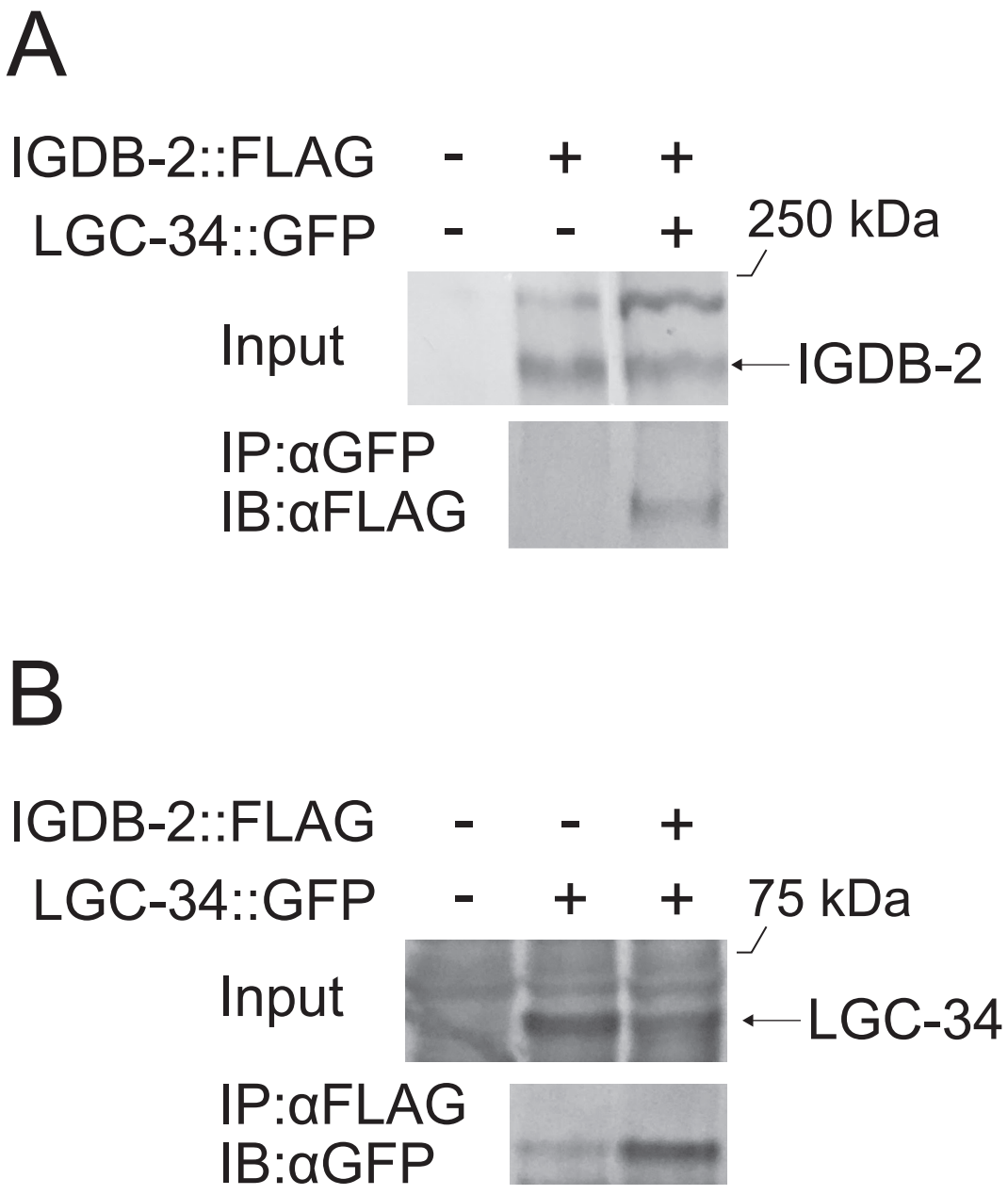

Figure 3.2. LGC-34 binds IGDB-2 in HEK293 cells. IGDB-2-FLAG and LGC-34-GFP were co-expressed in HEK293 cells. **(A)** IGDB-2 co-immunoprecipitates with LGC-34, purified with anti-GFP beads (top), and **(B)** vice versa, with anti-FLAG beads (bottom). Note: A residual amount of LGC-34::GFP was immunoprecipitated by anti-FLAG beads (left lane, bottom panel), but more protein was immunoprecipitated when co-expressed with IGDB-2-FLAG (right lane, bottom panel).

3.3 LGC-34 and IGDB-2 are co-expressed in some cells, including glia

The physical interaction suggests that IGDB-2 and LGC-34 may also be co-expressed in *C. elegans* cells. To verify this, we generated animals expressing *lgc-34* promoter::GFP and *igdb-2* promoter::nuclear-RFP transgenes. As shown in Figure 3.3A, *lgc-34* is expressed in a subset of *igdb-2*-positive cells (McKay et al., 2003; Meissner et al., 2011); however, glial co-localization is not observed, but this may be due to a lack of regulatory elements in the *lgc-34* promoter region used for these studies (McKay et al., 2003). In support of this, we analyzed previous AMsh glia expression profiling and found reads corresponding to both *lgc-34* and *igdb*-2 (Figure 3.3B; Wallace et al., 2016; and S.W. Wallace, unpublished results). Both were detected at higher levels than *daf-6*, previously reported to be expressed in AMsh glia (Perens and Shaham, 2005), suggesting that LGC-34 and IGDB-2 are likely co-expressed in glia.

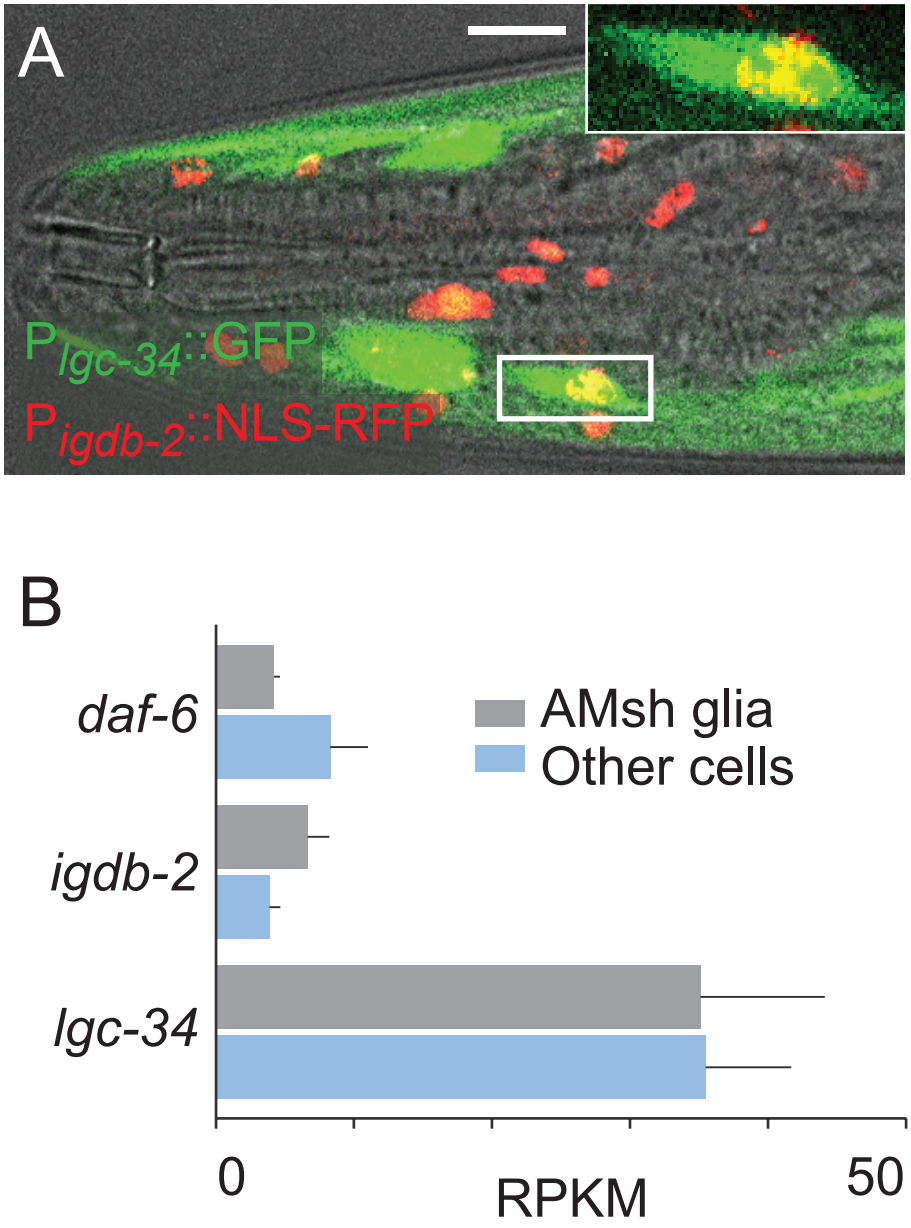

Figure 3.3. LGC-34 and IGDB-2 are co-expressed in a subset of cells in *C. elegans*. (A) An adult (head) co-expressing P_{lgc-34}::GFP (green) and P_{igdb-2}:: NLS-RFP (red). The outlined area is shown in greater detail in the inset. Scale bar, 5 µm. Left is anterior. **(B)** Gene expression profiling of daf-6, igdb-2, and lgc-34 in amphid sheath glia and other cells of the worm. RPKM, Reads Per Kilobase of transcript per Million mapped reads. Error bars, SEM, from 3 experiments.

3.4 LGC-34 restricts sensory compartment expansion and is inhibited by IGDB-2

To uncover possible *lgc-34* functions, I assessed whether *lgc-34* mutations affect amphid compartment morphology. *lgc-34*(*gk532*) contains a deletion spanning the *lgc-34* 5' UTR and the first 2 exons (Figure 3.4A). I found that *lgc-34*(*gk532*)*; igdb-2; daf-6* triple mutants had significantly reduced dye-filling, compared to *igdb-2*; *daf-6* double mutants (Figure 3.4B). To confirm this, I crossed a second *lgc-34* allele, *gk751837*, predicted to generate a truncated protein with no transmembrane domains, into *igdb-2*; *daf-6* double mutants. The resulting triple mutant also displayed a reduction in *igdb-2*-dependent *daf-6* suppression, with only 12% of triple mutants taking up dye. Since the *lgc-34* mutations suppressed the *igdb-2* phenotype, *lgc-34* acts in the opposite direction of *igdb-2* in amphid compartment morphogenesis. Surprisingly, neither *lgc-34* allele had a dye-filling defect on its own, and did not significantly restore dye filling to *daf-6* mutants (Figure S2). Thus, *lgc-34* participates in amphid compartment morphogenesis downstream of *igdb-2* and in the opposite manner, meaning it is inhibited by *igdb-2*.

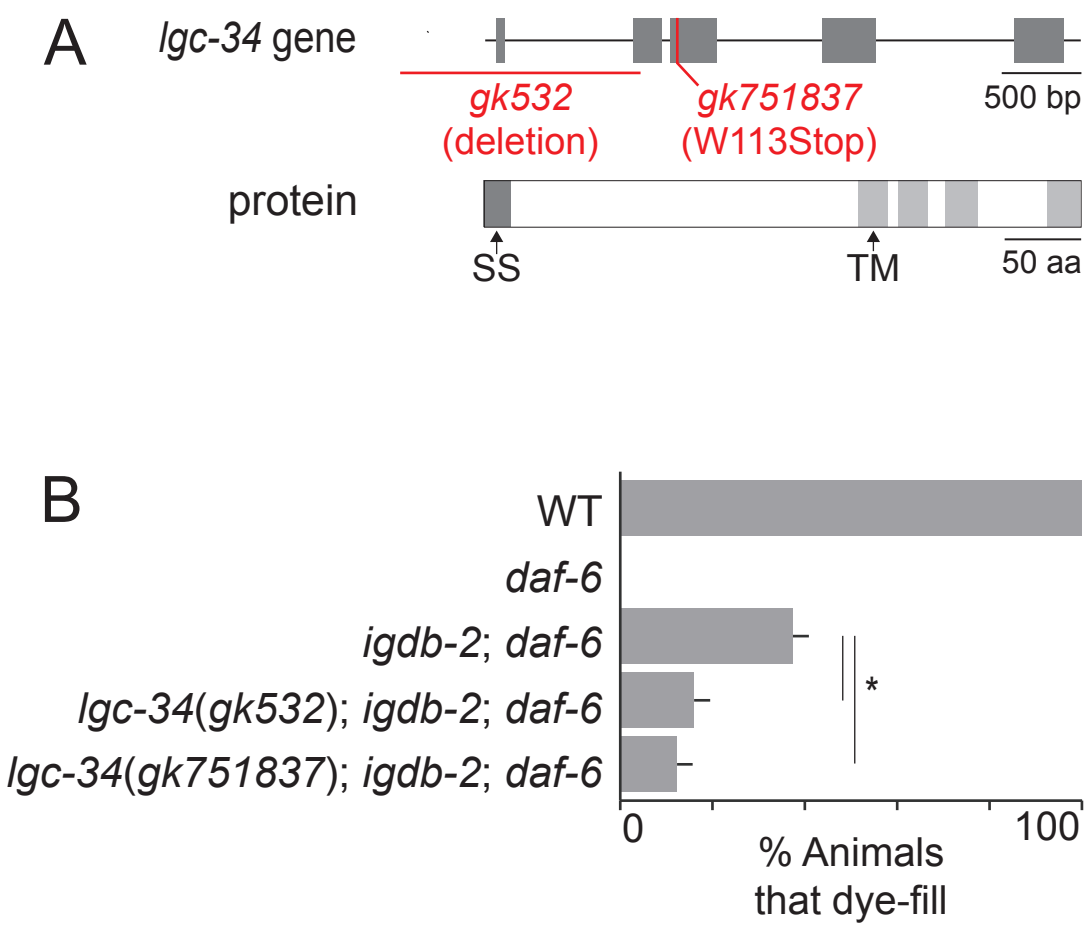

Figure 3.4. *lgc-34* restricts sensory compartment expansion and is inhibited by *igdb-2*. **(A)** Schematic of the *lgc-34* gene (top), marked with regions affected in the *gk532* and *gk751837* alleles, and LGC-34 protein (bottom). SS, signal sequence, and TM, transmembrane domain. **(B)** Dye-filling assay for indicated genotypes. Alleles used are: *daf-6*(*e1377*), *igdb-2*(*ns122*), *lgc-34*(*gk532*), and *lgc-34*(*gk751837*). $n \geq 100$. Error bars, SEM, from ≥ 3 experiments. *$p < 0.006$, unpaired *t*-test.

3.5 F42A8.1, an uncharacterized protein and IGDB-2 interactor candidate, is unlikely to be involved in sensory compartment morphogenesis

As previously stated, F42A8.1 peptides were the second most abundant to co-immunoprecipitate with IGDB-2, relative to the amount with LIT-1. To determine the functional relevance of F42A8.1 to sensory compartment morphogenesis, I sought to test whether *F42A8.1* mutations, like *lgc-34* mutations, affected dye-filling. However, there were no null alleles available for *F42A8.1*, so I used the CRISPR/Cas9 system to generate an allele encoding a truncated protein product. The resulting allele, *ns793*, was a deletion that removed the first splice acceptor site (Figure 3.5A). It was thus likely that the second exon would be skipped, and the first exon would be spliced to the third exon. This was predicted to shift the protein reading frame, and the resulting protein product was unlikely to be functional. Nevertheless, it would be best to confirm this by reverse transcription polymerase chain reaction (RT-PCR).

Assuming that *ns793* encoded a nonfunctional protein, I crossed this allele to both *daf-6* and *igdb-2*; *daf-6* mutants. However, there was no significant change in dye-filling in the resulting double and triple mutants (Figure 3.5B), which suggests that F42A8.1 is unlikely to function in sensory compartment morphogenesis or is functionally redundant with another regulator. However, given the number of remaining IGDB-2 interactor candidates, there are still likely functionally relevant IGDB-2 interactors that remain to be characterized (see Future directions, section 5.4).

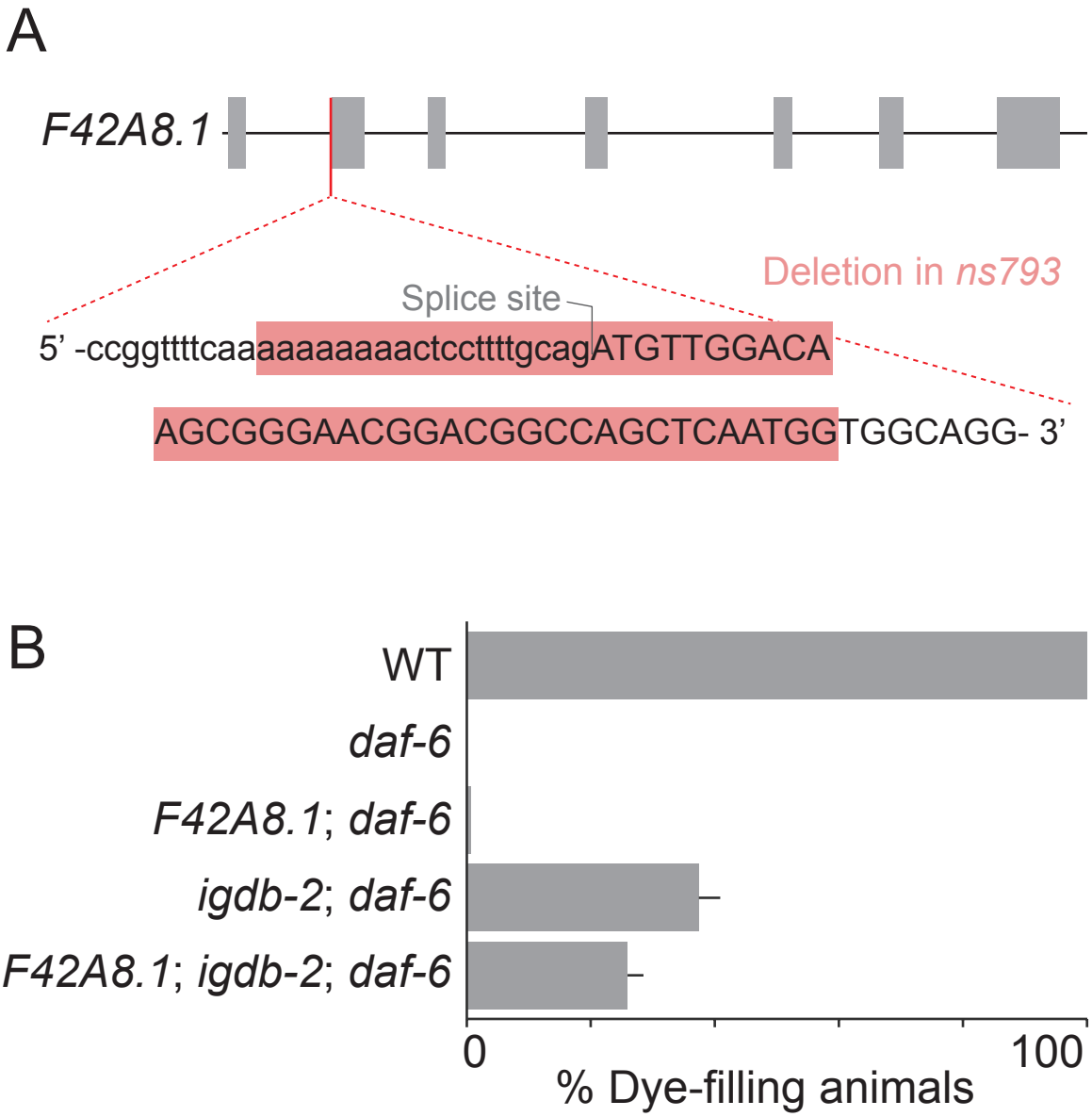

Figure 3.5. *F42A8.1* does not appear to be involved in sensory com-partment morphogenesis. (A) Schematic of the *F42A8.1* gene and the *ns793* deletion allele that removes a splice acceptor site. **(B)** Dye-filling assay for indicated genotypes. Alleles used are: *daf-6*(*e1377*), *igdb-2*(*ns122*), and *F42A8.1*(*ns793*). $n \geq 100$. Error bars, SEM, from ≥ 2 experiments, unpaired *t*-test.

Chapter 4: Discussion

4.1 A model for amphid compartment morphogenesis

The results presented here are consistent with a model in which *igdb-2* normally inhibits *lgc-34*, which in turn restricts sensory compartment growth (Figure 4.1). Since *lgc-34* mutations do not fully suppress *igdb-2* mutant defects, *igdb-2* also likely functions independently, and perhaps together with *lit-1* and *snx-1* to influence amphid channel morphogenesis.

We also demonstrated that *igdb-2* functions, at least in part, in the AMso glia. This was somewhat surprising, given that *daf-6* is required in the adjacent AMsh glia to restrict amphid channel expansion (Perens and Shaham, 2005). Thus, *igdb-2* could be opposing *daf-6* in a paracrine manner, or both could be acting from both the AMso and AMsh glia. We favor the latter model based on the following observations. First, both *igdb-2* and *daf-6* are expressed in AMso and AMsh glia (Wallace et al., 2016; S.W. Wallace, unpublished results; and Perens and Shaham, 2005). Second, AMso glia-specific expression of *igdb-2* rescues *ns122* defects, but to a lesser degree than expression under the *igdb-2* or pan-glial *mir-228* promoter. This suggests that *igdb-2* may be acting from other cells, like the AMsh glia. Third, infrared laser-induced expression of *daf-6* in the AMsh glia in *daf-6* mutants restores dye-filling, but only in 30% of animals (Singhal and Shaham, 2017). Thus, *daf-6* function may similarly be required in the AMso glia, where it may function with IGDB-2.

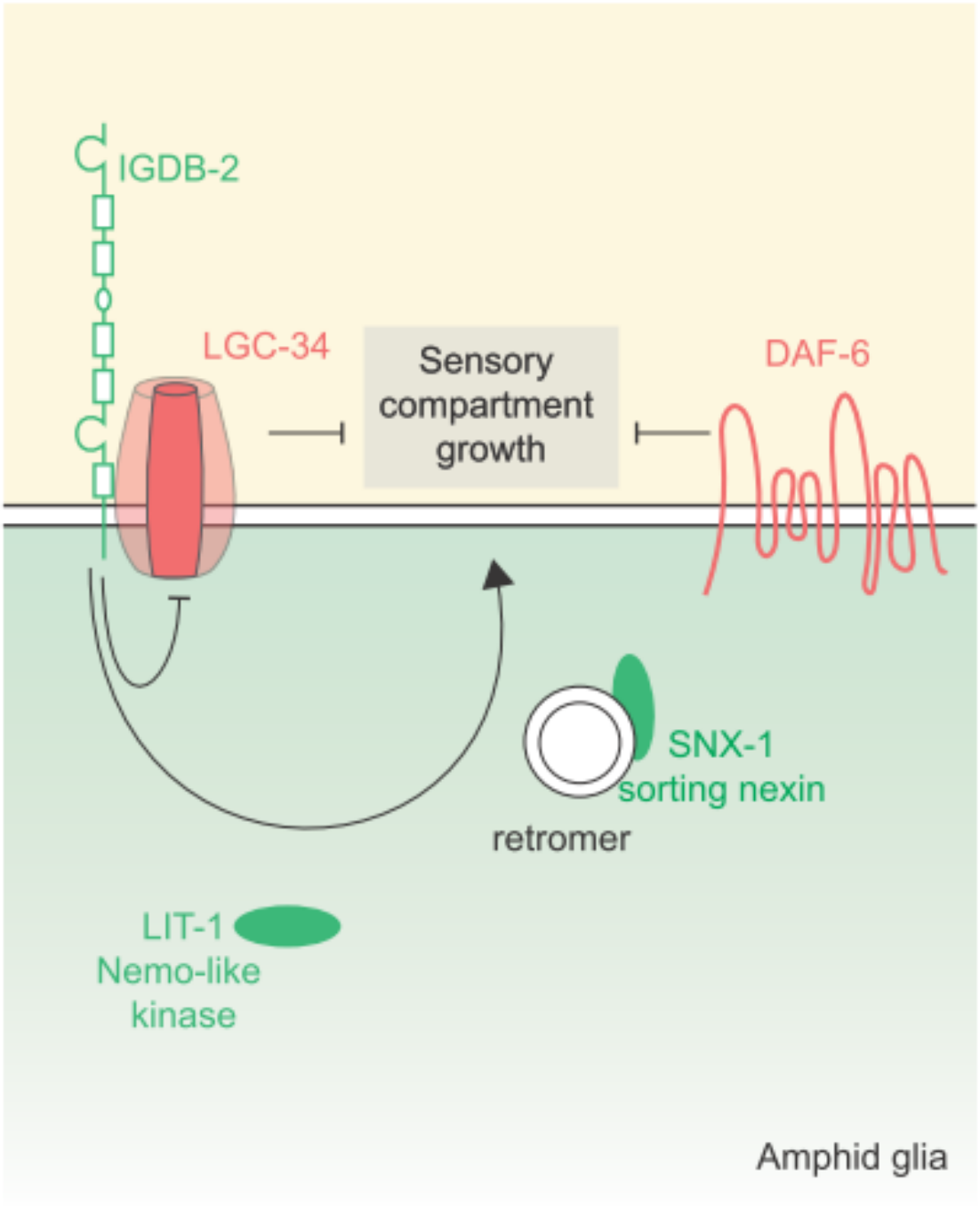

Figure 4.1. A model for sensory compartment morphogenesis.

4.2 IGDB-2 protein domains are found in other lumen-forming proteins

IGDB-2 contains Ig-like and FNIII domains, providing insight into how the amphid channel may form. Ig/FNIII proteins are classified as cell adhesion molecule (CAM) members of the immunoglobulin superfamily, and play prominent roles in neurodevelopment (Sytnyk et al., 2017). As mentioned in Chapter 1, several Ig/FNIII transmembrane proteins are involved in lumen formation in the nervous system. Neogenin, a Netrin receptor in the zebrafish, promotes neural tube formation (Mawdsley et al., 2004); *Neuroglian*, the *Drosophila* L1-CAM homolog, promotes formation of glial canals of the antennal lobe (Chen and Hing, 2008); and Robo, the Slit receptor, promotes formation of astrocytic tunnels leading to the olfactory bulb in mice (Kaneko et al., 2010). Given that Neogenin, *Neuroglian*, and Robo all function as membrane receptors for cell-cell communication, IGDB-2 may function in a similar manner, directing communication between the AMso and AMsh glia, or between the glia and amphid neurons.

In particular, the mechanism for Neogenin function suggests a possible interaction between IGDB-2 and the actin machinery. Neogenin interacts directly with the WAVE regulatory complex (WRC) through a WRC-interacting receptor sequence (WIRS) (Lee et al., 2016). This binding then recruits the WRC and Arp2/3 to adherens junctions. It is thus possible that IGDB-2 also regulates actin dynamics, especially since LIT-1, another regulator of sensory compartment morphogenesis, interacts with WSP-1 and actin (Figure 4.2) (Oikonomou et al., 2011). IGDB-2 may

recruit either WSP-1 or LIT-1 or a complex of both to the cell surface to promote actin nucleation near the cell surface and establish apical-basal polarity.

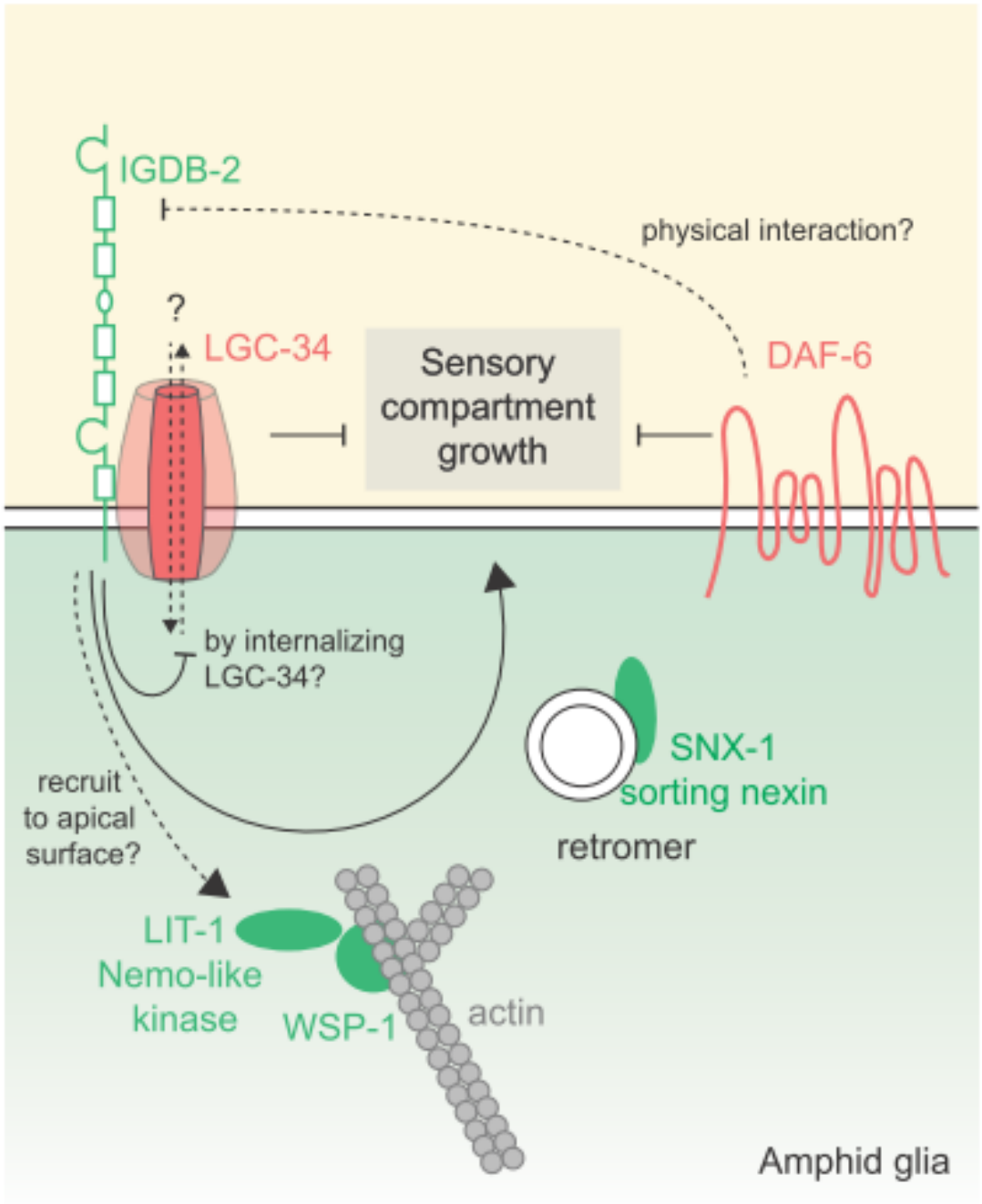

Figure 4.2. Possible mechanisms underlying sensory compartment morphogenesis in *C. elegans*

4.3 A comparison of IGDB-2-LGC-34 with protein complexes in Hedgehog signaling

My findings suggest that IGDB-2 functions through LGC-34 to control amphid channel morphogenesis. What could be the functional nature of this interaction? One hypothesis is that IGDB-2 may alter membrane localization or stability of LGC-34. This scenario is reminiscent of how another Ig/FNIII transmembrane protein and Hedgehog coreceptor, Cdo, regulates activity of the Kir2.1 K^+ channel: Cdo forms a complex with Kir2.1 and increases cell surface expression of Kir2.1 in differentiating myoblasts (Leem et al., 2016). Thus, the functional nature of the IGDB-2-LGC-34 interaction deserves further exploration.

Notably, the *Drosophila* homolog of Cdo, Ihog (Interference hedgehog), forms a complex with Patched and a related Ig/FNIII protein, Boi (Brother of Ihog) (Zheng et al., 2010). This is intriguing given the genetic interactions we uncovered between *igdb-2* and *daf-6*, encoding a Patched-related protein. Moreover, Ihog interacts with Hedgehog *in vitro* (Yao et al., 2006) and with Patched through its first and second FNIII domains (Zheng et al., 2010), respectively. Similarly, IGDB-2 structure-function analysis showed that the N-terminal membrane-distal domain, which contains its first two FNIII domains, is necessary for IGDB-2 function.

A physical interaction between IGDB-2 and DAF-6 (Figure 4.2) would be highly informative and exciting, since there is currently no complete Hh signaling pathway known in *C. elegans* (Bürglin and Kuwabara, 2006). Only select components appear conserved thus far: Dispatched (CHE-14, PTD-2), Patched (PTC-

1 and -3), and Ci (TRA-1). There are over 60 Hh-related proteins and 24 Ptc-related proteins (PTRs), one of which is DAF-6. Existence of a similar relationship between a PTR and Ptc in other systems would thus suggest more of the Hh signaling pathway is conserved in *C. elegans* than was previously thought.

4.4 A role for IGDB-2 and LGC-34 in glial osmolarity regulation

IGDB-2 may regulate the open/closed state of LGC-34, thus mediating ion flux across amphid glia, and possibly glial cell osmolarity. Consistent with this model, *igdb-2* lesions appear to enhance dye-filling defects of mutants carrying mutations in CHE-14, a Dispatched-related protein involved in osmoregulation and amphid channel morphogenesis (Michaux et al., 2000). Indeed, the expansion and contraction of the amphid channel could be consistent with changes in fluid accumulation and osmoregulation. To study whether LGC-34 affects osmolarity, we may first characterize LGC-34 ion selectivity and identify the ion(s) it conducts across the membrane (Figure 4.2).

4.5 A ligand for LGC-34 function

LGC-34 may also be gated by a specific ligand, since other LGC (ligand-gated ion channels of the Cys loop superfamily) proteins in *C. elegans* are neurotransmitter receptors. LGC-55 is a tyramine-gated chloride channel that likely functions in head neurons or GLR glia to regulate head movements (Ringstad et al., 2009). Given LGC-34 expression in muscle cells, LGC-34 may be an acetycholine or GABA receptor, which are both found in muscle (Hernando and Bouzat, 2014). In vertebrate glia, ligand-gated ion channels are known to activate downstream

signaling cascades and morphogenetic changes (Verkhratsky and Steinhäuser, 2000), providing possible clues for processes activated by LGC-34 and inhibited by IGDB-2.

However, based on sequence analysis, LGC-34 is highly divergent from other LGCs and has only an atypical cysteine loop; this is normally involved in ligand-binding and present in most other LGCs (Jones and Sattelle, 2008). Thus, it is also possible that LGC-34, along with IGDB-2, may be acting through a novel mechanism to regulate sensory compartment growth.

Chapter 5: Future directions

5.1 Structure-function analysis of the IGDB-2-LGC-34 interaction

From co-immunoaffinity purification of IGDB-2, followed by mass spectrometry analysis, LGC-34 was identified as an IGDB-2 interactor. Genetic analysis suggests *igdb-2* inhibits *lgc-34* to promote sensory compartment expansion. However, the significance of this interaction remains unclear. To address this question, structure-function analysis of the IGDB-2-LGC-34 interaction will be performed.

Since Cys-loop receptors traditionally have two N-terminal Cys-loops critical for receptor assembly (Green and Wanamaker, 1997) and channel gating (Grutter et al., 2005), the Cys-loop in LGC-34 is a good region for mutagenesis. Another region is the intracellular linker between the first and second transmembrane domains, which determines charge selectivity of the ion channel (Jensen et al., 2005). Testing whether these mutants can rescue the *lgc-34* dye-filling phenotype will reveal where these two regions are required for *lgc-34* function.

To determine if the LGC-34 domains required for function are also necessary for IGDB-2 interaction, we will test whether the mutant LGC-34 proteins can bind IGDB-2 by co-immunoprecipitation. Ideally, this would be performed i*n vivo*. However, previously, the interaction between epitope-tagged LGC-34 and IGDB-2 was not detectable *in vivo*. A possible reason is that sonication of the protein lysate, which is necessary to break the worm cuticle, may have disrupted weaker protein interactions. Thus, a cell culture system will be used to test for interactions. If any

LGC-34 domains required for function are also required for IGDB-2 interaction, it would suggest IGDB-2 inhibits LGC-34 through its interaction.

5.2 IGDB-2 regulates LGC-34 localization

Expression pattern studies demonstrated that IGDB-2 is expressed in several glia, including the AMso glia, and is enriched along the amphid channel. Both *igdb*-2 and *lgc*-34 expression were detected by AMsh glial expression profiling (Wallace et al., 2016, and S.W. Wallace, unpublished results). This suggests both proteins may be co-expressed in glia.

Another Ig/FNIII protein-ion channel complex consists of Cdo, the Hedgehog coreceptor, and Kir2.1, a K+ channel. Cdo increases cell surface expression of Kir2.1 in differentiating myoblasts (Leem et al., 2016). If IGDB-2 acts via a similar mechanism, IGDB-2 may also be regulating LGC-34 function by altering LGC-34 localization.

To examine this, LGC-34 localization will be analyzed in an *igdb-2* mutant background. This requires a visible LGC-34 reporter. Although LGC-34 expression was not detected in amphid glia using an endogenous promoter fragment, a strong glia-specific promoter (e.g. *T02B11.3* for AMsh glia, *itr-1* for AMso glia) can be used to drive *lgc-34* expression in the glia. Since *igdb-2* appears to inhibit *lgc-34* function, *igdb-2* may downregulate *lgc-34* surface expression.

5.3 Interaction between DAF-6 and IGDB-2

Our findings show that *igdb-2* opposes *daf-6* in promoting sensory compartment expansion. Both encode membrane proteins that are enriched along

the amphid channel. Additionally, we found that IGDB-2 is N-glycosylated, like many other cell surface proteins (Gahmberg and Tolvanen, 1996). These results suggest that DAF-6 and IGDB-2 may localize to the same areas on the cell surface. To test this, colocalization studies with DAF-6 and IGDB-2, expressed in either the AMsh glia or AMso glia, will be performed.

Ihog, the *Drosophila* Hedgehog coreceptor and Cdo homolog, forms a complex with Patched and Boi, another coreceptor. Since both Ihog and Boi are Ig/FNIII proteins, IGDB-2 may similarly form a complex with DAF-6, a Patched-related protein. This can be tested by co-immunoprecipitation experiments in cell culture.

Given that detecting the interactions of multi-pass membrane proteins by co-immunoprecipitation is usually challenging, this approach may fail. Alternatively, fluorescence resonance energy transfer (FRET), a method to determine protein-protein interaction based on energy transfer from a donor molecule to an acceptor molecule, could be used to examine IGDB-2 and DAF-6 interaction. For this purpose, IGDB-2 will be fused with GFP and DAF-6 will be fused with YFP.

5.4 Characterizing other IGDB-2 interactor candidates

To select which IGDB-2 interactor candidates to verify, they were ranked by quantity (or area under the curve plotting intensity of a particular mass/charge over time) in the IGDB-2 sample, relative to that in the LIT-1 sample (Table 1). LGC-34 was the highest-scoring protein, and its interaction with IGDB-2 was subsequently verified. However, there are still many other potential IGDB-2 interactors worth

verifying. If these interactors are also involved in sensory compartment morphogenesis, they may uncover mechanisms for IGDB-2 function.

One promising candidate is ARL-1, a member of the ADP ribosylation factor-like (ARL) family of small GTPases. Its vertebrate homolog, Arl1, localizes to the Golgi apparatus and regulates vesicle trafficking from the endosome to the *trans*-Golgi (Galindo et al., 2016). Since IGDB-2 is a membrane protein, ARL-1 may bind and regulate IGDB-2 trafficking.

To determine whether ARL-1 affects trafficking of IGDB-2, we can examine IGDB-2 localization in *arl-1* mutants. To test whether *arl-1* regulates *igdb-2* function, we can examine *arl-1* mutants for dye-filling phenotypes. A deletion allele, *arl-1*(*tm1938*), significantly enhances dye-filling in *igdb-2*; *daf-6* mutants, suggesting that *arl-1* may be involved in *igdb-2* function. This needs to be verified, for example with additional mutant alleles or rescue experiments.

5.5 LGC-34 and glial (and sensory compartment) osmolarity

Our results suggest that IGDB-2 inhibits LGC-34 to promote sensory compartment expansion. As previously mentioned, IGDB-2 may regulate the open/closed state of LGC-34 and mediate ion flux across amphid glia. This would alter osmolarity of the sensory compartment (extracellular space) and could explain the bloated sensory compartments in *daf-6* mutants. This is similar to how K^+ flux across glia in vertebrates can alter volumes of glial cells and extracellular space (Leiserson and Keshishian, 2011).

To explore this, we could examine whether changes ion flux across LGC-34 affect dye-filling. One approach is to alter external ion concentrations, by supplementing *C. elegans* growth medium with specific ions. Since the *lgc-34* phenotype is only seen in *igdb-2*; *daf-6* mutants, ionic imbalances affecting *lgc-34* ion flux would likely affect dye-filling in *igdb-2*; *daf-6* mutants. Our preliminary results show a nonspecific decrease in dye-filling in *igdb-2*; *daf-6* mutants, when supplementing with 150 mM NaCl, KCl, Na-acetate, or K-acetate (Figure 5.1). This result is intriguing, since it phenocopies the *lgc-34* mutant. However, the lack of ion specificity is puzzling. One explanation is that the ion concentration may be too high, producing a general change in the sensory compartment. Another is that the ion specific to LGC-34 has not actually been supplemented, such as Ca^{2+}, which interestingly is required for dye-filling of the IL2 neurons (Burket et al., 2006). More repetitions will need to be performed to confirm this finding (this was the first trial), and future experiments will further optimize ion concentrations and treatment duration.

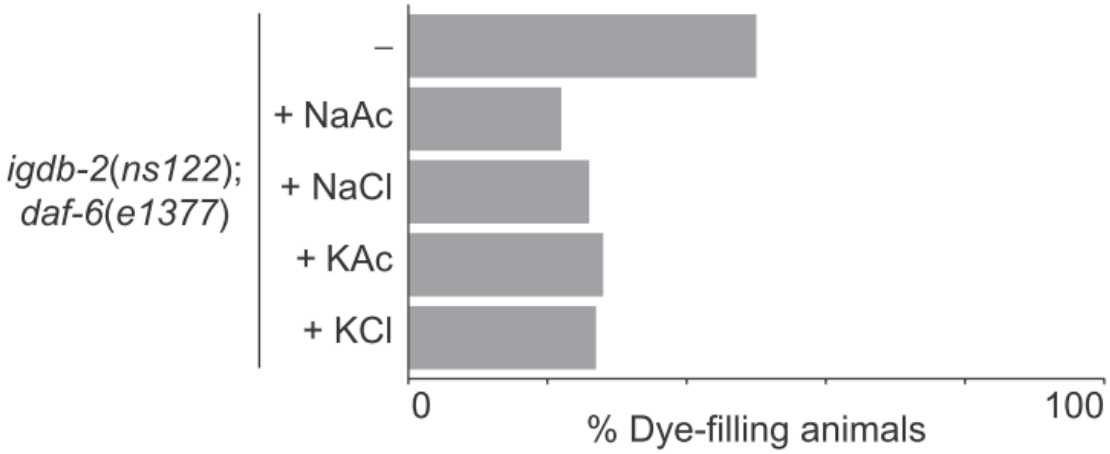

Figure 5.1. Environmental osmolarity affects dye-filling in *igdb-2*; *daf-6* mutants.

5.6 Characterizing *ns125*, another *daf-6* suppressor mutant

Our work on sensory compartment morphogenesis began with *daf-6* and its role in forming tubular structures. Subsequent findings, including mine, suggest mechanisms for *daf-6* action, including regulating actin dynamics, vesicle trafficking, and now protein trafficking and ion flux. This demonstrates how each *daf-6* suppressor mutant provides valuable insight.

Fortunately, there is another uncharacterized *daf-6* suppressor mutant, *ns125*. Cloning *ns125* will likely further our understanding of glial compartment morphogenesis. My preliminary mapping results suggest that *n125* is X-linked. Interestingly, a couple of backcrossed *ns125* lines show high penetrance levels (70-90% of animals dye-fill). This suggests *ns125* affects a novel gene that acts in a separate pathway from *lit-1*, *snx-1*, and *igdb-2*. Thus, identifying *ns125* should help complete our current model for sensory compartment morphogenesis.

Summary

The *C. elegans* amphid channel is an excellent model sensory compartment to study glial morphogenesis. In the studies presented here, I identify a novel regulator of amphid channel morphogenesis, IGDB-2, a single-pass Ig/FNIII transmembrane protein. IGDB-2 promotes sensory compartment expansion. I also identify LGC-34, a ligand-gated ion channel, as an IGDB-2 interactor. Genetic analysis shows that IGDB-2 inhibits LGC-34, but also acts with LIT-1 and SNX-1, to promote amphid channel expansion.

These results suggest exciting possible mechanisms underlying amphid channel morphogenesis. As an Ig/FNIII protein, IGDB-2 may signal to and/or recruit factors like WSP-1 to promote actin polymerization at the cell surface. As an ion channel, LGC-34 may regulate ion flux across glial cell membranes, to mediate amphid channel size. Further work to mechanistically characterize the IGDB-2-LGC-34 relationship may thus provide insights into amphid channel morphogenesis, and glial cell morphogenesis at large.

Chapter 6: Materials and methods

6.1 *C. elegans* strains

Strains were cultured as previously described (Brenner, 1974). All animals were maintained and scored at 20°C for at least two generations without starvation. N2 animals were used as wild-type. Alleles in this study were: linkage group II (LGII) *lgc-34*(*gk532*, *gk751837*), LGIII *lit-1*(*ns132*) (Oikonomou et al., 2011), LGIV *igdb-2*(*ns122*, *gk214668*), and LGX *snx-1*(*ns133*) (Oikonomou et al., 2012) and *daf-6*(*e1377*, *m186*) (Albert et al., 1981; Starich et al., 1995).

6.2 Identification of *igdb-2*(*ns122*)

SNP mapping was performed as described (Wicks et al., 2001). Briefly, CB4856 males were mated with *ns122*; *daf-6* hermaphodites (N2 background). F2 recombinants were cloned, and F3 animals were scored for dye-filling as described in *Section 2.6*. SNP mapping placed *ns122* in the region between +4.96 and +6.44 on LG IV. Fosmid rescue experiments narrowed the mapping interval to map units between LG IV +5.97 and +5.98. Whole genome sequencing of the *ns122*; *daf-6* strain was performed, and the results analyzed using galign (Shaham, 2009). Mutations were found in two genes in the relevant interval: *igdb-2* and *T04A11.1*. Rescue studies confirmed *igdb-2* is the relevant gene.

6.3 Extrachromosomal arrays

The following arrays were used in this study: *nsEx5869*, *nsEx5870*, and *nsEx5884* ($P_{T02B11.3}$::GFP and P_{gcy-5}::mCherry); *nsEx4695-nsEx4699* (WRM0629bG01 fosmid containing *igdb-2* and pMH135 (P_{pha-4}::GFP)); *nsEx4743-nsEx4747* (pWW3

and pMH135); *nsEx5663*, *nsEx5664*, and *nsEx5693* (pWW4 and $P_{unc-122}$::dsRed); *nsEx5233-nsEx5236* (pWW5 and $P_{unc-122}$::dsRed); *nsEx5436-nsEx5438* (pWW6 and $P_{unc-122}$::dsRed); *nsEx5453-nsEx5456* (pWW7 and $P_{unc-122}$::dsRed); *nsEx5373* (pWW8); Ex(pGT001(P_{itr-1}::GFP) and pRF4(*rol-6*(*su1006*))) (Gower et al., 2001); *nsEx5189*, *nsEx5190*, *nsEx5192*, *nsEx5195*, and *nsEx5232* (P_{igdb-2}::IGDB-2(N-terminal deletion)::GFP and $P_{unc-122}$::dsRed); *nsEx5124*, *nsEx5125*, *nsEx5156*, and *nsEx5796* (P_{igdb-2}::IGDB-2(middle deletion)::GFP and $P_{unc-122}$::dsRed); and *nsEx5155*, *nsEx5157*, *nsEx5158*, and *nsEx5201* (P_{igdb-2}::IGDB-2(C-terminal deletion)::GFP and $P_{unc-122}$::dsRed).

6.4 Integrated arrays

The following arrays were used: *nsIs98* ($P_{mir-228}$::GFP); *nsIs521* (pWW2 and $P_{unc-122}$::dsRed); *nsIs355* (pWW1 and pRF4); *nsIs370* (P_{daf-6}DAF-6::GFP::3xFLAG from the TransgeneOme project (Sarov et al., 2006)); and *sIs13244* (P_{lgc-34}::GFP and pCeh361(*dpy-5*(+))) (McKay et al., 2003).

6.5 Plasmid construction

pWW3 consists of P_{igdb-2}::IGDB-2 (genomic SacI-XbaI fragment from 5.4kb upstream of ATG to 0.4kb downstream of TAA, cloned into pBS). pWW4 was pBS containing P_{igdb-2}::IGDB-2(cDNA)::GFP with: 1) the same promoter fragment as pWW3, 2) the *igdb-2* cDNA amplified by polymerase chain reactions (PCR) from a mixed stage cDNA library, cloned into NheI-AscI sites, 3) GFP, and 4) *unc-54* 3'UTR. pWW5 consists of $P_{mir-228}$::IGDB-2(cDNA)::GFP ($P_{mir-228}$ (Miska et al., 2007) cloned into NotI-AscI and *igdb-2* cDNA into NheI-KpnI sites in pSM-GFP). pWW6 and

pWW7 are the same as pWW5 but with $P_{itr\text{-}1}$ (2.1kb) and $P_{dyf\text{-}7}$ (1.8kb) at NotI-XmaI, respectively (Gower et al., 2001; Heiman and Shaham, 2009). pWW8 is the same as pWW4, except with NLS-RFP fused to the *unc-54* 3'UTR, in place of IGDB-2(cDNA)::GFP, cloned with BamHI-MluI. pWW9, pWW10, and pWW11 are the same as pWW4, but with the following cDNA deletion mutants: IGDB-2Δ25aa-784aa, IGDB-2Δ786aa-1412aa, and IGDB-2Δ1441aa-1526aa, respectively. Plasmids used for worm co-immunoprecipitation studies were pWW1 and pWW2. pWW1 consists of $P_{T02B11.3}$::3xFLAG::GFP::LIT-1 (inserted 3xFLAG into the Acc65I site in pGO38) (Oikonomou et al., 2011). pWW2 consists of $P_{igdb\text{-}2}$::IGDB-2::GFP::3xFLAG (same as pWW3 but with GFP::3xFLAG fused to the 3' end of *igdb-2*, followed by the *unc-54* 3'UTR flanked by Acc65I sites). Plasmids used for cell culture co-immunoprecipitation studies were pWW12 (pLenti-CMV::LGC-34::GFP) and pWW13 (pLenti-CMV::IGDB-2::3xFLAG), which were made using the Gateway® cloning system (ThermoFisher). The plasmids used for CRISPR/Cas9 mutations were pWW14 and pWW15, which each consist of pJW1285, but with the 5'-ACGGACGGCCAGCTCAATGG-3' and 5'-TACTTTTATGAGTGTAGACG-3' as the *F42A8.1* sgRNAs, respectively. The sgRNAs were inserted as an SphI-KasI insert generated by overlap PCR.

6.6 Dye-filling assay

Animals were washed off nematode growth medium (NGM) plates into M9 buffer containing 10 µg/ml diI (1,1'-dioctadecyl-3,3,3',3'-tetramethylindocarbocyanine perchlorate) (ThermoFisher D282) and rotated at

20°C in the dark for 2 hours. They were then transferred to new NGM plates and scored for dye-filling (animals with any subset of dye-filled amphid neurons were considered positive for dye-filling). For transgenic strains, at least three lines were scored and averaged. Statistical analysis of all dye-filling values was performed with the unpaired *t*-test (GraphPad), except for epistasis analysis which was performed with the one-way ANOVA test with Bonferroni's multiple comparisons (GraphPad).

6.7 Fluorescence and transmission electron microscopy

Images were acquired with a DeltaVision Image Restoration microscope (Applied Precision) with an Olympus UPLSAPO (60X, 1.3NA) silicone oil objective for amphid channel morphology and with an inverted TCS SP8 laser scanning confocal microscope (Leica) with a PlanApo (either 63x, 1.40NA or 100x, 1.46NA) oil objective for expression pattern studies. Deltavision images were deconvolved with SoftWoRx (Applied Precision). All fluorescence images were analyzed with ImageJ (NIH). For transmission electron microscopy, animals were sectioned and imaged as previously described (Perens and Shaham, 2005; Wallace et al., 2016).

6.8 Co-immunoaffinity purification from worms and mass spectrometry

Mixed stage worms were grown on 50-100 15-cm peptone-enriched plates with HB101 bacteria, resuspended in homogenization buffer (50 mM HEPES-NaOH (pH 7.6), 1 mM EDTA, 150 mM NaCl, and 10% glycerol), and frozen as previously described (Mets and Meyer, 2009). Frozen worm powder was resuspended in homogenization buffer (with the addition of 1% NP-40 and Halt protease inhibitor (ThermoFisher 78429)), sonicated, and centrifuged at 20,000 *g* for 15 minutes at

4°C. The supernatant (2-3 mg/ml, 5-10 ml total) was incubated with 200 µl anti-FLAG® M2 affinity gel (Sigma A2220) for 2 hours. Beads were washed 3 times with homogenization buffer and proteins eluted with SDS loading buffer. One third of the total eluate was resolved by SDS-PAGE (4-12% gradient) to one third the length of the gel, and stained with Coomassie Blue (BioRad 1610436). The protein was then in-gel trypsinized, and the extracted peptides were identified by MS/MS mass spectrometry (Rockefeller University Proteomics Resource Center). Western blot analysis was performed with anti-GFP (polyclonal rabbit, gift from Baolin Wang) and anti-FLAG® M2 (monoclonal mouse, Sigma F3165) at 1:1000, and HRP-conjugated donkey anti-rabbit and anti-mouse at 1:5000 (Jackson ImmunoResearch 711-035-152 and 711-035-150, respectively).

6.9 Cell culture and co-immunoaffinity purification

HEK293 cells were cultured in DMEM (ThermoFisher 11995065), supplemented with 10% heat-inactivated fetal bovine serum (Sigma F4135) and penicillin/streptomycin (ThermoFisher 15140-122). Transfections were performed using FuGENE HD (Promega E2311) according to the manufacturer protocol. Transfected cells were lysed with homogenization buffer and centrifuged at 20,000 *g* for 10 minutes. The supernatant was incubated with either anti-FLAG® M2 affinity gel or anti-GFP, as was done with worm lysate (see above).

6.10 Immunofluorescence

HEK293 cells were transfected with a lentiviral construct containing LGC-34-GFP (pWW12) and lentiviral packaging plasmids. Two days later, the supernatant

was collected to transduce NIH-3T3 cells. To make the stable IGDB-2-3xFLAG cell line, NIH-3T3 cells were again transduced with a lentivirus expressing IGDB-2-3xFLAG (pWW13), but after two days, underwent puromycin selection (3 μg/ml).

For cell staining, the above protocol was used, but cells were grown on gelatin-coated coverslips. After the two-day infection, they were fixed with 4% paraformaldehyde for 15 minutes, washed with PBS, incubated with 0.2% Triton X-100 (TX-100) in PBS for 5 minutes, washed with PBS. The cells were then incubated with primary antibodies in a PBS solution of 2% BSA and 0.2 TX-100 for 1 hour, washed with PBS, and incubated with secondary antibodies in the same PBS solution. After washing, cells were mounted to a slide with mounting fluid containing DAPI. Primary antibodies were the same as those used for Western blot analysis, each at 1:2000 (see Section 6.8). Secondary antibodies were the Cy™3 AffiniPure Goat Anti-Mouse IgG (H+L) and Alexa Fluor® 488 AffiniPure Goat Anti-Rabbit IgG (H+L) (Jackson ImmunoResearch 115-165-146 and 111-545-144, respectively), each at 1:250.

6.11 PNGase F assay

The PNGase F assay was performed under denaturing conditions, according to the manufacturer protocol (NEB P0704S). 5 μl and 9 μl of supernatant from IGDB-2 ::GFP::3xFLAG- and DAF-6::GFP::3xFLAG-expressing worms (prepared as in section 6.8) were used per 10 μl reaction.

6.12 CRISPR/Cas9 generation of *ns793*

Deletion alleles were generated using a co-CRISPR strategy with *dpy-10* as a co-CRISPR marker (Arribere et al., 2014). pWW14 and pWW15 were injected into *daf-6*(*e1377*) animals, along with pDD162-*dpy-10*(sgRNA) and a *dpy-10* repair oligo.

Appendix.

This appendix provides supplemental data to more thoroughly support previous findings in Chapters 2 and 3. First, I provide an electron micrograph, taken by Yun Lu, of a complete cross-section through the amphid of an *igdb-2*; *daf-6* mutant. As discussed in Chapter 2, this animal dye-filled in one of its two amphid organs, and allows a comparison between the two amphids at the ultrastructural level. Second, a dye-filling assay was conducted for the (double or triple) mutants of several *igdb-2* interactor candidates. Third, a dye-filling assay was conducted for control strains for *lgc-34* (as previously mentioned, the *lgc-34* mutant phenotype is apparent in the *igdb-2*; *daf-6* mutants).

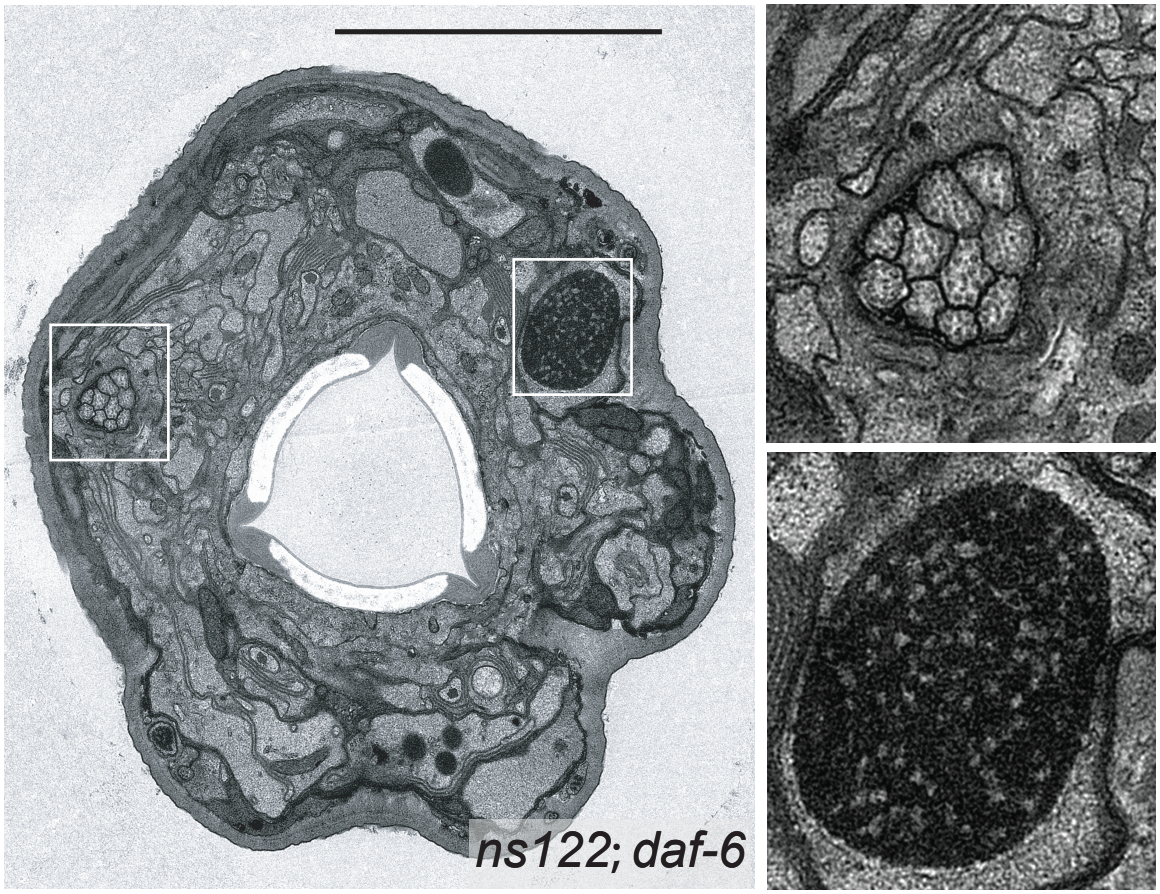

Figure S1. *ns122* suppression of the *daf-6* dye-filling defect correlates with normal amphid channel morphology.
TEM of a cross-section through the head of an *ns122; daf-6*(*e1377*) adult with one dye-filled amphid. The left and right amphid channels are outlined, and shown in greater detail in the top and bottom insets, respectively. Only the left amphid channel appears normal. The right channel is displaced and full of dark staining matrix. Scale bar, 5 μm.

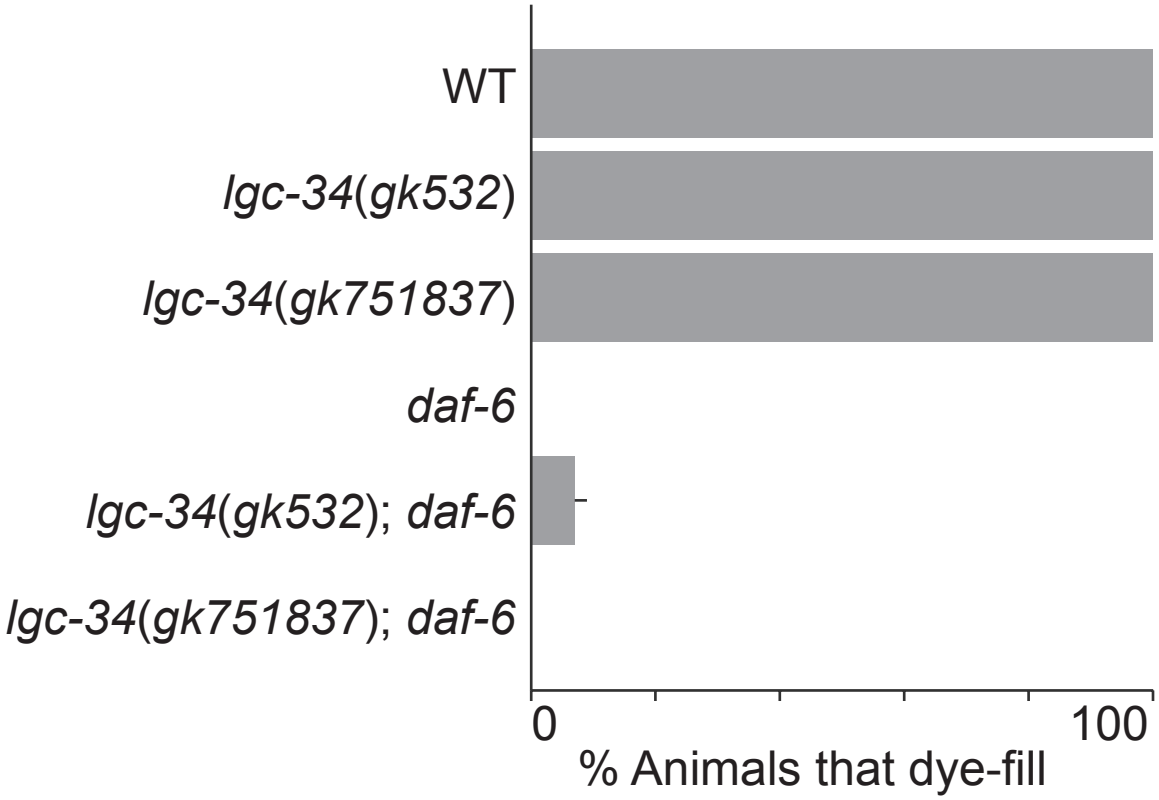

Fig. S2. *lgc-34* mutants show no significant dye-filling defects as single or double mutants with *daf-6.*
Dye-filling assay for indicated genotypes. Alleles used are: *daf-6*(*e1377*), *lgc-34*(*gk532*), and *lgc-34*(*gk751837*). $n \geq 100$. Error bars, SEM, from ≥ 3 experiments.

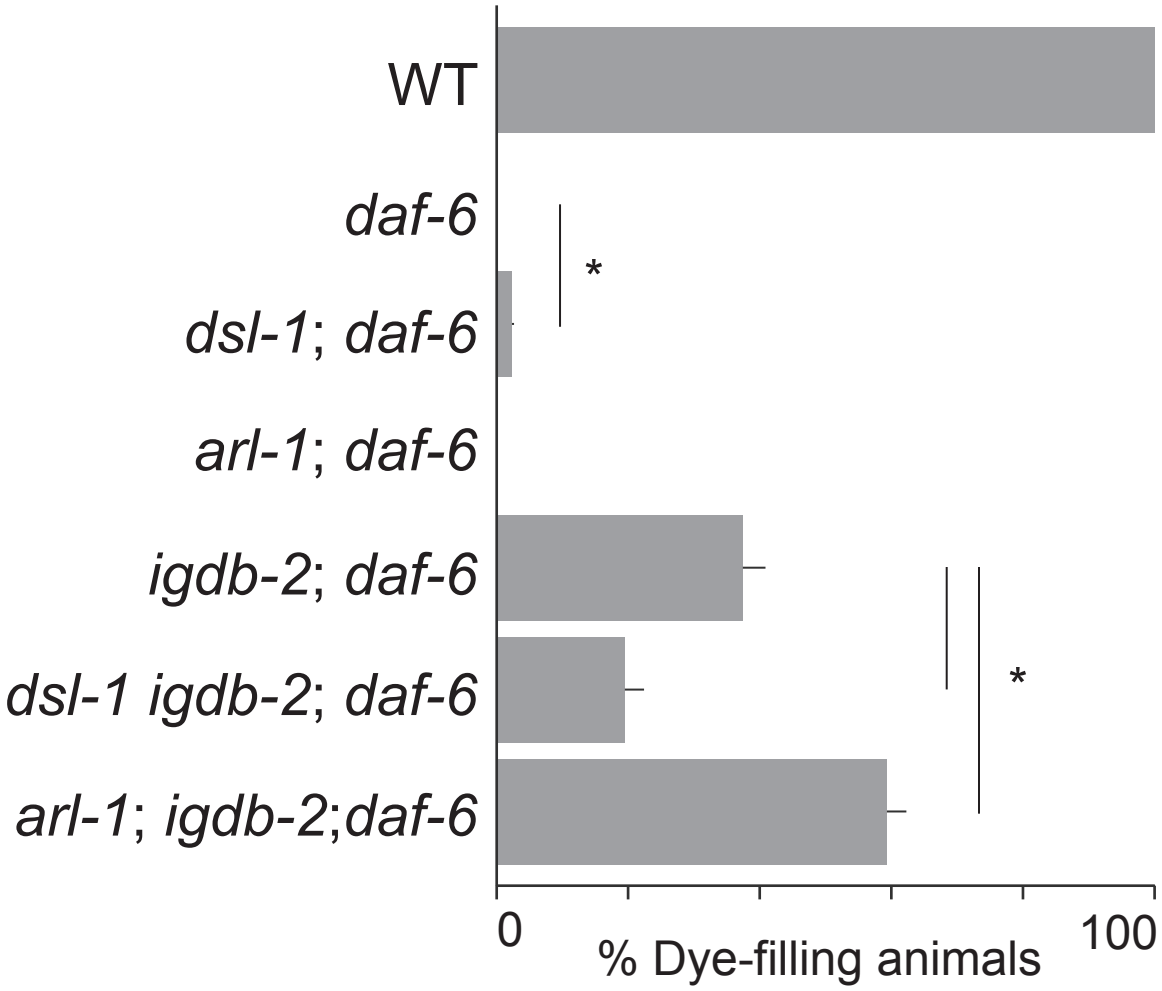

Figure S3. Potential IGDB-2 interactors have dye-filling phenotypes.
Dye-filling assay for indicated genotypes. Alleles used are: *daf-6*(*e1377*), *arl-1*(*tm1938*), *dsl-1*(*ok810*), and *igdb-2*(*ns122*). $n \geq 100$. Error bars, SEM, from ≥ 3 experiments. *$p < 0.0061$, n.s. not significant, unpaired *t*-test.

Table S1. List of abbreviations.

Abbreviation	Explanation
AFD neuron	Amphid finger cell D (thermosensory neuron)
AMsh cell	Amphid sheath cell
AMso cell	Amphid socket cell
AS-C	*achaete-scute* gene complex (four basic helix-loop-helix transcription factors) that regulates neuroblast fate specification
CAM	Cell adhesion molecule
CLIC	Chloride intracellular channel
FNIII	Fibronectin type III domain
GFAP	Glial fibrillary acidic protein
GLR cells	Three pairs of glia associated with the nerve ring and form gap junctions on head muscle cells
HGF	Hepatocyte growth factor
Ig-like	Immunoglobulin-like domain
IgCAM	Ig cell adhesion molecule
IGDB-2	Ig domain- and fibronectin type III domain-containing protein 2
IgSF	Ig superfamily
IPM	Interphotoreceptor matrix (between photoreceptors and retinal pigment epithelial cells)
LGC	Ligand-gated ion channel of the Cys-loop superfamily
LGIC	Ligand-gated ion channel
LGII, -III, -IV, -X	Linkage group (corresponds to chromosome) II, III, IV, X
NCAM-140	Neural cell adhesion molecule (140 kDa cytoplasmic isoform)
NGM	Nematode growth medium
NRE	Neuronal receptive ending
OHC	Outer hair cell
ORN	Olfactory receptor neuron
PATJ	PALS1 (protein-associated with Lin7, Stardust, MPP5)-associated tight junction protein (apical marker)
PTR	Patched-related protein
RGM	Repulsive guidance molecule
RMS	Rostral migratory stream (path between subventricular zone and olfactory bulb in mammals)
RPE cells	Retinal pigment epithelial cells
SOP cell	Sensory organ precursor cell
TIFR glia	Transient-Interhemispheric-Fibrous-Ring glia in *Drosophila*
VAC	Vacuolar apical compartment
WASP	Wiskott-Aldrich Syndrome Protein
WIRS	WRC-interacting receptor sequence

Table S1. List of abbreviations (continued).

Abbreviation	Explanation
WRC	WAVE regulatory complex: WASP-family verprolin homologous protein 1 (WAVE1), CYFIP1, ABI2, Nap1 and HSPC300
XLAG	X-linked lissencephaly with abnormal genitalia
ZP domain	Zona pellucida-like domain (functions in protein binding and polymerization)

References

Albert, P.S., Brown, S.J., Riddle, D.L., 1981. Sensory control of dauer larva formation in Caenorhabditis elegans. The Journal of comparative neurology 198, 435-451.

Alberts, B., Johnson, A., Lewis, J., et al. , 2002. Ion Channels and the Electrical Properties of Membranes. , Molecular Biology of the Cell., 4th edition ed. Garland Science, New York.

Allen, B.L., Song, J.Y., Izzi, L., Althaus, I.W., Kang, J.-S., Charron, F., Krauss, R.S., McMahon, A.P., 2011. Overlapping roles and collective requirement for the co-receptors Gas1, Cdo and Boc in Shh pathway function. Developmental cell 20, 775-787.

Anttonen, T., Kirjavainen, A., Belevich, I., Laos, M., Richardson, W.D., Jokitalo, E., Brakebusch, C., Pirvola, U., 2012. Cdc42-dependent structural development of auditory supporting cells is required for wound healing at adulthood. 2, 978.

Arey, B.J., 2012. The Role of Glycosylation in Receptor Signaling, in: Petrescu, S. (Ed.), Glycosylation. InTech, Rijeka, p. Ch. 12.

Arribere, J.A., Bell, R.T., Fu, B.X.H., Artiles, K.L., Hartman, P.S., Fire, A.Z., 2014. Efficient Marker-Free Recovery of Custom Genetic Modifications with CRISPR/Cas9 in *Caenorhabditis elegans*. Genetics 198, 837-846.

Ashmore, J., 2008. Cochlear Outer Hair Cell Motility. Physiological Reviews 88, 173-210.

Awasaki, T., Ito, K., 2004. Engulfing Action of Glial Cells Is Required for Programmed Axon Pruning during Drosophila Metamorphosis. Current Biology 14, 668-677.

Bacaj, T., Tevlin, M., Lu, Y., Shaham, S., 2008. Glia are essential for sensory organ function in C. elegans. Science 322, 744-747.

Barnett, S.C., Chang, L., 2004. Olfactory ensheathing cells and CNS repair: going solo or in need of a friend? Trends in neurosciences 27, 54-60.

Bayless, K.J., Davis, G.E., 2002. The Cdc42 and Rac1 GTPases are required for capillary lumen formation in three-dimensional extracellular matrices. Journal of cell science 115, 1123-1136.

Berry, K.L., Bülow, H.E., Hall, D.H., Hobert, O., 2003. A *C. elegans* CLIC-like Protein Required for Intracellular Tube Formation and Maintenance. Science 302, 2134-2137.

Bilder, D., Schober, M., Perrimon, N., 2003. Integrated activity of PDZ protein complexes regulates epithelial polarity. Nature cell biology 5, 53-58.

Binder, D.K., Nagelhus, E.A., Ottersen, O.P., 2012. Aquaporin-4 and epilepsy. Glia 60, 1203-1214.

Blockus, H., Chédotal, A., 2016. Slit-Robo signaling. Development 143, 3037-3044.

Bok, D., 1993. The retinal pigment epithelium: a versatile partner in vision. Journal of cell science. Supplement 17, 189-195.

Brenner, S., 1974. The genetics of *Caenorhabditis elegans.* Genetics 77, 71-94.

Bringmann, A., Biedermann, B., Reichenbach, A., 1999. Expression of potassium channels during postnatal differentiation of rabbit Muller glial cells. The European journal of neuroscience 11, 2883-2896.

Briscoe, J., Thérond, P.P., 2013. The mechanisms of Hedgehog signalling and its roles in development and disease. Nature reviews. Molecular cell biology 14, 416-429.

Buechner, M., 2002. Tubes and the single C. elegans excretory cell. Trends in cell biology 12, 479-484.

Bürglin, T.R., Kuwabara, P.E., 2006. Homologs of the Hedgehog signalling network in *C. elegans*. . WormBook.

Burket, C.T., Higgins, C.E., Hull, L.C., Berninsone, P.M., Ryder, E.F., 2006. The C. elegans gene dig-1 encodes a giant member of the immunoglobulin superfamily that promotes fasciculation of neuronal processes. Developmental biology 299, 193-205.

Burnashev, N., Khodorova, A., Jonas, P., Helm, P., Wisden, W., Monyer, H., Seeburg, P., Sakmann, B., 1992. Calcium-permeable AMPA-kainate receptors in fusiform cerebellar glial cells. Science 256, 1566-1570.

Camp, D., Currie, K., Labbé, A., van Meyel, D.J., Charron, F., 2010. Ihog and Boi are essential for Hedgehog signaling in Drosophila. Neural development 5, 28.

Caviglia, S., Brankatschk, M., Fischer, E.J., Eaton, S., Luschnig, S., 2016. Staccato/Unc-13-4 controls secretory lysosome-mediated lumen fusion during epithelial tube anastomosis. Nature cell biology 18, 727-739.

Chen, W., Hing, H., 2008. The L1-CAM, Neuroglian, functions in glial cells for Drosophila antennal lobe development. Developmental Neurobiology 68, 1029-1045.

Chun, T.-H., Sabeh, F., Ota, I., Murphy, H., McDonagh, K.T., Holmbeck, K., Birkedal-Hansen, H., Allen, E.D., Weiss, S.J., 2004. MT1-MMP–dependent neovessel formation

within the confines of the three-dimensional extracellular matrix. The Journal of cell biology 167, 757-767.

Chung, Y.D., Zhu, J., Han, Y., Kernan, M.J., 2001. nompA encodes a PNS-specific, ZP domain protein required to connect mechanosensory dendrites to sensory structures. Neuron 29, 415-428.

Colón-Ramos, D.A., Margeta, M.A., Shen, K., 2007. Glia Promote Local Synaptogenesis Through UNC-6 (Netrin) Signaling in C. elegans. Science (New York, N.Y.) 318, 103-106.

Connolly, C.N., Wafford, K.A., 2004. The Cys-loop superfamily of ligand-gated ion channels: The impact of receptor structure on function. Biochemical Society Transactions 32, 529-534.

Copley, C.O., Duncan, J.S., Liu, C., Cheng, H., Deans, M.R., 2013. Postnatal Refinement of Auditory Hair Cell Planar Polarity Deficits Occurs in the Absence of Vangl2. The Journal of Neuroscience 33, 14001-14016.

Cornell-Bell, A.H., Thomas, P.G., Smith, S.J., 1990. The excitatory neurotransmitter glutamate causes filopodia formation in cultured hippocampal astrocytes. Glia 3, 322-334.

Davis, G.E., Camarillo, C.W., 1996. An α2β1 Integrin-Dependent Pinocytic Mechanism Involving Intracellular Vacuole Formation and Coalescence Regulates Capillary Lumen and Tube Formation in Three-Dimensional Collagen Matrix. Experimental cell research 224, 39-51.

Davis, G.E., Koh, W., Stratman, A.N., 2007. Mechanisms controlling human endothelial lumen formation and tube assembly in three-dimensional extracellular matrices. Birth Defects Research Part C: Embryo Today: Reviews 81, 270-285.

Davis, G.E., Senger, D.R., 2005. Endothelial Extracellular Matrix. Biosynthesis, Remodeling, and Functions During Vascular Morphogenesis and Neovessel Stabilization 97, 1093-1107.

Devinsky, O., Vezzani, A., Najjar, S., De Lanerolle, N.C., Rogawski, M.A., 2013. Glia and epilepsy: excitability and inflammation. Trends in neurosciences 36, 174-184.

Dong, B., Hannezo, E., Hayashi, S., 2014. Balance between Apical Membrane Growth and Luminal Matrix Resistance Determines Epithelial Tubule Shape. Cell Reports 7, 941-950.

Eliceiri, B.P., Puente, X.S., Hood, J.D., Stupack, D.G., Schlaepfer, D.D., Huang, X.Z., Sheppard, D., Cheresh, D.A., 2002. Src-mediated coupling of focal adhesion kinase to

integrin αvβ5 in vascular endothelial growth factor signaling. The Journal of cell biology 157, 149-160.

Etienne-Manneville, S., Hall, A., 2001. Integrin-mediated activation of Cdc42 controls cell polarity in migrating astrocytes through PKCzeta. Cell 106, 489-498.

Felton, C.M., Johnson, C.M., 2011. Modulation of dopamine-dependent behaviors by the Caenorhabditis elegans Olig homolog HLH-17. Journal of neuroscience research 89, 1627-1636.

Fischer-Lougheed, J., Liu, J.H., Espinos, E., Mordasini, D., Bader, C.R., Belin, D., Bernheim, L., 2001. Human myoblast fusion requires expression of functional inward rectifier Kir2.1 channels. The Journal of cell biology 153, 677-686.

Freeman, M.R., 2010. Specification and Morphogenesis of Astrocytes. Science 330, 774-778.

Furman, D.P., Bukharina, T.A., 2008. How Drosophila melanogaster Forms its Mechanoreceptors. Current Genomics 9, 312-323.

Gahmberg, C.G., Tolvanen, M., 1996. Why mammalian cell surface proteins are glycoproteins. Trends in Biochemical Sciences 21, 308-311.

Galindo, A., Soler, N., McLaughlin, S.H., Yu, M., Williams, R.L., Munro, S., 2016. Structural Insights into Arl1-Mediated Targeting of the Arf-GEF BIG1 to the trans-Golgi. Cell Rep 16, 839-850.

Galliot, B., de Vargas, C., Miller, D., 1999. Evolution of homeobox genes: Q50 Paired-like genes founded the Paired class. Development genes and evolution 209, 186-197.

García-Bellido, A., de Celis, J.F., 2009. The Complex Tale of the achaete–scute Complex: A Paradigmatic Case in the Analysis of Gene Organization and Function During Development. Genetics 182, 631-639.

Getchell, T.V., 1986. Functional properties of vertebrate olfactory receptor neurons. Physiological Reviews 66, 772-818.

Gettner, S.N., Kenyon, C., Reichardt, L.F., 1995. Characterization of beta pat-3 heterodimers, a family of essential integrin receptors in C. elegans. The Journal of cell biology 129, 1127-1141.

Ghosh, A., Manrique-Hoyos, N., Voigt, A., Schulz, J.B., Kreutzfeldt, M., Merkler, D., Simons, M., 2011. Targeted Ablation of Oligodendrocytes Triggers Axonal Damage. PloS one 6, e22735.

Goulding, S.E., zur Lage, P., Jarman, A.P., 2000. amos, a Proneural Gene for Drosophila Olfactory Sense Organs that Is Regulated by lozenge. Neuron 25, 69-78.

Gower, N.J.D., Temple, G.R., Schein, J.E., Marra, M., Walker, D.S., Baylis, H.A., 2001. Dissection of the promoter region of the inositol 1,4,5-trisphosphate receptor gene, itr-1, in C. elegans: a molecular basis for cell-specific expression of IP3R isoforms1. Journal of molecular biology 306, 145-157.

Green, W.N., Wanamaker, C.P., 1997. The Role of the Cystine Loop in Acetylcholine Receptor Assembly. Journal of Biological Chemistry 272, 20945-20953.

Grutter, T., de Carvalho, L.P., Dufresne, V., Taly, A., Edelstein, S.J., Changeux, J.-P., 2005. Molecular tuning of fast gating in pentameric ligand-gated ion channels. Proceedings of the National Academy of Sciences of the United States of America 102, 18207-18212.

Hartenstein, V., Posakony, J.W., 1989. Development of adult sensilla on the wing and notum of Drosophila melanogaster. Development 107, 389-405.

Hayashi, S., Dong, B., 2017. Shape and geometry control of the Drosophila tracheal tubule. Development, Growth & Differentiation 59, 4-11.

Hedgecock, E.M., Culotti, J.G., Hall, D.H., 1990. The unc-5, unc-6, and unc-40 genes guide circumferential migrations of pioneer axons and mesodermal cells on the epidermis in C. elegans. Neuron 4, 61-85.

Hegg, C.C., Irwin, M., Lucero, M.T., 2009. Calcium store-mediated signaling in sustentacular cells of the mouse olfactory epithelium. Glia 57, 634-644.

Heiman, M.G., Shaham, S., 2009. DEX-1 and DYF-7 establish sensory dendrite length by anchoring dendritic tips during cell migration. Cell 137, 344-355.

Herman, R.K., 1987. Mosaic Analysis of Two Genes That Affect Nervous System Structure in Caenorhabditis elegans. Genetics 116, 377-388.

Hernando, G., Bouzat, C., 2014. Caenorhabditis elegans Neuromuscular Junction: GABA Receptors and Ivermectin Action. PloS one 9, e95072.

Hibino, H., Inanobe, A., Furutani, K., Murakami, S., Findlay, I., Kurachi, Y., 2010. Inwardly Rectifying Potassium Channels: Their Structure, Function, and Physiological Roles. Physiological Reviews 90, 291-366.

Hochman, D.W., 2012. The extracellular space and epileptic activity in the adult brain: Explaining the antiepileptic effects of furosemide and bumetanide. Epilepsia 53, 18-25.

Holtzclaw, L.A., Gallo, V., Russell, J.T., 1995. AMPA receptors shape Ca2+ responses in cortical oligodendrocyte progenitors and CG-4 cells. Journal of neuroscience research 42, 124-130.

Hortsch, M., Bieber, A.J., Patel, N.H., Goodman, C.S., 1990. Differential splicing generates a nervous system—Specific form of drosophila neuroglian. Neuron 4, 697-709.

Hu, P.J., 2007. Dauer. WormBook.

Hutterer, A., Betschinger, J., Petronczki, M., Knoblich, J.A., 2004. Sequential Roles of Cdc42, Par-6, aPKC, and Lgl in the Establishment of Epithelial Polarity during Drosophila Embryogenesis. Developmental cell 6, 845-854.

Inglis, P.N., Ou, G., Leroux, M.R., Scholey, J.M., 2007. The sensory cilia of *Caenorhabditis elegans*. WormBook.

Iruela-Arispe, M.L., Beitel, G.J., 2013. Tubulogenesis. Development 140, 2851-2855.

Iruela-Arispe, M.L., Davis, G.E., Cellular and Molecular Mechanisms of Vascular Lumen Formation. Developmental cell 16, 222-231.

Jendelová, P., Syková, E., 1991. Role of glia in K+ and pH homeostasis in the neonatal rat spinal cord. Glia 4, 56-63.

Jensen, M.L., Schousboe, A., Ahring, P.K., 2005. Charge selectivity of the Cys-loop family of ligand-gated ion channels. Journal of neurochemistry 92, 217-225.

Joberty, G., Petersen, C., Gao, L., Macara, I.G., 2000. The cell-polarity protein Par6 links Par3 and atypical protein kinase C to Cdc42. Nature cell biology 2, 531-539.

Jones, A.K., Sattelle, D.B., 2008. The cys-loop ligand-gated ion channel gene superfamily of the nematode, Caenorhabditis elegans. Invertebrate Neuroscience 8, 41-47.

Kaneko, N., Marín, O., Koike, M., Hirota, Y., Uchiyama, Y., Wu, J.Y., Lu, Q., Tessier-Lavigne, M., Alvarez-Buylla, A., Okano, H., Rubenstein, J.L.R., Sawamoto, K., 2010. New Neurons Clear the Path of Astrocytic Processes for Their Rapid Migration in the Adult Brain. Neuron 67, 213-223.

Kang, J.-S., Yi, M.-J., Zhang, W., Feinleib, J.L., Cole, F., Krauss, R.S., 2004. Netrins and neogenin promote myotube formation. The Journal of cell biology 167, 493-504.

Kato, M., Das, S., Petras, K., Kitamura, K., Morohashi, K., Abuelo, D.N., Barr, M., Bonneau, D., Brady, A.F., Carpenter, N.J., Cipero, K.L., Frisone, F., Fukuda, T., Guerrini, R., Iida, E., Itoh, M., Lewanda, A.F., Nanba, Y., Oka, A., Proud, V.K., Saugier-Veber, P.,

Schelley, S.L., Selicorni, A., Shaner, R., Silengo, M., Stewart, F., Sugiyama, N., Toyama, J., Toutain, A., Vargas, A.L., Yanazawa, M., Zackai, E.H., Dobyns, W.B., 2004. Mutations of ARX are associated with striking pleiotropy and consistent genotype-phenotype correlation. Human mutation 23, 147-159.

Kee, N., Wilson, N., De Vries, M., Bradford, D., Key, B., Cooper, H.M., 2008. Neogenin and RGMa Control Neural Tube Closure and Neuroepithelial Morphology by Regulating Cell Polarity. The Journal of Neuroscience 28, 12643-12653.

Kee, N., Wilson, N., Key, B., Cooper, H.M., 2013. Netrin-1 is required for efficient neural tube closure. Developmental Neurobiology 73, 176-187.

Kidd, T., Bland, K.S., Goodman, C.S., 1999. Slit Is the Midline Repellent for the Robo Receptor in *Drosophila*. Cell 96, 785-794.

Kitamura, K., Yanazawa, M., Sugiyama, N., Miura, H., Iizuka-Kogo, A., Kusaka, M., Omichi, K., Suzuki, R., Kato-Fukui, Y., Kamiirisa, K., Matsuo, M., Kamijo, S., Kasahara, M., Yoshioka, H., Ogata, T., Fukuda, T., Kondo, I., Kato, M., Dobyns, W.B., Yokoyama, M., Morohashi, K., 2002. Mutation of ARX causes abnormal development of forebrain and testes in mice and X-linked lissencephaly with abnormal genitalia in humans. Nature genetics 32, 359-369.

Knutson, P., Ghiani, C.A., Zhou, J.M., Gallo, V., McBain, C.J., 1997. K+ channel expression and cell proliferation are regulated by intracellular sodium and membrane depolarization in oligodendrocyte progenitor cells. The Journal of neuroscience : the official journal of the Society for Neuroscience 17, 2669-2682.

Krasnow, M.A., Manning, G., 1993. Development of the *Drosophila* tracheal system., in: Bate, M., Ariase, M.-A. (Ed.), The Development of *Drosophila melanogaster*. Cold Spring Harbor Laboratory Press, Cold Spring Harbor, New York, USA., pp. 609-685.

Landmann, F., Quintin, S., Labouesse, M., 2004. Multiple regulatory elements with spatially and temporally distinct activities control the expression of the epithelial differentiation gene lin-26 in C. elegans. Developmental biology 265, 478-490.

Lee, N.K., Fok, K.W., White, A., Wilson, N.H., O'Leary, C.J., Cox, H.L., Michael, M., Yap, A.S., Cooper, H.M., 2016. Neogenin recruitment of the WAVE regulatory complex maintains adherens junction stability and tension. 7, 11082.

Leem, Y.-E., Jeong, H.-J., Kim, H.-J., Koh, J., Kang, K., Bae, G.-U., Cho, H., Kang, J.-S., 2016. Cdo Regulates Surface Expression of Kir2.1 K+ Channel in Myoblast Differentiation. PloS one 11, e0158707.

Leiserson, W.M., Keshishian, H., 2011. Maintenance and regulation of extracellular volume and the ion environment in Drosophila larval nerves. Glia 59, 1312-1321.

Leung, B., Hermann, G.J., Priess, J.R., 1999. Organogenesis of the Caenorhabditis elegans intestine. Developmental biology 216, 114-134.

Lipschutz, J.H., Guo, W., O'Brien, L.E., Nguyen, Y.H., Novick, P., Mostov, K.E., 2000. Exocyst Is Involved in Cystogenesis and Tubulogenesis and Acts by Modulating Synthesis and Delivery of Basolateral Plasma Membrane and Secretory Proteins. Molecular Biology of the Cell 11, 4259-4275.

Lipschutz, J.H., Lingappa, V.R., Mostov, K.E., 2003. The Exocyst Affects Protein Synthesis by Acting on the Translocation Machinery of the Endoplasmic Reticulum. Journal of Biological Chemistry 278, 20954-20960.

Liu, H.N., Almazan, G., 1995. Glutamate induces c-fos proto-oncogene expression and inhibits proliferation in oligodendrocyte progenitors: receptor characterization. The European journal of neuroscience 7, 2355-2363.

Lubarsky, B., Krasnow, M.A., 2003. Tube Morphogenesis. Cell 112, 19-28.

Luschnig, S., Bätz, T., Armbruster, K., Krasnow, M.A., 2006. serpentine and vermiform Encode Matrix Proteins with Chitin Binding and Deacetylation Domains that Limit Tracheal Tube Length in Drosophila. Current Biology 16, 186-194.

Macias, H., Moran, A., Samara, Y., Moreno, M., Compton, J.E., Harburg, G., Strickland, P., Hinck, L., 2011. SLIT/ROBO1 signaling suppresses mammary branching morphogenesis by limiting basal cell number. Developmental cell 20, 827-840.

MacVicar, B.A., Feighan, D., Brown, A., Ransom, B., 2002. Intrinsic optical signals in the rat optic nerve: role for K(+) uptake via NKCC1 and swelling of astrocytes. Glia 37, 114-123.

Maley, F., Trimble, R.B., Tarentino, A.L., Plummer, T.H., Jr., 1989. Characterization of glycoproteins and their associated oligosaccharides through the use of endoglycosidases. Analytical biochemistry 180, 195-204.

Marmorstein, A.D., Finnemann, S.C., Bonilha, V.L., Rodriguez-Boulan, E., 1998. Morphogenesis of the Retinal Pigment Epithelium: Toward Understanding Retinal Degenerative Diseasesa. Annals of the New York Academy of Sciences 857, 1-12.

Martin-Belmonte, F., Gassama, A., Datta, A., Yu, W., Rescher, U., Gerke, V., Mostov, K., 2007. PTEN-Mediated Apical Segregation of Phosphoinositides Controls Epithelial Morphogenesis through Cdc42. Cell 128, 383-397.

Matusek, T., Djiane, A., Jankovics, F., Brunner, D., Mlodzik, M., Mihály, J., 2006. The *Drosophila* formin DAAM regulates the tracheal cuticle pattern through organizing the actin cytoskeleton. Development 133, 957-966.

Mawdsley, D.J., Cooper, H.M., Hogan, B.M., Cody, S.H., Lieschke, G.J., Heath, J.K., 2004. The Netrin receptor Neogenin is required for neural tube formation and somitogenesis in zebrafish. Developmental biology 269, 302-315.

McKay, S.J., Johnsen, R., Khattra, J., Asano, J., Baillie, D.L., Chan, S., Dube, N., Fang, L., Goszczynski, B., Ha, E., Halfnight, E., Hollebakken, R., Huang, P., Hung, K., Jensen, V., Jones, S.J.M., Kai, H., Li, D., Mah, A., Marra, M., Mcghee, J., Newbury, R., Pouzyrev, A., Riddle, D.L., Sonnhammer, E., Tian, H., Tu, D., Tyson, J.R., Vatcher, G., Warner, A., Wong, K., Zhao, Z., Moerman, D.G., 2003. Gene Expression Profiling of Cells, Tissues, and Developmental Stages of the Nematode C. elegans. Cold Spring Harbor symposia on quantitative biology 68, 159-170.

McKeown, C., Praitis, V., Austin, J., 1998. sma-1 encodes a betaH-spectrin homolog required for Caenorhabditis elegans morphogenesis. Development 125, 2087-2098.

McMahon, A.P., Ingham, P.W., Tabin, C.J., 2003. 1 Developmental roles and clinical significance of Hedgehog signaling. Current topics in developmental biology 53, 1-114.

McNaughton, L.A., Hunt, S.P., 1992. Regulation of gene expression in astrocytes by excitatory amino acids. Molecular Brain Research 16, 261-266.

Medioni, C., Astier, M., Zmojdzian, M., Jagla, K., Sémériva, M., 2008. Genetic control of cell morphogenesis during Drosophila melanogaster cardiac tube formation. The Journal of cell biology 182, 249-261.

Meissner, B., Rogalski, T., Viveiros, R., Warner, A., Plastino, L., Lorch, A., Granger, L., Segalat, L., Moerman, D.G., 2011. Determining the Sub-Cellular Localization of Proteins within Caenorhabditis elegans Body Wall Muscle. PloS one 6, e19937.

Mets, D.G., Meyer, B.J., 2009. Condensins regulate meiotic DNA break distribution, thus crossover frequency, by controlling chromosome structure. Cell 139, 73-86.

Michaux, G., Gansmuller, A., Hindelang, C., Labouesse, M., 2000. CHE-14, a protein with a sterol-sensing domain, is required for apical sorting in C. elegans ectodermal epithelial cells. Current Biology 10, 1098-1107.

Miska, E.A., Alvarez-Saavedra, E., Abbott, A.L., Lau, N.C., Hellman, A.B., McGonagle, S.M., Bartel, D.P., Ambros, V.R., Horvitz, H.R., 2007. Most Caenorhabditis elegans microRNAs Are Individually Not Essential for Development or Viability. PLOS Genetics 3, e215.

Monk, K.R., Feltri, M.L., Taveggia, C., 2015. New insights on schwann cell development. Glia 63, 1376-1393.

Montesano, R., Schaller, G., Orci, L., 1991. Induction of epithelial tubular morphogenesis in vitro by fibroblast-derived soluble factors. Cell 66, 697-711.

Murai, K.K., Nguyen, L.N., Irie, F., Yamaguchi, Y., Pasquale, E.B., 2003. Control of hippocampal dendritic spine morphology through ephrin-A3/EphA4 signaling. Nature neuroscience 6, 153-160.

Nelson, K.F., Albert, P.S., Riddle, D.L., 1983. Fine structure of the Caenorhabditis elegans secretory—excretory system. Journal of Ultrastructure Research 82, 156-171.

Oikonomou, G., 2011. Sensory Organ Morphogenesis in *Caenorhabditis elegans*, Developmental Genetics. Rockefeller University, New York.

Oikonomou, G., Perens, E.A., Lu, Y., Shaham, S., 2012. Some, but not all, retromer components promote morphogenesis of C. elegans sensory compartments. Developmental biology 362, 42-49.

Oikonomou, G., Perens, E.A., Lu, Y., Watanabe, S., Jorgensen, E.M., Shaham, S., 2011. Opposing activities of LIT-1/NLK and DAF-6/patched-related direct sensory compartment morphogenesis in C. elegans. PLoS biology 9, e1001121.

Oikonomou, G., Shaham, S., 2011. The glia of Caenorhabditis elegans. Glia 59, 1253-1263.

Olsen, M.L., Khakh, B.S., Skatchkov, S.N., Zhou, M., Lee, C.J., Rouach, N., 2015. New Insights on Astrocyte Ion Channels: Critical for Homeostasis and Neuron-Glia Signaling. The Journal of Neuroscience 35, 13827-13835.

Perea, G., Araque, A., 2005. Glial calcium signaling and neuron–glia communication. Cell Calcium 38, 375-382.

Perens, E.A., 2006. The roles of *daf-6* and cell-cell interactions in sensory organ morphogenesis., Developmental Genetics. Rockefeller University, New York.

Perens, E.A., Shaham, S., 2005. C. elegans daf-6 encodes a patched-related protein required for lumen formation. Developmental cell 8, 893-906.

Perkins, L.A., Hedgecock, E.M., Thomson, J.N., Culotti, J.G., 1986. Mutant sensory cilia in the nematode Caenorhabditis elegans. Developmental biology 117, 456-487.

Pollack, A.L., Runyan, R.B., Mostov, K.E., 1998. Morphogenetic mechanisms of epithelial tubulogenesis: MDCK cell polarity is transiently rearranged without loss of cell-cell contact during scatter factor/hepatocyte growth factor-induced tubulogenesis. Developmental biology 204, 64-79.

Ramón-Cueto, A., Valverde, F., 1995. Olfactory bulb ensheathing glia: A unique cell type with axonal growth-promoting properties. Glia 14, 163-173.

Ribeiro, C., Neumann, M., Affolter, M., 2004. Genetic Control of Cell Intercalation during Tracheal Morphogenesis in Drosophila. Current Biology 14, 2197-2207.

Ringstad, N., Abe, N., Horvitz, H.R., 2009. Ligand-Gated Chloride Channels Are Receptors for Biogenic Amines in *C. elegans.* Science 325, 96-100.

Rio, C., Dikkes, P., Liberman, M.C., Corfas, G., 2002. Glial fibrillary acidic protein expression and promoter activity in the inner ear of developing and adult mice. The Journal of comparative neurology 442, 156-162.

Robert, A., Magistretti, P.J., 1997. AMPA/kainate receptor activation blocks K+ currents via internal Na+ increase in mouse cultured stellate astrocytes. Glia 20, 38-50.

Rocheleau, C.E., Yasuda, J., Shin, T.H., Lin, R., Sawa, H., Okano, H., Priess, J.R., Davis, R.J., Mello, C.C., 1999. WRM-1 activates the LIT-1 protein kinase to transduce anterior/posterior polarity signals in C. elegans. Cell 97, 717-726.

Rodriguez, S., Sickles, H.M., DeLeonardis, C., Alcaraz, A., Gridley, T., Lin, D.M., 2008. Notch2 is required for maintaining sustentacular cell function in the adult mouse main olfactory epithelium. Developmental biology 314, 40-58.

Santiago-Martinez, E., Soplop, N.H., Patel, R., Kramer, S.G., 2008. Repulsion by Slit and Roundabout prevents Shotgun/E-cadherin-mediated cell adhesion during Drosophila heart tube lumen formation. The Journal of cell biology 182, 241-248.

Sarov, M., Schneider, S., Pozniakovski, A., Roguev, A., Ernst, S., Zhang, Y., Hyman, A.A., Stewart, A.F., 2006. A recombineering pipeline for functional genomics applied to Caenorhabditis elegans. Nat Meth 3, 839-844.

Sato, K., Nakano, A., 2007. Mechanisms of COPII vesicle formation and protein sorting. FEBS Letters 581, 2076-2082.

Seaman, M.N., 2005. Recycle your receptors with retromer. Trends in cell biology 15, 68-75.

Shaham, S., 2005. Glia-neuron interactions in nervous system function and development. Current topics in developmental biology 69, 39-66.

Shaham, S., 2009. galign: a tool for rapid genome polymorphism discovery. PloS one 4, e7188.

Shaham, S., 2010. Chemosensory organs as models of neuronal synapses. Nature reviews. Neuroscience 11, 212-217.

Shanbhag, S.R., Müller, B., Steinbrecht, R.A., 2000. Atlas of olfactory organs of Drosophila melanogaster. Arthropod Structure & Development 29, 211-229.

Shin, T.H., Yasuda, J., Rocheleau, C.E., Lin, R., Soto, M., Bei, Y., Davis, R.J., Mello, C.C., 1999. MOM-4, a MAP kinase kinase kinase-related protein, activates WRM-1/LIT-1 kinase to transduce anterior/posterior polarity signals in C. elegans. Molecular cell 4, 275-280.

Singhal, A., Shaham, S., 2017. Infrared laser-induced gene expression for tracking development and function of single C. elegans embryonic neurons. Nature Communications 8, 14100.

Singhvi, A., Liu, B., Friedman, Christine J., Fong, J., Lu, Y., Huang, X.-Y., Shaham, S., 2016. A Glial K/Cl Transporter Controls Neuronal Receptive Ending Shape by Chloride Inhibition of an rGC. Cell 165, 936-948.

Srinivasan, K., Strickland, P., Valdes, A., Shin, G.C., Hinck, L., 2003. Netrin-1/Neogenin Interaction Stabilizes Multipotent Progenitor Cap Cells during Mammary Gland Morphogenesis. Developmental cell 4, 371-382.

Starich, T.A., Herman, R.K., Kari, C.K., Yeh, W.H., Schackwitz, W.S., Schuyler, M.W., Collet, J., Thomas, J.H., Riddle, D.L., 1995. Mutations affecting the chemosensory neurons of Caenorhabditis elegans. Genetics 139, 171-188.

Strauss, O., 2005. The Retinal Pigment Epithelium in Visual Function. Physiological Reviews 85, 845-881.

Stromme, P., Mangelsdorf, M.E., Scheffer, I.E., Gecz, J., 2002. Infantile spasms, dystonia, and other X-linked phenotypes caused by mutations in Aristaless related homeobox gene, ARX. Brain & development 24, 266-268.

Sulston, J.E., Albertson, D.G., Thomson, J.N., 1980. The Caenorhabditis elegans male: Postembryonic development of nongonadal structures. Developmental biology 78, 542-576.

Sundaram, M.V., Buechner, M., 2016. The *Caenorhabditis elegans* Excretory System: A Model for Tubulogenesis, Cell Fate Specification, and Plasticity. Genetics 203, 35-63.

Suzuki, A., Ohno, S., 2006. The PAR-aPKC system: lessons in polarity. Journal of cell science 119, 979-987.

Suzuki, N., Buechner, M., Nishiwaki, K., Hall, D.H., Nakanishi, H., Takai, Y., Hisamoto, N., Matsumoto, K., 2001. A putative GDP–GTP exchange factor is required for development of the excretory cell in *Caenorhabditis elegans*. EMBO reports 2, 530-535.

Suzuki, Y., Takeda, M., Farbman, A.I., 1996. Supporting cells as phagocytes in the olfactory epithelium after bulbectomy. The Journal of comparative neurology 376, 509-517.

Svoboda, J., Sykova, E., 1991. Extracellular space volume changes in the rat spinal cord produced by nerve stimulation and peripheral injury. Brain research 560, 216-224.

Swoboda, P., Adler, H.T., Thomas, J.H., 2000. The RFX-Type Transcription Factor DAF-19 Regulates Sensory Neuron Cilium Formation in C. elegans. Molecular cell 5, 411-421.

Sytnyk, V., Leshchyns'ka, I., Schachner, M., 2017. Neural Cell Adhesion Molecules of the Immunoglobulin Superfamily Regulate Synapse Formation, Maintenance, and Function. Trends in neurosciences 40, 295-308.

Teichmann, S.A., Chothia, C., 2000. Immunoglobulin superfamily proteins in Caenorhabditis elegans1. Journal of molecular biology 296, 1367-1383.

Tonning, A., Hemphälä, J., Tång, E., Nannmark, U., Samakovlis, C., Uv, A., 2005. A Transient Luminal Chitinous Matrix Is Required to Model Epithelial Tube Diameter in the Drosophila Trachea. Developmental cell 9, 423-430.

Tsarouhas, V., Senti, K.-A., Jayaram, S.A., Tiklová, K., Hemphälä, J., Adler, J., Samakovlis, C., 2007. Sequential Pulses of Apical Epithelial Secretion and Endocytosis Drive Airway Maturation in Drosophila. Developmental cell 13, 214-225.

Tucker, M., Sieber, M., Morphew, M., Han, M., 2005. The Caenorhabditis elegans aristaless Orthologue, alr-1, Is Required for Maintaining the Functional and Structural Integrity of the Amphid Sensory Organs. Molecular Biology of the Cell 16, 4695-4704.

Ullian, E.M., Sapperstein, S.K., Christopherson, K.S., Barres, B.A., 2001. Control of synapse number by glia. Science 291, 657-661.

Vega-Salas, D.E., Salas, P.J., Rodriguez-Boulan, E., 1987. Modulation of the expression of an apical plasma membrane protein of Madin-Darby canine kidney epithelial cells: cell-cell interactions control the appearance of a novel intracellular storage compartment. The Journal of cell biology 104, 1249-1259.

Verkhratsky, A., Steinhäuser, C., 2000. Ion channels in glial cells. Brain research reviews 32, 380-412.

Wallace, Sean W., Singhvi, A., Liang, Y., Lu, Y., Shaham, S., 2016. PROS-1/Prospero Is a Major Regulator of the Glia-Specific Secretome Controlling Sensory-Neuron Shape and Function in C. elegans. Cell Reports 15, 550-562.

Wang, S., Jayaram, S.A., Hemphälä, J., Senti, K.-A., Tsarouhas, V., Jin, H., Samakovlis, C., 2006. Septate-Junction-Dependent Luminal Deposition of Chitin Deacetylases Restricts Tube Elongation in the Drosophila Trachea. Current Biology 16, 180-185.

Wang, V.Y., Hassan, B.A., Bellen, H.J., Zoghbi, H.Y., 2002. Drosophila atonal Fully Rescues the Phenotype of Math1 Null Mice. Current Biology 12, 1611-1616.

Ward, S., Thomson, N., White, J.G., Brenner, S., 1975. Electron microscopical reconstruction of the anterior sensory anatomy of the nematode caenorhabditis elegans. The Journal of comparative neurology 160, 313-337.

Wicks, S.R., Yeh, R.T., Gish, W.R., Waterston, R.H., Plasterk, R.H.A., 2001. Rapid gene mapping in Caenorhabditis elegans using a high density polymorphism map. Nature genetics 28, 160-164.

Wilson, N.H., Key, B., 2006. Neogenin interacts with RGMa and Netrin-1 to guide axons within the embryonic vertebrate forebrain. Developmental biology 296, 485-498.

Wilson, N.H., Key, B., 2007. Neogenin: One receptor, many functions. The International Journal of Biochemistry & Cell Biology 39, 874-878.

Wolff, J.R., Bär, T., 1972. 'Seamless' endothelia in brain capillaries during development of the rat's cerebral cortex. Brain research 41, 17-24.

Yang, Z., Wang, K.K.W., 2015. Glial fibrillary acidic protein: from intermediate filament assembly and gliosis to neurobiomarker. Trends in neurosciences 38, 364-374.

Yao, S., Lum, L., Beachy, P., 2006. The Ihog Cell-Surface Proteins Bind Hedgehog and Mediate Pathway Activation. Cell 125, 343-357.

Yu, N., Zhao, H.B., 2009. Modulation of outer hair cell electromotility by cochlear supporting cells and gap junctions. PloS one 4, e7923.

Zallen, J.A., Yi, B.A., Bargmann, C.I., 1998. The Conserved Immunoglobulin Superfamily Member SAX-3/Robo Directs Multiple Aspects of Axon Guidance in *C. elegans*. Cell 92, 217-227.

Zhang, X., Bi, E., Novick, P., Du, L., Kozminski, K.G., Lipschutz, J.H., Guo, W., 2001. Cdc42 Interacts with the Exocyst and Regulates Polarized Secretion. Journal of Biological Chemistry 276, 46745-46750.

Zheng, X., Mann, R.K., Sever, N., Beachy, P.A., 2010. Genetic and biochemical definition of the Hedgehog receptor. Genes & development 24, 57-71.

Zinn, K., Özkan, E., 2017. Neural immunoglobulin superfamily interaction networks. Current opinion in neurobiology 45, 99-105.

Zovein, A.C., Luque, A., Turlo, K.A., Hofmann, J.J., Yee, K.M., Becker, M.S., Fassler, R., Mellman, I., Lane, T.F., Iruela-Arispe, M.L., 2010. β1 Integrin Establishes Endothelial Cell Polarity and Arteriolar Lumen Formation via a Par3-Dependent Mechanism. Developmental cell 18, 39-51.